

Tectonostratigraphic Analysis Case Studies from British Columbia, Canada UAV Photogrammetry and 3D Seismic of Bohai Bay, China

By
Keaton Denzer

A Thesis Submitted to the Department of Earth and Atmospheric Sciences,
College of Natural Sciences and Mathematics
University of Houston

In Partial Fulfillment of the requirements
for the Degree of Master of Science
In Geology

Chair of Committee: Jonny Wu
Committee Member: Yin Liu
Committee Member: Michael Murphy
Committee Member: Nicholas Perez

May 2022

Acknowledgements

My special thanks go to Dr. Jonny Wu, Ph.D., for his guidance, support, and patience throughout this endeavor. Furthermore, I am incredibly grateful to my thesis committee members, Dr. Yin Liu, Ph.D., Dr. Michael Murphy, Ph.D., and Dr. Nicholas Perez, Ph.D., for the insights they too have provided throughout this project. I would also like to thank my research group mates and fellow graduate students Ozzy Tirmizi and Spencer Fuston for the help and advice they have provided me on numerous occasions. I would also like to thank those who have funded me; The Texas GURI Funds administered by Dr. Suppe, funding this research through the summer of 2021, NSF EAR-1848327 which funded my travel to the GSA short course which helped me to develop the 3D spatial skills needed to create a virtual field trip using virtual outcrop models, Advisor start up funds which funded the trip to Canada, and NSF GEOAllies which funded my trip to New Mexico. Finally, I am eternally grateful for the support of my family and close friends who have encouraged me throughout my pursuit of higher education.

Abstract

This thesis covers two tectonostratigraphic analysis case studies for geoscience education and petroleum geoscience structural analysis, respectively. The first study involves development of Unmanned Aerial Vehicle (UAV) drone surveys to address gaps in field geoscience education. Four UAV surveys were conducted including a 378,200 m² outcrop survey of the Taylor Creek Group in the South Chilcotin Mountains of British Columbia, Canada. We created a series of virtual field trip 'video game'-style lab exercises from the UAV imagery that are PC, phone and tablet-accessible and do not require additional software.

The second study involves the Dongying Depression, Bohai Bay, China, the second largest petroleum field in China. The region has been heavily faulted and has experienced multi-phase deformation including pure extension, transtension, and thermal subsidence. We interpret 20 extracted raster seismic cross sections from a 1600 km² 3D seismic volume and from a proprietary sequence stratigraphic framework. Isochron maps show that deposited sediments between 46 Ma to the Present within the Dongying Depression form a thickness of 1500 ms two-way-time (~4 km). Older depocenters are centered in the north near the master listric normal faults whereas younger sediments are deposited near the central depression. Tectonostratigraphic interpretation showed the following history: 1) between 64 to 44 Ma, active extension occurred along half-grabens bounded by listric normal faults; 2) between 44 to 24 Ma, extension continued but was punctuated by pulses of compression and inversion of the listric normal faults between 44 and 32 Ma. A regional angular unconformity formed at ~24 Ma; and, 3) from 24 to 0 Ma, widespread, minor extensional growth occurred that is

attributed to thermal subsidence. The most significant period of fault reorganization that occurred between 44 to 32 Ma could be linked to changes in the plate tectonic boundary conditions (i.e. Pacific-Eurasia subduction).

Table of Contents

Chapter 1: Introduction	1
Chapter 2: UAV Photogrammetry for Developing Geoscience Education Virtual Field Trips	3
2.1 Introduction	3
2.1.1 <i>Purpose of the Study</i>	3
2.1.2 <i>Review of UAVs in Geoscience</i>	4
2.2 Method Development	6
2.2.1 Acquisition	6
2.2.2 Processing.....	12
2.2.3 Export.....	12
2.2.4 VFT Development.....	13
2.3 Results of Surveys	15
2.3.1 Survey 1 - Katy Home	16
2.3.2 Survey 2 - Reimers Ranch.....	22
2.3.3 <i>Survey 3 - Pedernales River</i>	28
2.3.4 <i>Survey 4 - Taylor Creek Group</i>	29
2.3.5 <i>Survey 5 - The Florida Mountains, Deming, New Mexico</i>	35
2.4 Virtual Field Trip (VFT) Development	39
2.4.1 <i>Conceptual Model VFT ‘Methoda Fields’</i>	39
2.4.2 <i>Real-world VFT ‘Taylor Creek Group’</i>	41
2.5 Discussion: Comparison to Previous UAV Studies	48
2.6 Conclusion	50
Chapter 3: Structural Analysis of the Dongying Depression, Bohai Bay Basin, China	52
3.1 Introduction	52
3.2 Geologic Setting	54
3.2.1 <i>Structural Setting</i>	54

3.2.2 Stratigraphy.....	55
3.3 Methods and Data	56
3.3.1 Dataset.....	56
3.4 Results	58
3.4.1 Seismic stratigraphy.....	58
3.4.2 Regional Tectonostratigraphy.....	64
3.4.3 Stratigraphic styles	78
3.4.5 Structural Styles.....	89
3.4.6 Fault Analysis.....	94
3.4.7 Seismic Reconstruction.....	97
3.5 Discussion.....	101
3.5.1 Tectonostratigraphic evolution	101
3.5.2 Comparison to Previous Studies.....	103
3.6 Conclusion	105
Chapter 4: Conclusion	105
Bibliography	108
Appendix.....	A
<i>The TCG Virtual Field Trip Stops.....</i>	<i>A</i>
<i>Written Assignment (Blank).....</i>	<i>D</i>
<i>Key to Assignment</i>	<i>K</i>

List of Tables

2.1 Result of Surveys.....	15
2.2 Individual surveys of the Taylor Creek Group outcrop	31

List of Figures

2.1 Workflow for developing a virtual field trip	6
2.2 Map view showing potential survey flight paths	8
2.3 Conceptual image of drone survey camera angles	10
2.4 Conceptual image of various UAV survey plans for steep topography	11
2.5 In game image of VFT showing the strike and dip function	14
2.6 Map view image of Survey 1 location with dimensions	17
2.7 Examples of images taken from Survey 1	19
2.8 Images demonstrating overlap issues in Survey 1	20
2.9 Image of VOM generated from Survey 1	21
2.10 Resolution comparison between satellite imagery and an image of the Reimers Ranch outcrop	23
2.11 Flight path of Survey 2 overlaid on Reimers Ranch Outcrop	24
2.12 Image of model generation broken down by phase	26
2.13 Image of VOM generated from Survey 2	27
2.14 Map view image of Taylor Creek Group location	29
2.15 Map view image of Taylor Creek Group surveys on satellite imagery of the outcrop	30
2.16 Oblique image comparison between the Taylor Creek Group VOM and satellite imagery of the outcrop	33
2.17 Images of the Taylor Creek Group outcrop after being cropped	34
2.18 Map view of the Florida Mountain survey location	36
2.19 Zoomed in oblique image of the upper Florida Mountain VOM	37
2.20 Zoomed in oblique image of the lower Florida Mountain VOM	38
2.21 In VFT image of the Methoda Fields model	40
2.22 In VFT image of game functions on the Methoda Fields model	41
2.23 In VFT view of spawn point in the Taylor Creek Group VFT	44
2.24 Stop 3 in the Taylor Creek Group VFT	45
2.25 Stops 4 and 8 in the Taylor Creek Group VFT	46
2.26 Stop 10 in the Taylor Creek Group VFT	47
2.27 Stop 9 in the Taylor Creek Group VFT	48
3.1 Tectonic Map of the Bohai Bay Basin, eastern China	53
3.2 Regional plate tectonic history modified from Liang et al., 2016	54
3.3 Basemap of Dongying Depression with transect locations	57
3.4 Seismostratigraphic column	60
3.5 Isochron maps of the Dongying Depression	63

3.6	<i>Two representative regional seismic transects</i>	64
3.7	<i>Two representative regional seismic transects 1:1 scale</i>	66
3.8	<i>Interpreted N-S seismic transects</i>	69
3.9	<i>Uninterpreted N-S seismic transects</i>	72
3.10	<i>Interpreted E-W seismic transects</i>	76
3.11	<i>Uninterpreted E-W seismic transects</i>	77
3.12	<i>Angular unconformity locations on Dongying Depression Basemap</i>	79
3.13	<i>Example of the regional unconformity 24 Ma</i>	80
3.14	<i>Example of a local Shahejie angular unconformity</i>	81
3.15	<i>Example Kongdian - Shahejie angular unconformity</i>	82
3.16	<i>Example of the Kongdian - Cretaceous angular unconformity</i>	83
3.17	<i>Example of Kongdian onlap onto Cretaceous horizons</i>	85
3.18	<i>Interpreted example of Clinofolds</i>	87
3.19	<i>Uninterpreted example of Clinofolds</i>	88
3.20	<i>Example of half graben geometries of the depression</i>	90
3.21	<i>Location of upward fault terminations after 24 Ma erosional event</i>	91
3.22	<i>Location of upward fault terminations between 24 Ma to 43.5 Ma</i>	92
3.23	<i>Location of upward fault terminations before 43.5 Ma</i>	93
3.24	<i>Example of fault truncation patterns</i>	94
3.25	<i>Example if inversion</i>	96
3.26	<i>Reconstruction of Transect 2656</i>	100

Chapter 1: Introduction

This M.S. thesis consists of two case studies on structural geology. Study 1 is focused on the use of Unmanned Aerial Vehicle (UAV) imagery and photogrammetry for geoscience education. In this study we will develop a work-flow for students and professors in the geosciences to create virtual field trips for education. This includes planning and acquisition of UAV data to a final product in the form of a virtual assignment. Many studies have used UAVs to analyze flat lying stratigraphy (Nesbit et al., 2018; Madjid et al., 2018; Zahm et al., 2016; Viana et al., 2018) and gently dipping beds (Tavani et al., 2014) where they have followed similar but different methods to achieve a similar goal. While these studies analyze how VOM's can be useful in interpreting geologic features, they do not mention the possibility of these models being used to educate students and to bridge the gap between classroom and field learning. In this study, we investigate the use of UAVs (Unmanned Aerial Vehicles) in order to develop a detailed UAV photogrammetry workflow to acquire a VOM good enough for a virtual field trip and explore the potential of using virtually created outcrops to introduce geological field mapping concepts that will be found in real outcrops through the development of a platform to deliver a pilot assignment to students in an inexpensive and easily accessed manner on widely-used digital devices.

Study 2 involves a structural analysis of large-scale structures using seismic images in the Dongying Depression located in southeastern Bohai Bay Basin, China. The Dongying Depression is located in southeastern Bohai Bay Basin, in eastern China. The Dongying Depression is of interest because of its large petroleum prospects with an area which contains the second largest oil field in China exceeding 800 MMBOE in

place (Li, 2003). The petroleum prospectivity has driven this area to be well imaged through 3D seismic data. The aim of this study is to deduce the history of structural deformation that has shaped the area. The approach will consist of: 1) a stratigraphic analysis of growth and erosional features; 2) a structural analysis of basin evolution from fault geometries and styles; 3) proposing a tectonostratigraphic evolution from the analyses in this study.

Chapter 2: UAV Photogrammetry for Developing Geoscience Education Virtual Field Trips

2.1 Introduction

2.1.1 Purpose of the Study

During the COVID-19 pandemic, in the Spring 2021 semester the University of Houston class 'GEOL3340 Geologic Field Methods' used Google Earth satellite imagery as an alternative means to teach geologic field mapping. This was due to classes being held online. We had to find new ways to offer students the opportunity to map geologic structures without actually being in the field (i.e. virtual field trips). Our use of Google Earth allowed more accessibility than a traditional field trip. Students were also able to see larger-scale (~10's to 1000's of meter-scale) views of geologic structures. However, one serious drawback was the lack of field-scale (i.e. 1 meter-scale) resolution in Google Earth imagery, which meant that the virtual learning was not fully portable to in-person field experiences. For example, our students did not have the opportunity to observe and measure field-scale rock attitudes (i.e. bedding dips and strikes). Furthermore, we observed that Google Earth did not offer students the opportunity to develop 3D spatial skills associated with making observations on topography. One example is the well-known advantage of making long-range observations from a topographic high (i.e. hilltop or mountain lookout) relative to a viewpoint from a valley floor.

In this study, we investigate the use of UAVs (Unmanned Aerial Vehicles), also known as drones, for bridging the apparent field-scale (~1 meter-scale) observational gap between in-person field experiences and Google Earth. The study aims are as

follows:

- 1) Develop a detailed UAV photogrammetry workflow starting from outcrop selection and flight planning to virtual field trip (VFT) development that can be implemented using the technical capability of most geoscience instructors;
- 2) Develop a platform to deliver a pilot assignment to students in an inexpensive and easily accessed manner on widely used digital devices (i.e. laptop, phone or tablet); and,
- 3) Explore the potential of using virtually created outcrops to introduce geological field mapping concepts that will be found in real outcrops.

2.1.2 Review of UAVs in Geoscience

Many studies have used UAVs to analyze flat lying stratigraphy (Nesbit et al., 2018; Madjid et al., 2018; Zahm et al., 2016; Viana et al., 2018) and gently dipping beds (Tavani et al., 2014) where they have followed similar but different methods to achieve a similar goal. Flying a UAV comes with several challenges that need to be avoided to allow for a good seamless series of surveys. Current UAVs challenges can be divided into three categories: natural, technological, and legal (Jordan, 2015). Natural limitations include large areas of vegetation and bad weather (high winds or storms). Large amounts of vegetation will make imaging geologic features near impossible either because they obstruct the structure or make it to where the drone cannot fly close enough for high resolution images (Madjid et al., 2018). High winds will make the drone unstable in flight, causing low quality images or blowing the drone into obstacles (Jordan, 2015). Technological barriers include camera resolution and flight time limitations because of battery capacity (Hodgetts, 2013). Laws about UAV use is the

last factor limiting the use of UAVs in geosciences (Jordan, 2015). On top of this they have caused many issues regarding privacy (Flacy, 2014). This study is designed to address these challenges in producing UAV-supported educational materials for those who are limited in travel to good geologic features. Another factor of consideration is the type of drone being flown, being that this study was done by a quadcopter, I will focus on survey planning for this type of drone.

The usage of UAVs in geosciences has been on the rise over the past few years (e.g. Hodgetts, 2013; James et al. 2017, Madjid et al. 2018). Geologic fields that have utilized UAVs include natural hazards (Jordan and Napier, 2016; Mateos et al., 2017; Serban et al., 2016; Tamminga et al., 2015), sedimentary geology (Chesley et al., 2017; Nieminski and Graham, 2017; Nesbit et al., 2018), environmental science (Hird et al., 2017; Mlambo et al., 2017), and structural geology (Bemis et al., 2014; Viana et al., 2018; Bistacchi et al., 2015, Uzkeda et al., 2022). While these studies used drones to analyze data, or map geologic features, more workflows are needed to bring these techniques for educational use, especially near Houston.

2.2 Method Development

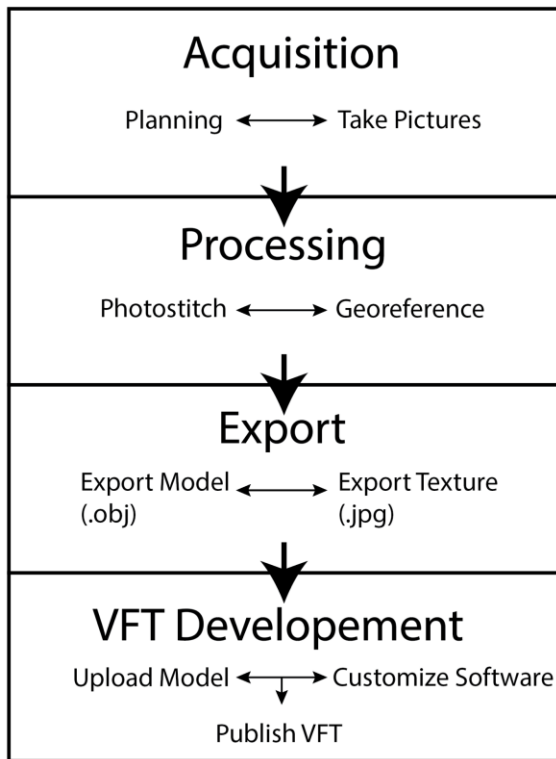


Figure 2.1: Workflow for developing a Virtual Field Trip; starting from the initial planning of the UAV survey to the publishing of the VFT for students to use. Modified from Zahm et al. 2016

2.2.1 Acquisition

The acquisition process involves two steps: planning the survey by finding the best location for a survey and programming a preflight plan into drone software and capturing the inflight pictures through the programmed survey or by manually taking them as the UAV pilot. These steps are crucial and lay the foundation on which the rest of the project will be built. Outcrop selection and survey planning work together because each outcrop is different in size and orientation and not all outcrops can be surveyed because of this. Finding the right geologic outcrop or part of an outcrop is important to ensure a survey can be run to its full resolution capabilities. Outcrops with vertical faces will need to be surveyed differently from a flat lying geologic feature.

When an outcrop is only vertical or horizontal, the survey process is fairly straightforward; the struggle in survey planning comes from when the geologic outcrop is a combination of vertical and horizontal features. The different software that allows for pre-flight survey planning typically have several flight plan options. Some of the options are not as practical for outcrop models, and do not need to be mentioned. The typical flight path used to map surfaces for 2-D maps can be seen in Figure 2.2a. The flight plan only runs in two directions, N-S or E-W. While this type of survey is good for 2-D maps and flat surfaces, it does not image an outcrop well enough to create a high resolution 3-D model. Therefore, a flight plan that looks like Figure 2.2b is best for 3-D models. With paths running N-S and E-W, the model can be imaged from all sides, ensuring full coverage of the outcrop. Survey planning can be done in a number of ways: setting waypoints and taking manual pictures (Survey 1), planning a manual flight and manually taking the pictures (Survey 2), and using software to create a survey path for the drone to follow that automatically takes pictures (Surveys 3, 4, 5). For all three of these options, the Pilot needs to ensure to follow a similar path to Figure 2.2 and ensure the correct amount of overlap between each image. Pix4DMapper was chosen for this study because it has an automated process where a 2D rectangle can be drawn and the software will propagate a flight path into the rectangle and calculate the image overlap. The application gives the surveyor several options when creating the survey including photo overlap, flight elevation, camera angle, and UAV speed. One of the difficulties in the planning is that the flight elevation does not change with topography, but instead is set at the height above wherever the drone lifts off from. This can cause some problems when trying to be effective with survey length time and area covered.

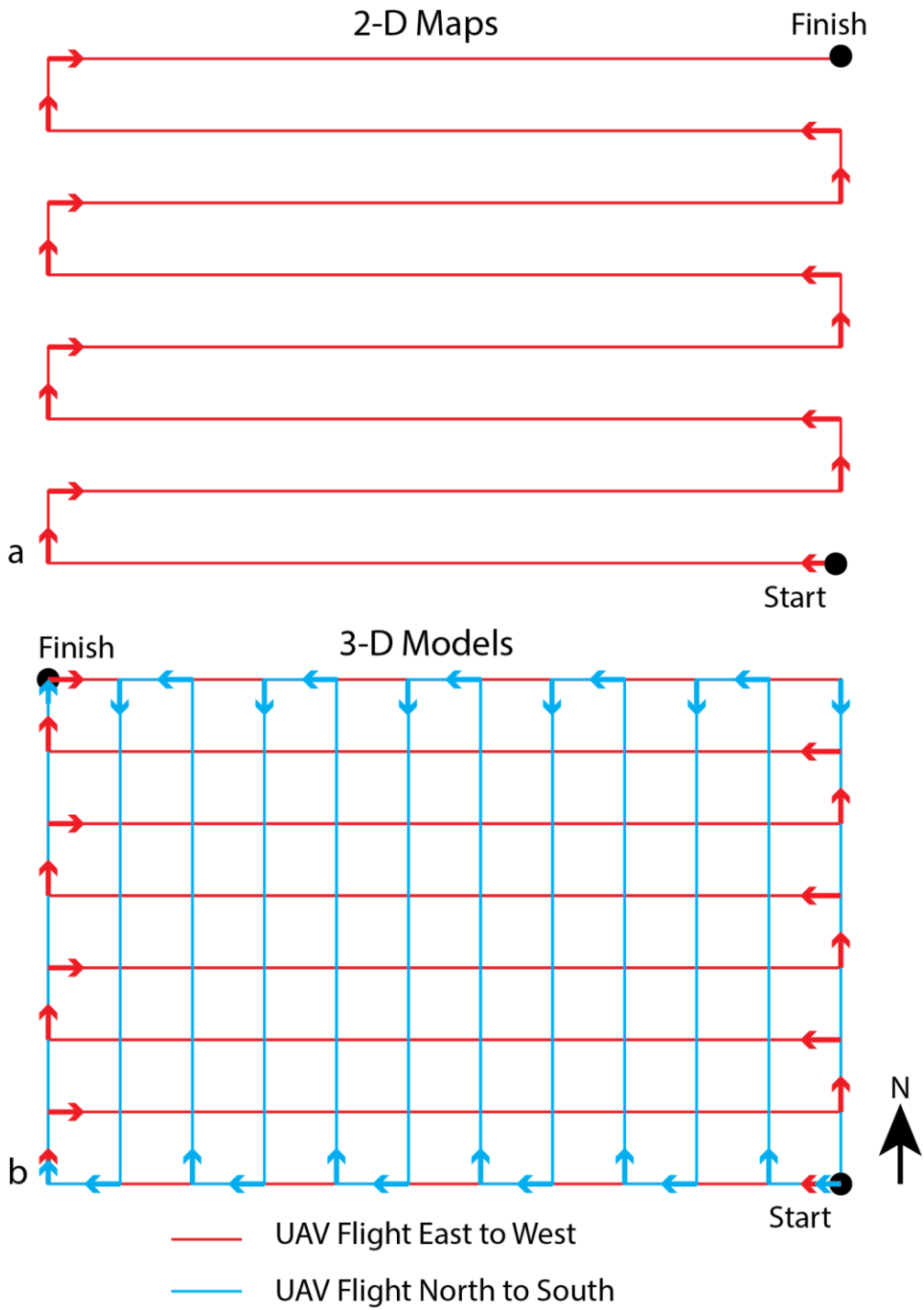


Figure 2.2: Map view image showing potential survey flight paths. Figure 2.2a is an image of a flight path that is good for the creation of 2-D maps. The drone survey starts where the word start is and ends where the word finish is. Figure 2.2b is an image of a flight path that is good for creating 3-D models. The first half of the survey is like Figure 2.2a, but continues in a N-S flight over the area after flying over the full area E-W.

What dictates the total amount of images taken in a single survey is the pre-set overlap percentage between each photo, the higher the percentage, the more images that are taken. It is important to have a high amount of overlap otherwise the model will not be created correctly. The camera angle affects how well an outcrop is imaged and how much overlap there is of high relief or strongly dipping beds, therefore it needs to be adjusted for optimal coverage when planning the survey (Fig. 2.3). Depending on the type of terrain, a low camera angle off-nadir will cause large sections of the outcrop to not be modeled in certain flight directions. This means that when the model is being made, there will not be as much image overlap of the outcrop, which will decrease the resolution of the model dramatically (Figs. 3.3b and 3.3c)

The image taking process can be affected by a variety of variables, stemming from the flight capabilities of the drone, such as bad weather, high wind speeds, and low cloud cover. Each of these factors need to be considered when choosing a location and date and time of day to fly the UAV. The time of day affects the model extremely because of shadows that can cover the outcrop and ruin the 3d model. The survey needs to be planned in accordance with a time that the least amount of shadows are present or on a day that is overcast.

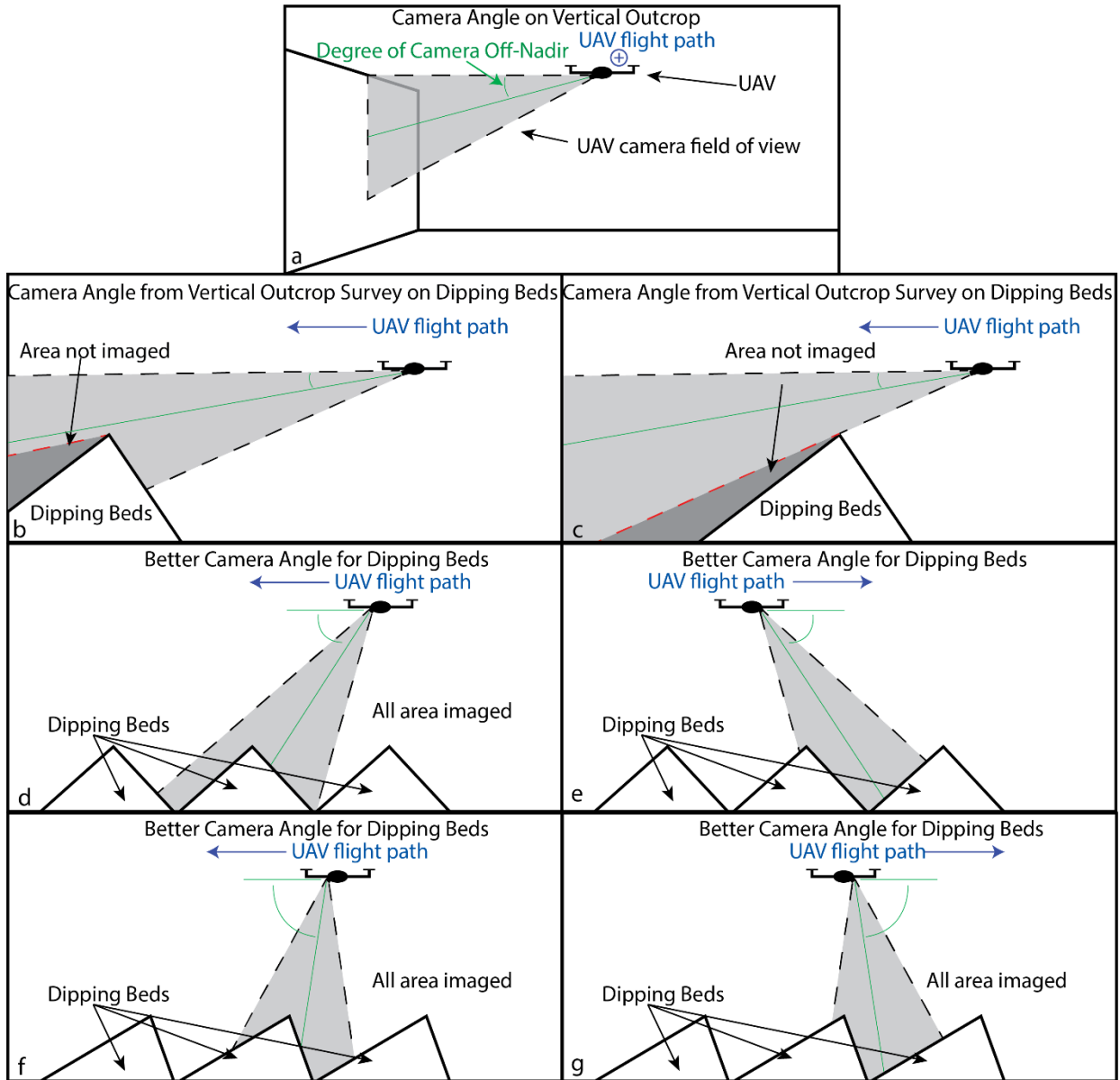


Figure 2.3: Side view images of a drone imaging various terrain to show how camera angle and drone location over the outcrop effect how well the outcrop is imaged, not drawn to scale. Figure 2.3a is a good camera angle which allows the UAV (Unmanned Aerial Vehicle) to image the vertical outcrop well. Figure 2.3b is an example of flying over a dipping bed outcrop where using the same camera angle as when imaging a vertical outcrop does not work well. Figure 2.3c is the same example as Figure 2.3b but the drone is flying in the opposite direction. Figures 2.3d and 2.3e are an example of flying over a dipping bed outcrop with a significantly larger camera angle off-nadir. Figures 2.3f and 2.3g are examples changing the camera angle to an even larger degree to ensure good picture coverage.

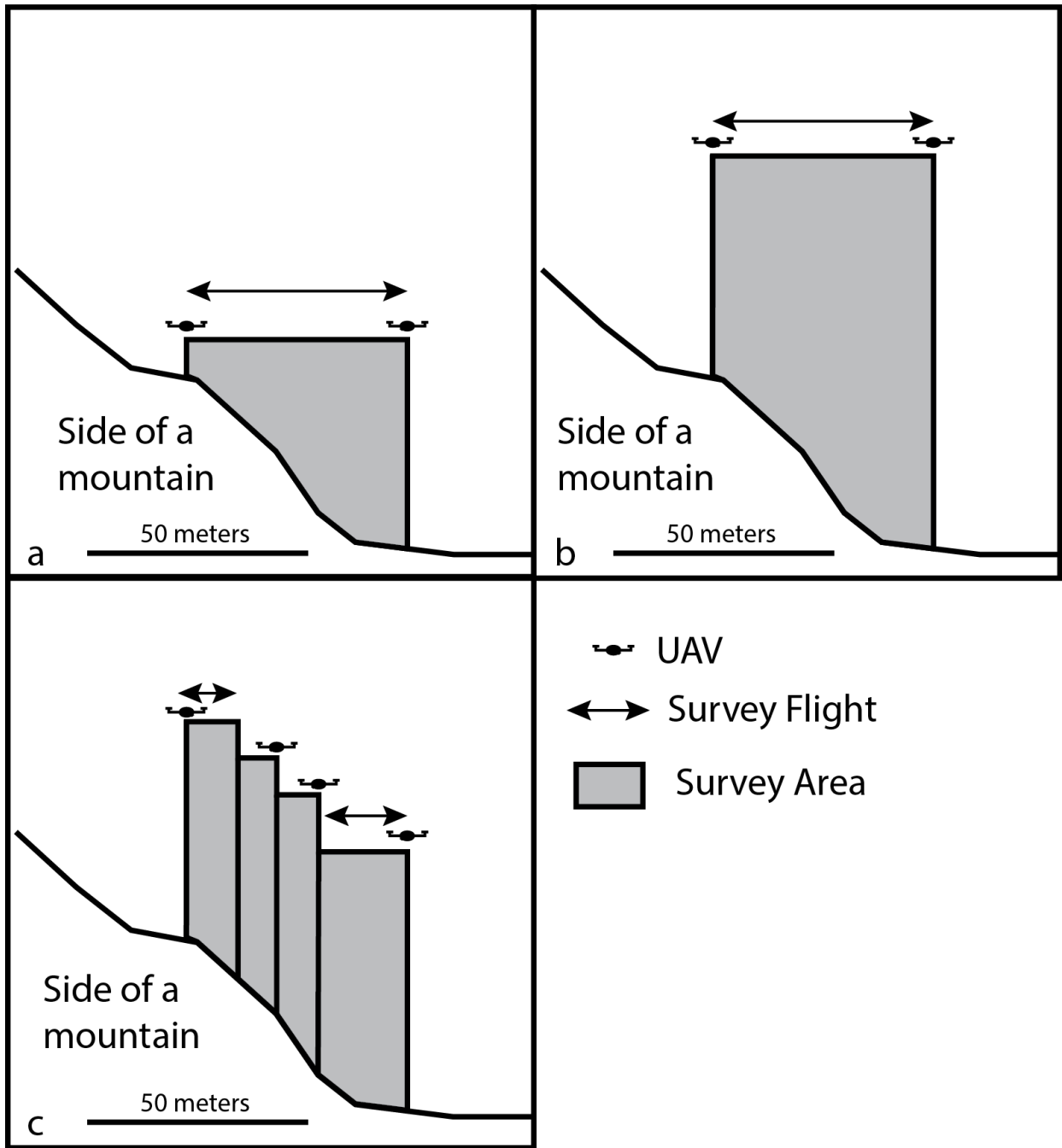


Figure 2.4: 2D side view images of various UAV survey plans on the side of a high relief outcrop on the side of a mountain. Figure 2.4a shows a survey planned 50 meters above the lift off point at the base of the outcrop. Figure 2.4b shows a survey planned 50 meters above the lift off point at the top of the outcrop. Figure 2.4c shows a series of surveys that are 50 meters above the lift off points, but with 4 separate take off points to accommodate for the high relief. Overall, this figure demonstrates a solution to losing resolution due to the high elevation change of an outcrop.

2.2.2 Processing

Photogrammetry is the 3-dimensional rendering of any object or structure by stitching together images taken of the object or structure and is possible through software such as Pix4DMapper (Pix4D, 2017; Nesbit and Hugenholtz, 2019; Madjid et al. 2018), and Agisoft Metashape Professional (Agisoft, 2020; Zahm et al., 2016). The software Agisoft is noted to be the most popular by Viana et al. (2018). We employed an academic license to use Agisoft due to its popularity, as this allows our workflows to be useful to the broadest population of educators . Agisoft Metashape Professional takes uploaded images captured from georeferenced locations and stitches them together to create a scaled 3-dimensional rendering of whatever was imaged. A large limit of this study was the processing time of the models because many outcrops are large in size and require several surveys to cover the whole area.

2.2.3 Export

Once a 3D model is fully rendered, with a mesh and texture, it can be exported to various software that allow for 3D model interpretation of viewing. Some of these programs include OpenPlot (Tavani et al., 2014), Skua-Gocad (Bistacchi et al., 2015) or Pix4Dmapper (Nesbit et al., 2018). Others have used ArcGIS to map linear features (Madjid et al., 2018; Zahm et al., 2016). The exportation of the model includes two separate files, the 3D model mesh (Wavefront OBJ file) and the associated texture(s) of the model (JPG file). When exporting large models that were made in separate chunks and merged, multiple textures may be created and exported for one model. Agisoft Allows you to export both files with one process. After selecting 'export model' and selecting the desired location to export the files to, Agisoft gives the option to export the

texture with the model and gives options as to which type of file to export the texture.

2.2.4 VFT Development

A video-game-like virtual field trip (VFT) can be created once the geologic model has been created and exported. The process to create these VFTs is through uploading the model and texture into Unity (Unity - Game Engine, 2019), a game engine that allows for people to design their own games and game software. The game software in Unity used for this study was developed by a group of students at The University of Washington in Seattle, Washington. The group, led by PhD student Max Needle, made the software code openly accessible here:

github.com/uwrealitylab/structuralquerytoolkit to clone the URL to Unity Hub (Github, 2020). This 'structural query tool kit' makes it so that the basic game code is already created and the creator of the VFT only needs to edit what has already been created. Once the software is cloned, the VFT creator can upload their own outcrop model and any modifications can be made. There are limitations in the size of the model that can be uploaded to ensure a smooth VFT assignment. Things that can be changed include the title page, the about page which also includes acknowledgments, the pictures, and the model that is being played on. Max Needle has created a manual on how to clone the URL and make changes to the game on the following website:

<https://github.com/UWRealityLab/StructuralQueryToolkit/wiki/3.1-Creating-your-model's-material-with-one-texture>.

What turns this game into a VFT is the addition of 'stops' throughout the model (Fig. 2.5), which are added to the game in the form of a floating, spinning rock hammer. In the VFT, the hammer can be clicked on and an in-game window will pop up with text

and images. The text and images on this pop up can be edited by the creator of the game with instructions, information on the model, and/or pictures from the area that the model was created.

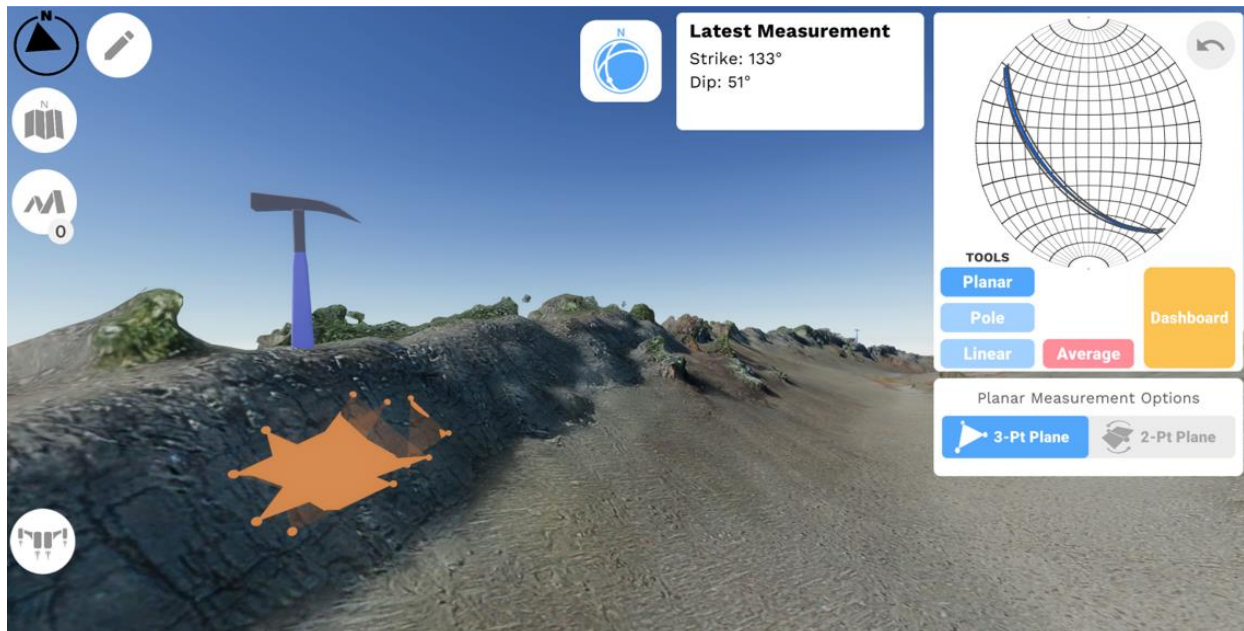


Figure 2.5: In game image of a stop in the VFT. Here, students can make strike and dip measurements and plot them on a stereonet. The orange area on the rock surface is the 3-point plane generated to measure the strike and dip. The hammer is a stop in the VFT that asks students what the strike and dip is.

Once the game has been created and finished, it can be published through a free account on itch.io, a website built to share games and is free to the general public to play games as well. Games created here can be left public or be made password protected if it is desired. Itch.io allows for the game creator to post the game as an HTML that can be played in a browser and does not require any special software.

2.3 Results of Surveys

Survey Name	Location	Date(s)	Total Images Taken	Area of Survey (m ²)	Style of Terrain	Type/Aim
1) Katy Home	Katy, Tx	3/8/ 2021	400	7,407	Flat with little vegetation	Preliminary, Test Drone Survey Feasibility
2) Reimers Ranch	Dripping Springs, Tx	3/18/ 2021	231	269	10-meter-tall cliff with surrounding flat terrain, light vegetation	Preliminary, Test possibility of resolution of outcrop models
3) Pedernales River	Johnson City, Tx	8/5/ 2021	366	600	Flat, tall grass and vegetation	Preliminary, Field Test of automated survey
4) Taylor Creek Group (TCG)	South Chilcotin Mountains, British Columbia, Canada	9/15/ 2021	1,266	378,200	Large, lightly vegetated area with small ridges and valleys	3D photogrammetry of an actual field area; develop a pilot virtual lab exercise
5) Florida Mountains	Deming, NM	2/26- 28/ 2022	2,626	200,000	High relief mountainous region that is mostly unvegetated	Develop a large-scale 3D model for a virtual field trip designed for the UH class Historical Geology

Table 2.1: Surveys flown for this study in the order that they were flown. The table includes the Survey name, location of the survey, date(s) that the survey was flown, total number of pictures taken in the survey, the type of terrain, and the aim of the study. The first two surveys were flown with a Fimi X8Se UAV and Surveys 3, 4, and 5 were flown with a DJI Mavic Pro 2.

Surveys 1,2 and 3 were preliminary surveys that were designed to test logistics, resolution, and acquisition capability. Survey 4 was the main survey used for the results of this study. Survey 5 was a large-scale survey flown at the request of University of Houston faculty teaching the class 'GEOL1376 Historical Geology' based on the encouraging results from Survey 4. Survey 5 is included and briefly described in this thesis to provide documentation for any future research or curriculum developed from the dataset.

2.3.1 Survey 1 - Katy Home

Survey 1 imaged a house in Katy, Texas (Fig. 2.6). The survey was acquired on 3/8/2021 with a solar noon estimated to be 12:30 pm. The UAV flight began at 1 pm to ensure minimum shadows. The imaging process took approximately 1 hour, separated between two 30-minute flights. The weather that day was sunny and 74 degrees, wind was a steady 5-7 meters per second (m/s) with good visibility.



Figure 2.6: Map view image of the area mapped in Survey 1. The image includes the dimensions of each side along the perimeter of the survey box.

Survey 1 was flown by creating a series of waypoints but manually taking the pictures; the survey proceeded as follows:

- 1) The first set of images was taken with the camera directly down at 80 meters from launch elevation and set to follow a predetermined horizontal path. Images were taken every 2-3 sec while the drone flew approximately 5 m/s.
- 2) The second set of images were taken with the camera directly down at 50 meters from launch elevation and set to follow a predetermined horizontal path, not the same as the path before. Images were taken every 2-3 sec while the drone flew approximately 5 m/s.
- 3) The third set of images were taken 25-30 meters from launch elevation with

varying angles of camera to fit objects in the image. These were taken in custom horizontal paths north to south. The drone traveled north until the end of the property, turned 180 degrees, and followed the same path back. Once this was done, the drone was rotated 90 degrees and followed a similar flight path east to west.

- 4) The fourth set of images were taken 10-15 meters from launch elevation to avoid power lines and the drone orbited the property and the camera angle was adjusted accordingly.
- 5) The fifth set of images were taken at selected areas that needed more detail, often between 3-6 meters above launch elevation, with the camera nearly horizontal to the ground. As locations were chosen, the drone would be rotated 360 degrees and images would be taken while the drone spun to acquire additional data.



Figure 2.7 - Images taken from Survey 1. Figure 2.7a is taken as the drone is flying north during the first set of images. Figure 2.7b is from the second set of images. Figure 2.7c is from the third set of images. Figure 2.7d is from the fourth set of images.

Approximately 400 photos were taken during this process. After uploading them to Agisoft, it was learned that not all images were able to be used. This is because of a lack of overlap between the two stages, where one stage ended and the next began. The images removed and not used were from the fourth and fifth set of images. This is because there was no overlap in the pictures as stage 3 ended and stage 4 began. (Fig. 2.8) The images were so far from where they needed to be I could not fix the error and therefore the final 3-d rendering is not as detailed as it could be (Fig. 2.9).



Figure 2.8: Two successive photographs a) photo 162 and b) photo 163 taken from the drone Survey 1 of a residential property near Houston. Agisoft software could not stitch together the images for photogrammetry due to the large spatial gap between the images. Therefore, in subsequent surveys the acquisition sequence was adjusted to avoid large spatial gaps in the photographs.



Figure 2.9: Image of the full 3D model in Agisoft. The survey demonstrated that a 3D photogrammetric model could be created successfully using our methods and equipment. Figure 2.9a is an image of the Katy House model from the south looking north. Figure 2.9b is an image of the Katy House model from the north looking to the south.

Based on the success of Survey 1, we proceeded to undertake Survey 2 of a geological outcrop in Central Texas.

2.3.2 Survey 2 - Reimers Ranch

Survey 2 was undertaken at an area called Reimers Ranch, a popular rock-climbing area in Dripping Springs, Texas, USA. The imaged area is significantly smaller than Survey 1 at 269 m². This area was chosen to test the potential resolution of an outcrop that could be produced in a 3D model in Agisoft. The vertical walls in this area are about 10-13 meters high and nearly horizontally continuous for hundreds of meters. The section of the wall in the final 3D model was roughly 25 meters long and was chosen because of the clearance without trees, which can be seen in Figure 2.10. The imaging took place on 3/18/2021 when the solar noon is estimated to be 1:30. The flight began at 3 pm, so the shadows have more of a factor on the final 3D model. The wind was between 5 - 7 m/s, there were no clouds and visibility was high. The flight lasted about 15 minutes. Both the survey path was flown, and the images taken manually.

Survey 2 was flown as follows:

1. Because of the small area of imaging, the first image was taken about 5 meters above the base of the wall and about 20 meters away from the wall. The image captured includes the entire 10 x 25 meter section shown in Figure 2.10a.
2. After the first image, the drone was flown closer to the wall and images were taken during this process to ensure a strong sequential order.
3. The second set of images consisted of flying a single rectangle, starting on the top right, working left, imaging every 2-3 seconds to ensure plenty of overlap between images. Then from top left to the bottom left corner and then to the

bottom right corner, finishing back in the top right corner (Fig. 2.11).

4. The third set of images began by flying closer to the top right of the wall. The pattern used in this step is imaged in Figure 2.11. Images were taken every 2-3 seconds to ensure plenty of overlap.
5. The fourth set of images were taken at an oblique angle once the drone was rotated 45 degrees from perpendicular to the wall to the right and following the path in Figure 2.11. When the drone reached the end of the path, the drone was rotated 45 degrees the other way and followed the same path.
6. The fifth set of images were taken with the drone camera 45 degrees below horizontal and perpendicular to the wall, following the same path seen in Figure 2.11.



Figure 2.10: Images comparing between a UAV image taken in the Reimers Ranch Survey and the same location viewed on Google Earth. Figure 2.10a shows a UAV overview image of the outcrop used in Survey 2. The latitude and longitude from where the UAV image was taken was used to find the exact location of the drone on Google Earth, seen in Figure 2.10b. Figure 2.10b shows the extremely low resolution image of the outcrop from Google Earth. The UAV image has far better resolution than the satellite image and proves that this method will allow students to see geologic outcrops better.

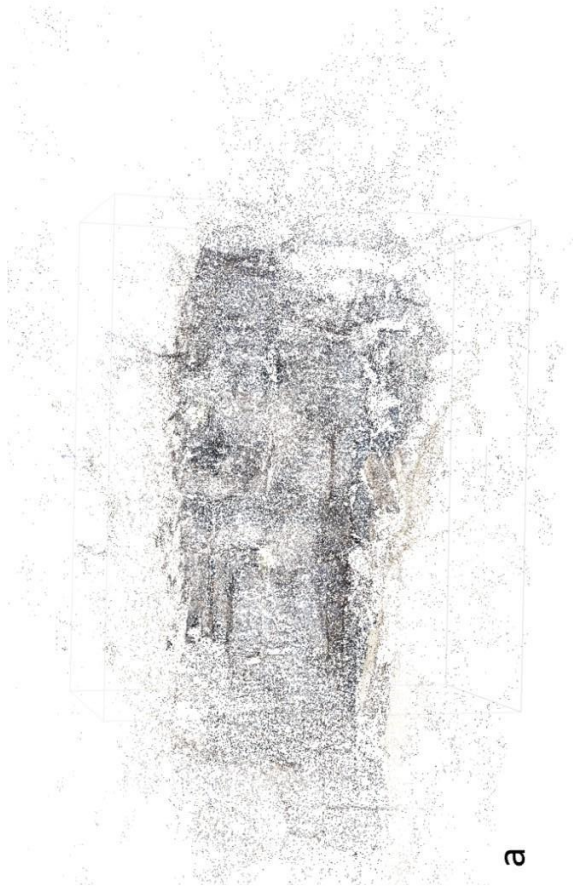


Figure 2.11: Flight paths superimposed onto the first image of the Reimers Ranch Outcrop. Each path progressively gets closer to the wall.

All 231 images taken were able to be aligned in Agisoft and Point Cloud was generated (Fig. 2.12a). From the Point Cloud, a Dense Cloud was able to be made (Fig. 2.12b), then a mesh which forms the shaded model (2.10c), and lastly a texture which forms a Textured Model (Fig. 2.11d).

Once textured, the 3D rendering of the wall was so detailed one can see the blades of grass on the plant on one of the ledges of the cliff (Fig. 2.11) or even the small climbing bolts on the wall (Fig. 2.12). The size of the bolts is approximately 25 cm tall, which shows that the survey can distinguish features on the order of ~ 20 - 30 cm thick.

Figure 2.12: Uploading and processing of Survey 2 images in Agisoft to produce a 3D photogrammetry model. a) point cloud created after uploading the images and aligning them. b) density cloud. c) shaded model. d) textured model. Image b (density cloud) has several gaps in the model, which can be seen in the lowest part of the image. The shaded model (image c) fills these gaps but without detail. The textured model gives better detail to the model and refines the colors.



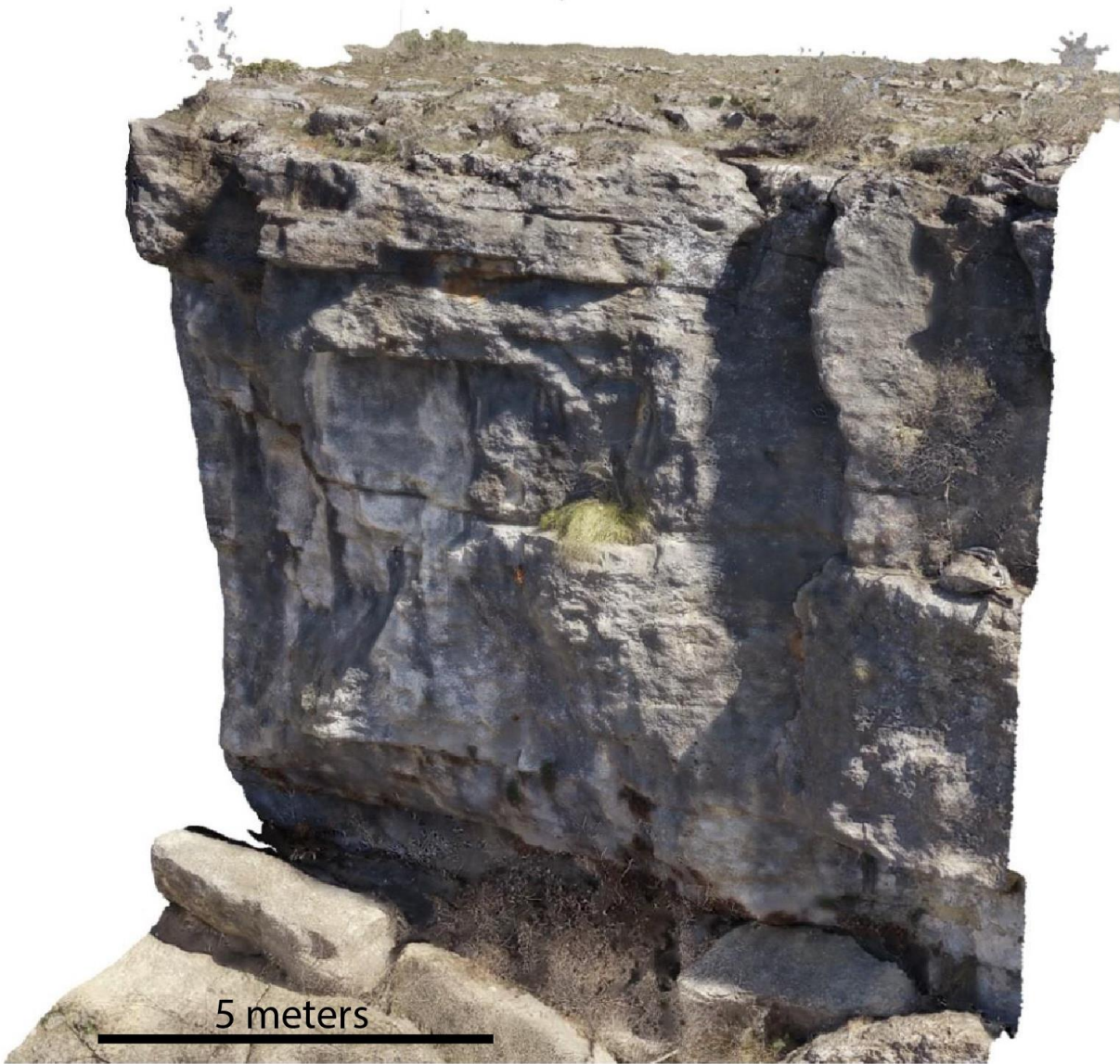


Figure 2.13: Zoomed in image of the 3D model on Agisoft of the left side of the photogrammetry model from Survey 2. This image shows that the model was a success because the green plant on the ledge has enough resolution to discern blades of the leaves on the plant are visible.

2.3.3 Survey 3 - Pedernales River

Survey 3 was conducted along the Pedernales River, about 1 mile west of Pedernales State Park. The location was chosen based on satellite images on Google Earth. The area was chosen because of its exposed dipping beds, similar in appearance to those in the state park, but on a much smaller scale. This survey represents the first time the Pix4DMapper application was used to pre-plan, fly and take pictures of the study area. Pix4DMapper was downloaded for free from the google play store directly onto the UAV controller from this link:

<https://play.google.com/store/apps/details?id=com.pix4d.pix4dmapper>

While the survey was successful in completion, the results were not good enough to be used for any form for educational purposes. This was because of the vegetation that grew between the different beds of rock. The tall grass effectively removed the ability of a student to see the dip of the bedding as well as skewed the resolution of the model because of its obstruction to the rock. This is something that needs to be carefully considered when planning a geologic UAV survey. Although the area can be analyzed in person and the vegetation does not affect a person's view of the rocks on the ground, it can be detrimental to a UAV survey.

2.3.4 Survey 4 - Taylor Creek Group

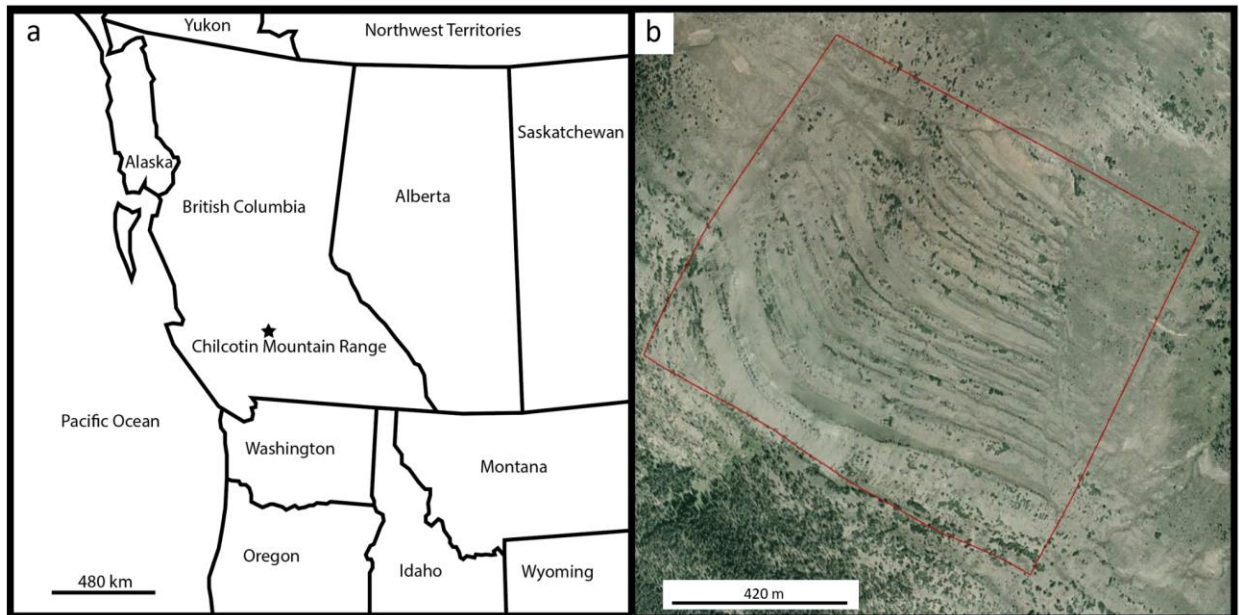


Figure 2.14: Map view of the location of the Taylor Creek Group Outcrop. Figure 2.14a is a regional map showing the outcrops' location in the Chilcotin Mountain Range, British Columbia, Canada. Figure 2.14b is a zoomed in image of the Taylor Creek Group from Google Earth. The red rectangle is the full extent of the 3D model created from the survey.

The UAV survey was flown over a remote outcrop in the South Chilcotin Mountains in British Columbia, Canada (Fig. 2.14a). The outcrop, located at latitude $51^{\circ} 9' 3.2''$ N and longitude $122^{\circ} 50' 10.14''$ W, consists of roughly $400,000 \text{ m}^2$ of exposed TCG (Taylor Creek Group) (Fig. 2.14b). The terrain of the outcrop was lightly vegetated with small trees and shrubbery spread throughout the area. This allowed for a straightforward flight plan to be created for the UAV to follow and take pictures using Pix4DMapper. The TCG outcrop is located on top of a remote mountain, making charging and recharging drone batteries very difficult; meaning, flight time is limited by the amount of charged batteries brought into the field without an opportunity to recharge them. I had a total of four fully charged batteries, limiting me to three drone flights approximately 20-25 minutes long with one extra battery in case of anything going

wrong. Because of the size of the area and the max flight time capable of one battery, the UAV was unable to image the entire area in one survey with the desired detail needed for the model. To obtain a desired resolution needed in the model, and image the largest amount of the model as possible, the flight elevation was set at 70 meters above the ground and three separate surveys were planned (Fig. 2.15a). The camera angle was set to be 55 degrees off nadir to best image the outcrops vertical ridges. Overall, the full survey took roughly 90 minutes to cover 130,000² m and 1,266 photos were taken. This is the area of what the drone flew, not the final size of the model (Fig. 2.15b).

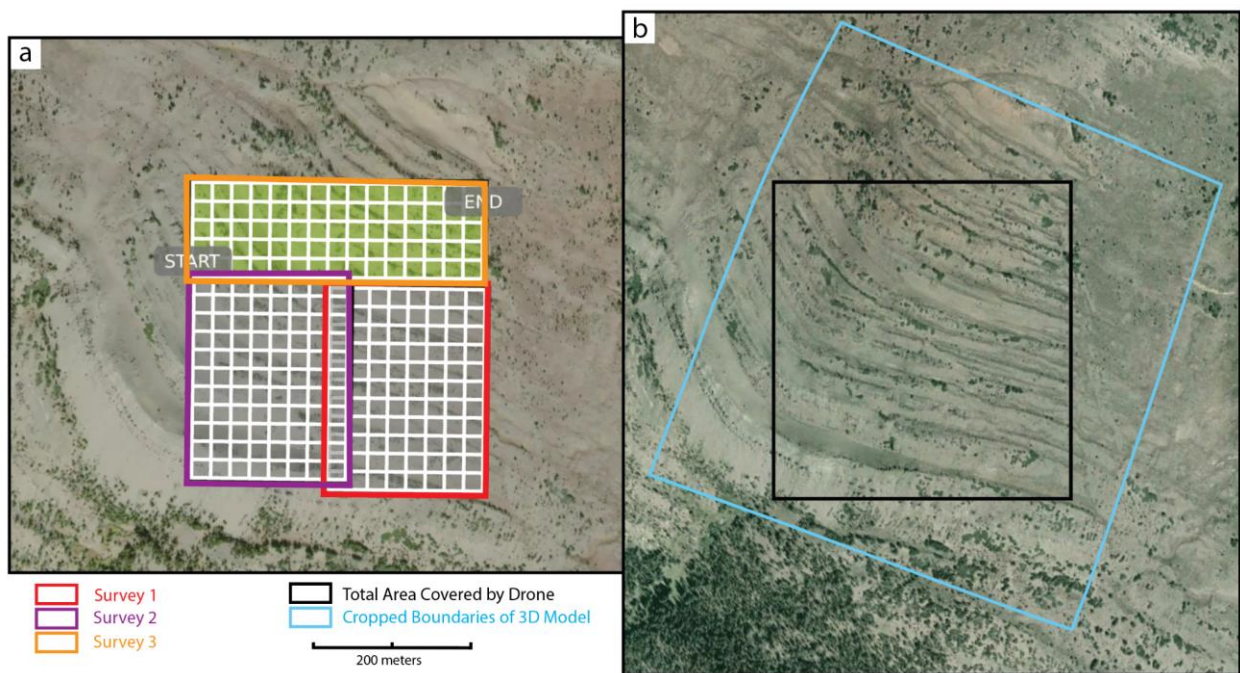


Figure 2.15: Map view of the surveys flown over the TCG outcrop. Figure 2.15a is a screenshot from the Pix4DMapper app and shows the 3 separate surveys as well as the drones path followed for the surveys. The overlapping between each survey was to ensure a seamless stitch between the surveys. Figure 2.15b compares the size of the flight path area to the area imaged by the drone and turned into part of the model.

forecasting is difficult and fairly unreliable. The top of the mountain can experience rapid changes in weather and cloud coverage, which was the case on the day of the flight. There was intermittent extreme cloud cover, snow, and haze which forced the UAV to be grounded between each individual survey. Because of the battery constraints, there was not enough time to be able to ground the drone in the middle of its flight if bad weather hits. There are a few locations of the model that appear to have lower resolution because of this.

TCG Survey	Date	Time	Dimensions	Camera angle	Images	Flight Time
1	Sep 15, 2021	1:27 pm	268m x 207m	55	432	19 min 45 s
2	Sep 15, 2021	2:00 pm	268m x 207m	55	431	20 min 08 s
3	Sep 15, 2021	3:00 pm	380m x 130m	55	403	19 min 30 s

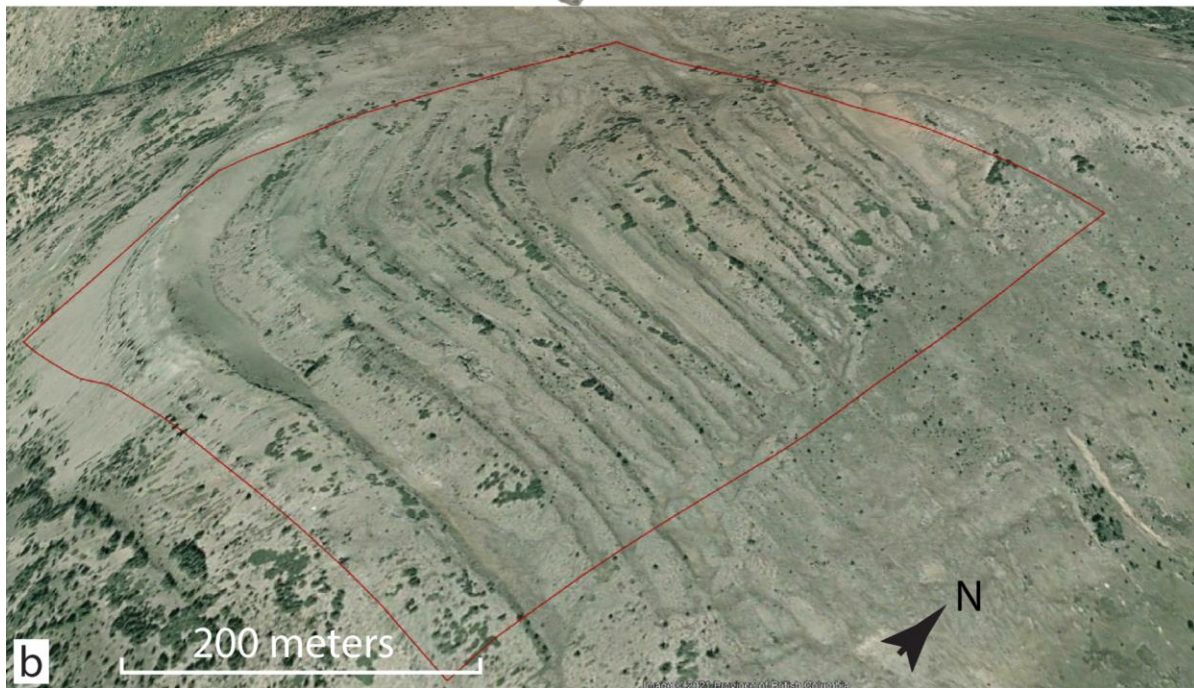
Table 2.2: List of the component surveys flown over the TCG outcrop with their individual properties: Date of flight, the time of when the drone began the survey, the perimeter dimensions of the rectangular survey, the angle of the camera off nadir, how many pictures were taken in each survey, and how long each survey lasted.

The creation of a point cloud took approximately 1 day of processing and consisted of the initial uploading of the photos and the stitching of them together. The next step in the process is the creation of a dense cloud, which took roughly 4 days of processing. Once rendered, the dense cloud was then broken into 12 individual chunks. This had to be done because the model was too big to render a mesh for the model as a whole. Each individual chunk had its own mesh and texture rendered, which took

approximately 1 hour for each chunk. After all the chunks are fully meshed and textured, they can be merged back together without the dense cloud, keeping the file size smaller. The mesh and texture resolution are what dictate the size of the file of the 3D model. This means that the higher the resolution, the larger the file. Because of the constraints needed for a smooth gaming experience in Unity, the file needed to be downsized from its full scale. The full-scale model dimensions are 610 m x 620 m (Fig. 2.16). While the mesh could not be rendered to its highest resolution, the highest texture resolution could be used. The settled model size for the VFT was 350 meters by 250 meters. Once this was completed, the model was rendered with a medium sized mesh and a 16k resolution for the texture. The model contains 2,454,360 faces and 1,231,217 vertices and a file size of 205 MB (Figure 2.17).

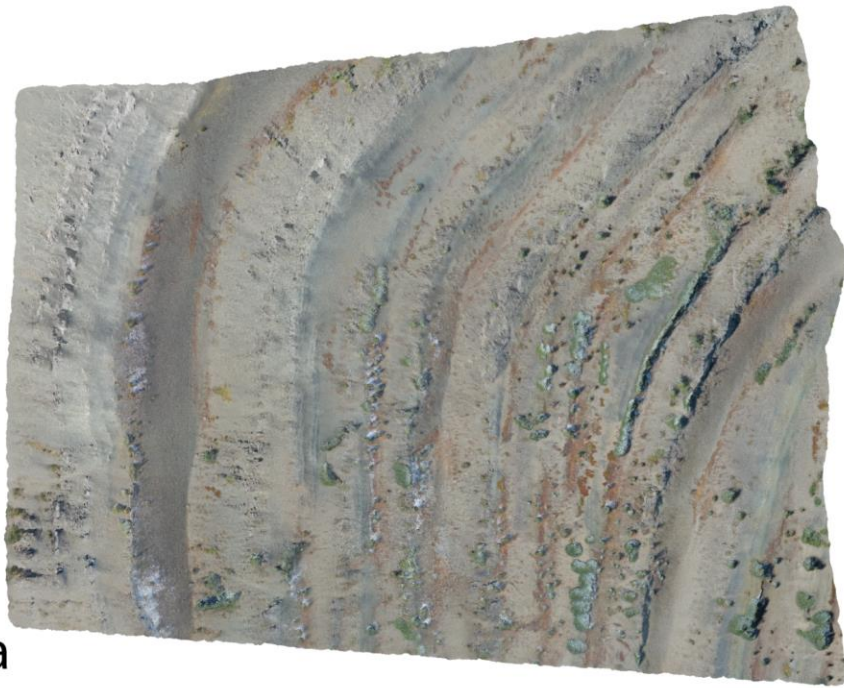


a



b

Figure 2.16: Oblique images of the Taylor Creek Group outcrop. Figure 2.16a is the virtual outcrop model rendered from Agisoft Professional. Figure 2.16b is an oblique image from satellite imagery on Google Earth.



a



b

Figure 2.17: Images of the cropped TCG virtual outcrop model that is used for the VFT. Figure 2.17a is a map view of the model and Figure 2.17b is an oblique view of the model.

2.3.5 Survey 5 - *The Florida Mountains, Deming, New Mexico*

Survey 5 was planned and flown with the intention of creating a high-resolution large scale virtual outcrop model for Historical Geology students at the University of Houston. The survey flight plan was created based on satellite imagery on google earth overlaid with a geologic map created by De los Santos et al., 2018 (Fig. 2.18a). The planned area within the Florida Mountains was in the Capitol Dome region and included a wide age range of geologic units, largely dipping beds, and small dikes throughout the area. The survey in total took two days, composed of 10 separate flights to encompass the full area (Fig. 2.18b). Each survey was flown in accordance with the contours of the high relief area ranging from 40-60 meters above the ground from its take off location. The surveys were made to be very narrow to accommodate for the high relief (Fig. 2.4). The virtual outcrop model created has high resolution, allowing for students to see features down to 10 cm in size, even in shadows (Fig. 2.19). The protruding stratigraphic units can be seen and interpreted very well from close (Fig. 2.20a) and far (Fig. 2.20b).

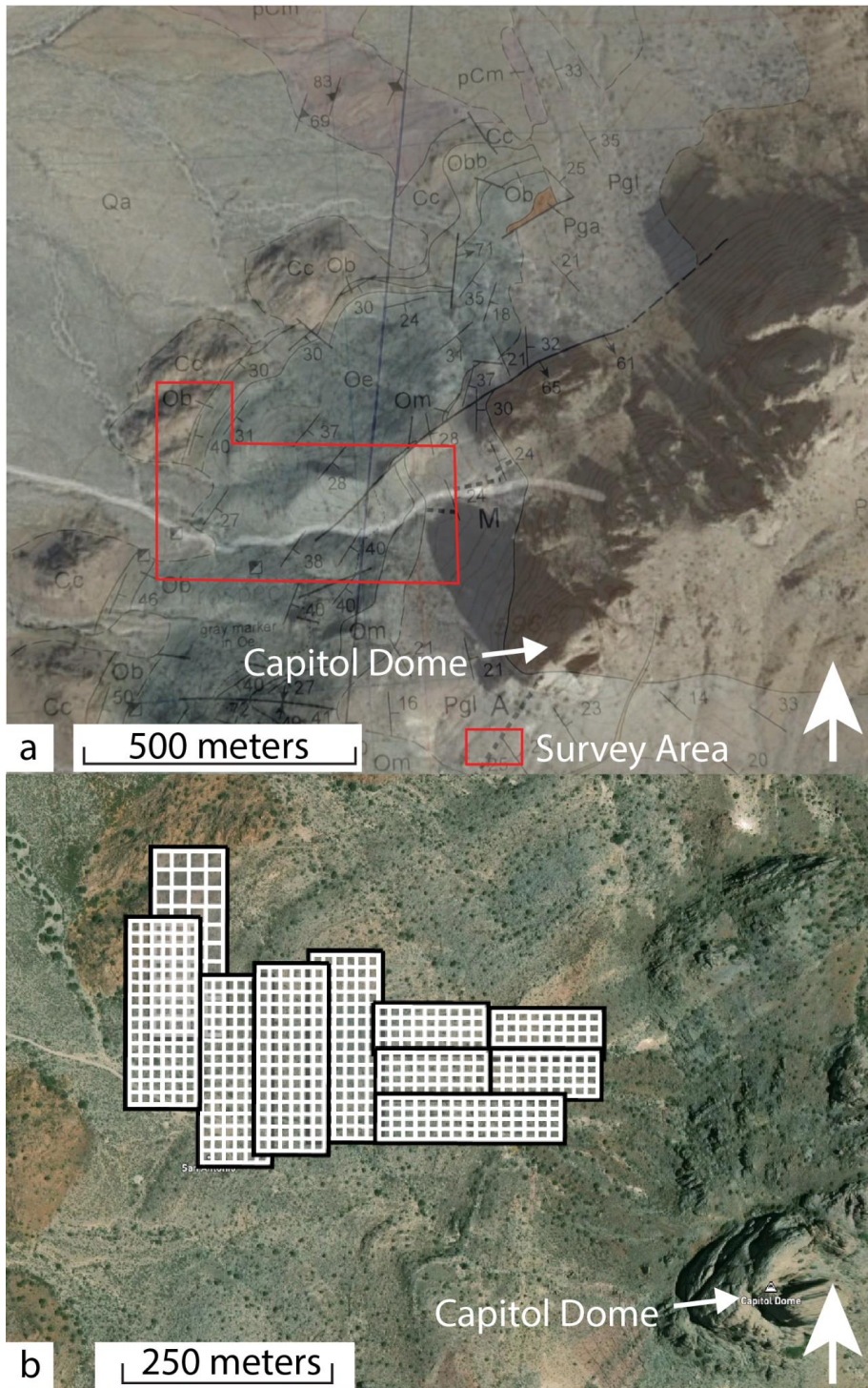


Figure 2.18: Map view images of the Capitol Dome region. Figure 2.18a shows a geologic map from De los Santos et al. (2018) overlaid onto a satellite image of the area from Google Earth. The red box is the area that the full survey covered. Figure 2.18b shows the flight plans for each individual survey flown. The grids in each box are the flight paths that automatically populate when creating the survey in Pix4DMapper.



Figure 2.19: Oblique image of a ridge in the Florida Mountains model. The high resolution can be seen in both where there are no shadows and where there are.



Figure 2.20: Oblique images of the lower section of the Florida Mountain model. Figure 2.20a is zoomed in on a section of the model that is also visible in Figure 2.20b. Figure 2.20a demonstrates the high-resolution potential of the model and Figure 2.20b show what the model looks like when zoomed out.

2.4 Virtual Field Trip (VFT) Development

2.4.1 Conceptual Model VFT 'Methoda Fields'

A conceptual model VFT 'Methoda Fields' was first developed to assist in learning the operations of the VFT and to be a bridge between classroom learning and virtual outcrop learning (Fig 2.21). For this project, the conceptual model was made in Blender, an open-source 3D design program with several advanced capabilities (Blender, 2021). The model is designed to be a simple dipping structure with distinct differential erosion, linear bedding planes, and a dried riverbed which has cut through perpendicular to the strike of the beds (Fig. 2.21). Along with this, a side view of the model allows for the student to see what the area would look like as a cross section (Figure 2.21).

The conceptual model is designed to walk the student through the game functions, such as how to move, take strike and dip measurements, and fly around the area, as well as introduce them to simple geologic concepts that will be experienced/seen on the TCG model (Appendix). While there are several critical things the student learns, one of the most basic, yet difficult concepts are how the strike and dip of a lithologic unit correlates from a 3D surface to a 2D map. This virtual model allows for a student to draw the symbol on the unit while in 3D view, and then view their drawing in map view, illustrating how the two are related (Fig. 2.22).

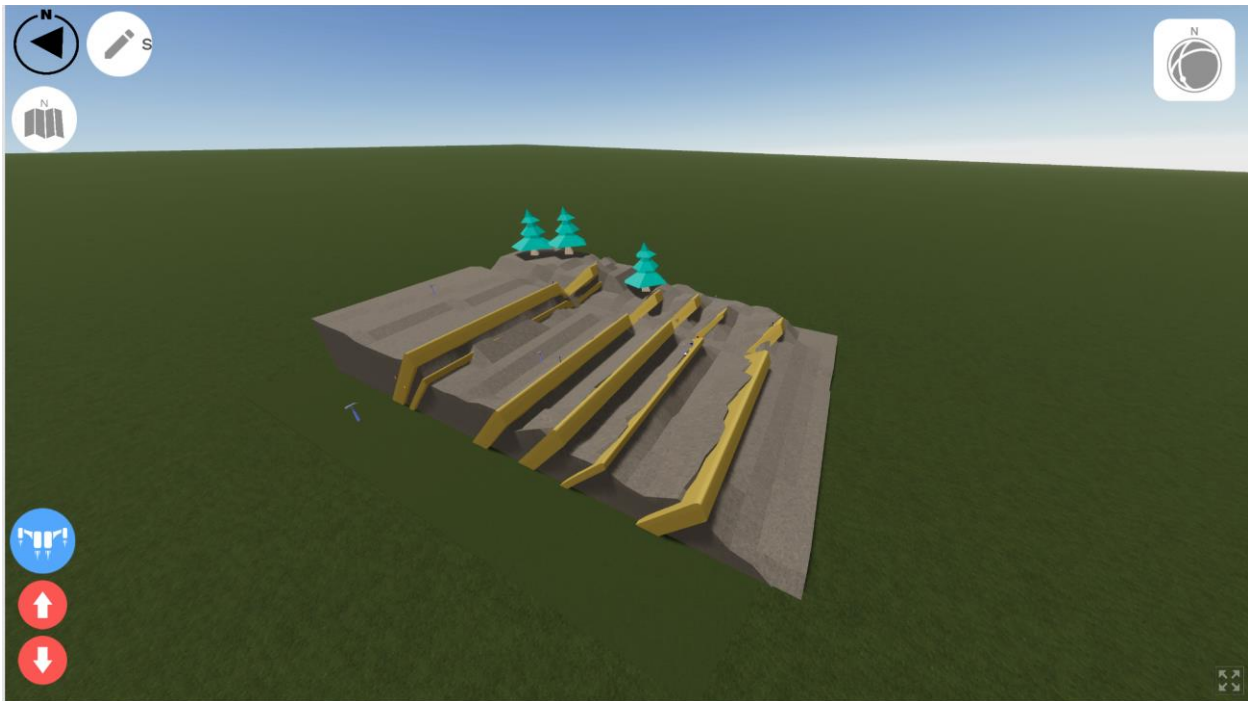


Figure 2.21: Oblique image of the conceptual model portion of the virtual field trip. The outcrop can be seen to have strong dipping units as well as soft eroded away units. The model also contains a channel cut and vegetation to make the model more realistic.

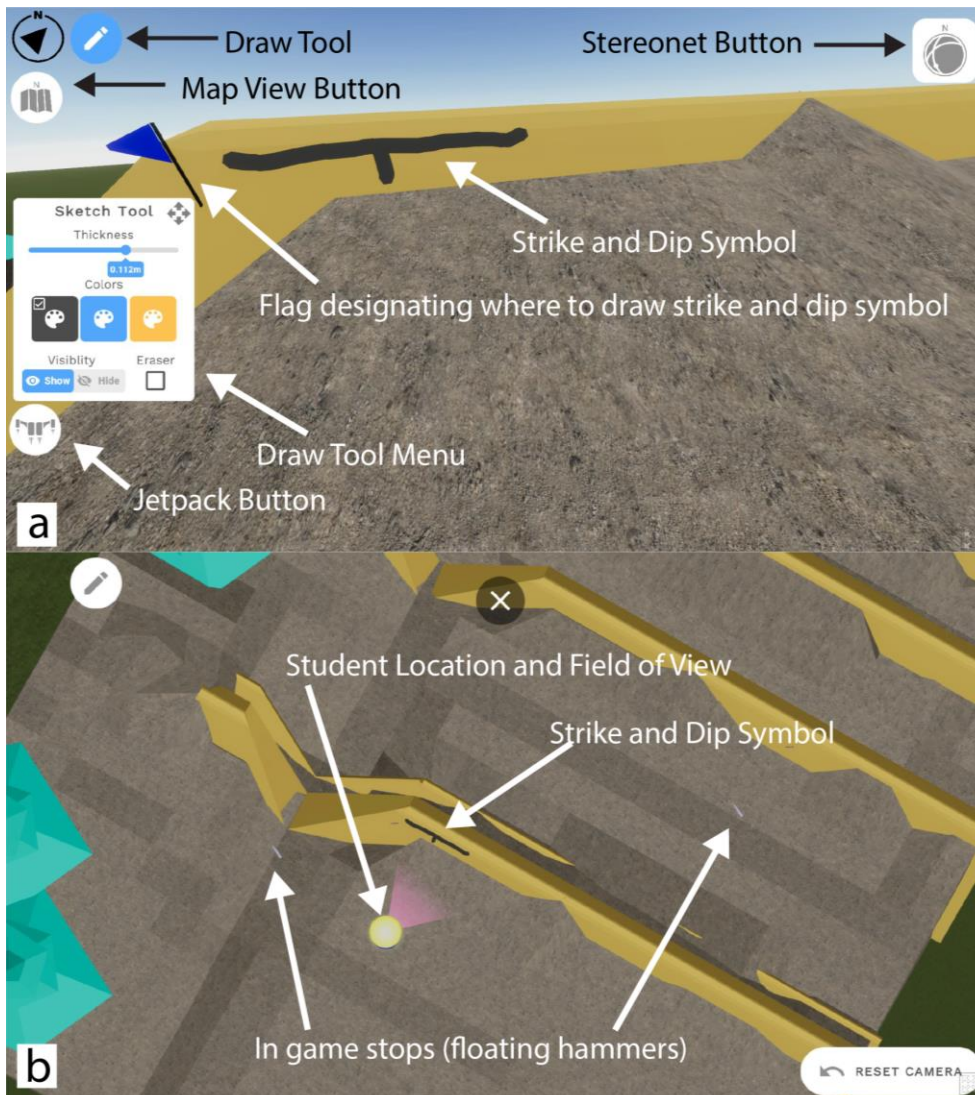


Figure 2.22: Image showing the correlation between drawing a strike and dip symbol on the model in first person view (Fig. 2.22a) and what this looks like when switched to 'Map View' button (Fig. 2.22b). The figure includes labeled 'Draw Tool,' Map View Button, Stereonet Button, and Jetpack Button.

2.4.2 Real-world VFT 'Taylor Creek Group'

The Taylor Creek Group (TCG) VFT was created to demonstrate the full potential of the video-game-like field trip. The full assignment includes both a virtual and written part (Appendix). The written portion of the assignment corresponds with the numbered stops that are spread throughout the TCG outcrop (Appendix), and during their

exploration of the outcrop, students are asked to fill out a geologic map with bedding surfaces and strike and dip symbols. Each stop was made with a specific topic in mind for the students to learn. The stops in the assignment are not designed to have to be done in any specific order, each stop is described in detail in the Appendix at the end of this study.

The first goal of the real-world outcrop is to give students the feeling of what it is like to look at a large outcrop in the field, obstructed views, having the walk the full model to understand what is happening while making stops to take measurements and other notes, and the lack of an aerial view of the area. Because of these goals, the jetpack button and map view are turned off for the first part of the TCG assignment. It is in this mode that students are expected to 'walk' the entire outcrop and stop at all of the floating hammers.

When a student first loads into the game, they are spawned between two ridges that obstruct their view of the full outcrop (Fig. 2.23). From here the students are expected to wander the outcrop and stop at a hammer when they find one. There are a total of 11 stops for the students to find. While the stops are numbered 1-11 they students do not have to follow this order and can fill out the assignment in the order they find the hammers.

Stop 3 is located next to a large, dipping rock layer that the students can take a good strike and dip measurement. Along with the stop telling them to take the strike and dip, the stop also includes information on the types of rocks found in the area and a picture of the rocks (Fig. 2.24). Stop 4 and Stop 8 work together to help students understand the structure of the outcrop. If the student walks the ridge between these

two stops, they will notice it is the same bed of rock that folds and changes strike (Fig. 2.25). Other stops are included to teach generic geology knowledge about vegetation patterns that can hint at geologic information of the area (Fig. 2.26). In many cases, even at great resolution, the virtual outcrop model may not show specific features you want them to see, so stops can be added at these locations and pictures can be put with these stops to allow students to see these smaller features or for them to be asked critical questions about what is there. This is done at Stop 9 (Fig. 2.27).

After the students have completed all the stops and their geologic map, they are asked to describe what they think the structure of the area is and the geologic story behind its formation.

Once they have done this, they can be given access to the final part of the assignment. This final part allows them access to the jetpack and map view of the area. The written portion asks the students if the new aerial news of the outcrop helps them understand the area better, and if they had interpreted the outcrop correctly before being given this ability.

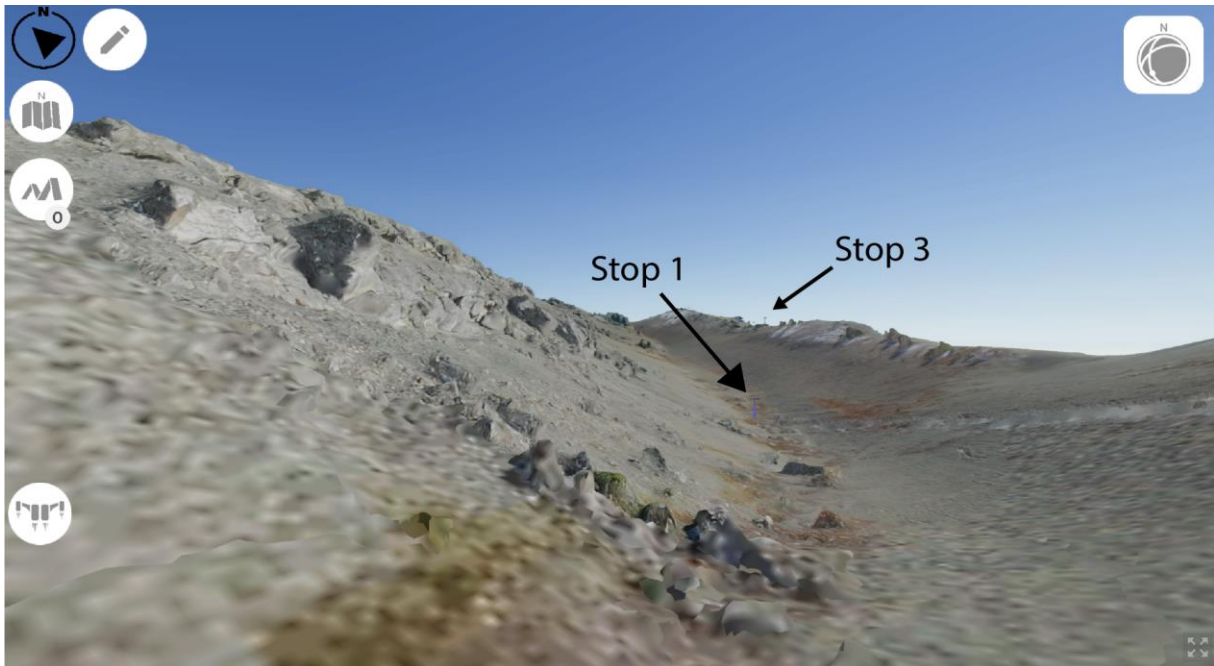
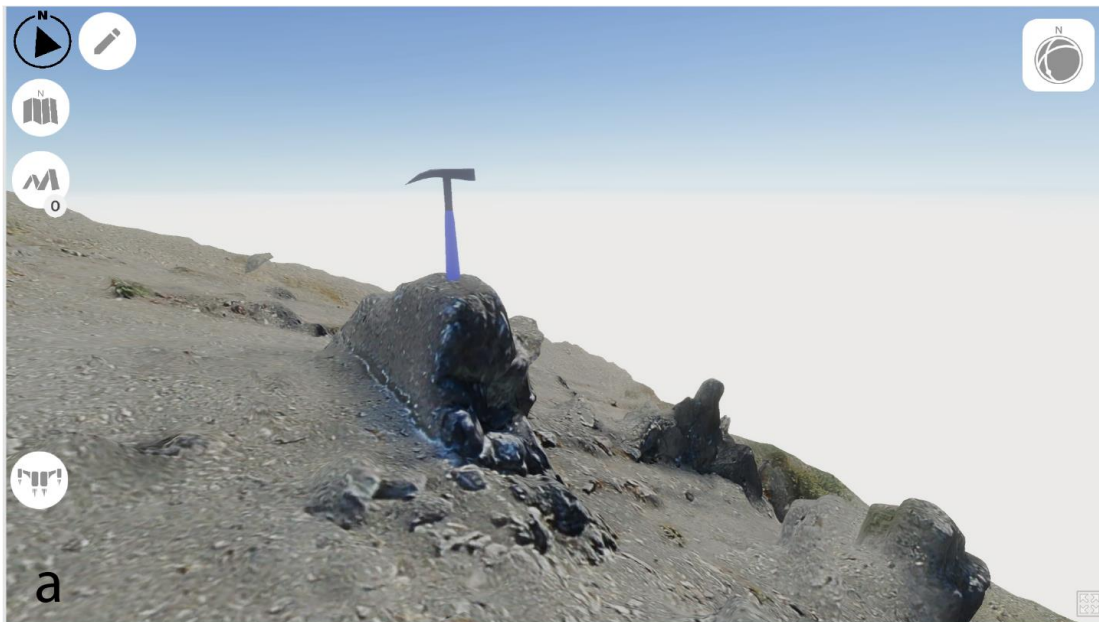


Figure 2.23: Image of where the student spawns into the VFT. Stop 1 and Stop 3 are visible from this location and Stop 2 is located over the ridge to the right.



Stop 3

Measure the strike and dip.

What makes this location good for taking a strike and dip? How do we know which face to measure on? In other words, what are some indicators we can use that help us decide which side is the correct bedding plane? (Hint: this was covered in part 1)

This image was not taken at this location, but is a good visualization of what the rocks looked like. This bed is a large clast conglomerate rock with interbedded sands as well as some igneous boulders spread throughout the unit. The ridge forming units in this area are all the same lithology as what is imaged here.

What may have been the depositional environment of a unit such as this one? (deep marine, shallow marine, deltaic, desert, etc.)



Figure 2.24: Images of Stop 3. Figure 2.24a is what the stop looks like before the student clicks on the hammer. Figure 2.24b is what the screen looks like once the student clicks on the hammer. This screen includes the questions that need to be answered from the written portion of the assignment as well as a description of the rocks present in the outcrop.

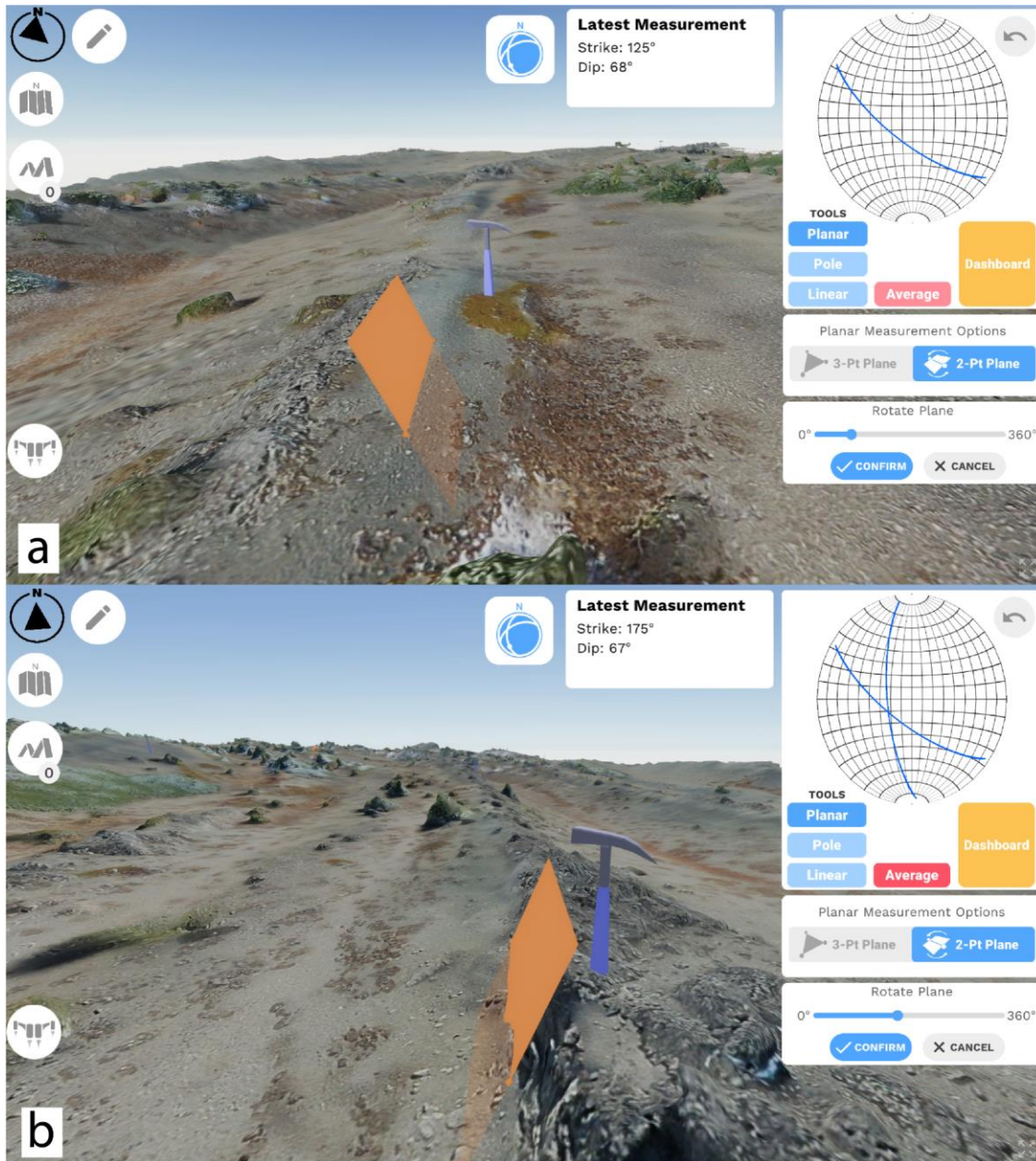
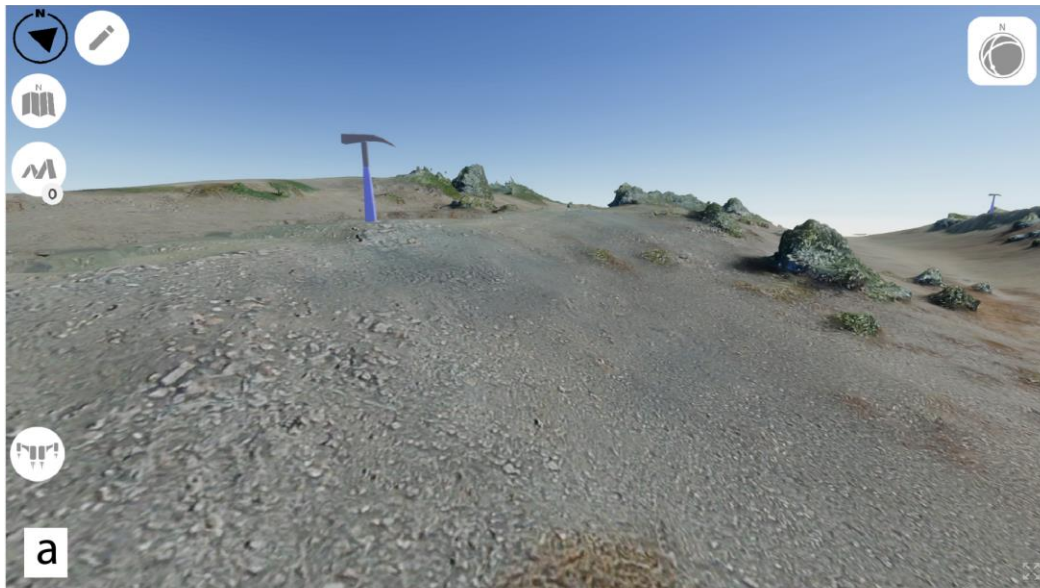


Figure 2.25: Images from two stops in the VFT. Figure 3.25a is at Stop 4, where the student is asked what the strike of the unit is. Figure 3.25b is at Stop 8, where the student is asked to measure the strike of the unit and compare it to Stop 4. The figures show a change in strike of the unit.



Figure 2.26: Image of vegetation along a small ridge at Stop 10. The vegetation does not have high resolution but can be seen to follow the ridge.



Stop 9 ✕

These images were taken at this location. What you are looking at is a shale with iron concretions. The hard iron concretions erode significantly slower than the shale, causing it to stick out of the bed much like a harder lithologic bed would, but these are individual pieces of rock. This creates linear patterns throughout the shale where the concretions have been eroded out but remain in the pattern they were deposited in. Would this deposition likely be marine or terrigenous in origin?




Figure 2.27: Image of Stop 9 in the VFT. Figure 2.27a is what the stop looks like before the hammer is clicked. Figure 2.27b is what the screen looks like after the stop is clicked. The stop includes images of the exact same location as in the real outcrop.

2.5 Discussion: Comparison to Previous UAV Studies

Acquisition of data through photogrammetry for virtual outcrop models has been noted to be extremely useful in doing large scale structural and stratigraphic analysis (Chesley et al., 2017; Nieminski and Graham, 2017; Nesbit et al., 2018; Hird et al., 2017; Mlambo et al., 2017; Bemis et al., 2014; Viana et al., 2018; Bistacchi et al., 2015,

Lambert, 2016, Uzkeđa et al., 2022). The methods used by many of these studies differ in their intentions of use for the model. To create and present a virtual outcrop model to students to learn from, a variety of criteria needs to be met to ensure a smooth learning process where the students can walk on the models and see the structures and stratigraphy at high resolution.

Nesbit et al. (2018) discusses the use of fixed wing UAV surveys being used to create a large-scale model to analyze the stratigraphy of fluvial deposits in southeastern Alberta, Canada in a study area that is 0.52 km² (520,000 m²). The methods used by this paper would be largely impractical for this study because of two things, the size of the study area and the resolution needed for the model's application. Survey planning and acquisition between a fixed wing drone and a quadcopter are very different, as can be seen in Nesbit et al. (2018), where the flight is programmed in a two-part fashion at high elevations to ensure optimal coverage. The problem with this large-scale coverage is a loss in potential resolution of the outcrop model. For a stratigraphic analysis such as the one employed in the Nesbit et al (2018) study, the obtained resolution is good. The problem arises zooming into the model and the stratigraphy begins to blur and be very difficult to see, this is not good if the model were to be used for a virtual field trip, where a student walks on the surface of the model.

Other studies, such as Viana et al. (2018) use structure from motion - multi view stereo to image a small road outcrop from a single location. While this method worked very well for viewing and analyzing the dikes in the outcrop, images taken from one location will not generate a high-quality 3D model that students can walk around virtually.

Lambert (2016) follows a very similar acquisition workflow to the one used in this study, but differs from our study in the survey flight path flown by their drone. Lambert (2016) surveys an outcrop with the camera 90 degrees off nadir (perpendicular to the ground), creating a virtual 2D map instead of a 3D model. The map created is great for digital elevation modeling and dip analysis of the beds, but the model created cannot be made into a 3D model because of its lack in dimensionality.

Uzkeda et al. (2022) presents a variety of methods in creating virtual outcrops, including a large-scale drone survey for structural analysis of a high relief folded structure. The model shown is from the Cantabrian Mountains, which is part of a foreland fold and thrust belt (Julivert et al., 1972). Model locations such as this one are perfect to develop a potential VFT for students, but the structure will need to be imaged by significantly closer surveys to ensure the best resolution for up close interpretation.

2.6 Conclusion

Results and discussion presented in this study encourage educators to take the opportunity to create virtual field trips through the creation of virtual outcrop models. Large scale virtual outcrop models can be used in an academic setting, and it creates the opportunity for students to see amazing geologic structures in places where access to these areas are extremely limited. The creation of these virtual field trips (VFT) needs to have several considerations to ensure its smooth acquisition to creation.

- Model selection is critical in finding large well exposed outcrops with uncomplicated terrain to make survey pre-flight plans. The optimal outcrop has limited vegetation and distinct protruding geologic beds and

other geologic features such as dykes, channels, etc. The terrain can be a mixture of dipping and flat terrain, but issues will arise if the outcrop has vertical walls and lateral extents to the outcrop as well.

- Survey plans need to be adjusted to the terrain style of each outcrop. This includes carefully selected camera angles, height, size, and shape of survey. Plan the survey during the time of year with the smallest chance of bad weather during flight and cloud coverage and movement is limited to ensure a smooth model without random shadows.
- A limiting factor of how well resolved a model can be is the size of file required to create a large model with high resolution.
- When exporting a model with the intention of putting it in Unity software, be sure to export it with only one texture for the whole model to limit complications when creating the virtual field trip.
- Create several stops throughout the VFT that walk the student through the process of how to interpret the geology of the area. The order of the stops is not critical, but they need to tie to one another and build the students' knowledge of the area.
- Use conceptual models to introduce the virtual field trip game functions and specific geologic features to watch for that will help on the real model.

Chapter 3: Structural Analysis of the Dongying Depression, Bohai Bay Basin, China

3.1 Introduction

The Dongying Depression is located in southeastern Bohai Bay Basin, in eastern China (Fig. 3.1). The Dongying Depression is of interest because of its large petroleum prospects with an area which contains the second largest oil field in China exceeding 800 MMBOE in place (Li, 2003). The petroleum prospectivity has driven this area to be well imaged through 3D seismic data. This area has been studied for many years, but questions still remain on fault growth histories (e.g. Chen et al., 2017). One reason is that the faults play a critical role in sealing or migration of hydrocarbons based on their formation and termination timing (Lampe et al., 2012). Other studies have also attempted to relate the fault histories to changes in Pacific plate motions (Fig. 3.2) (Liang et al. 2016).

In this project we interpret 2D transects across the Dongying Depression from a recent industry 3D seismic dataset (Fig. 3.3). The aim of this study is to deduce the history of structural deformation that has shaped the area. The approach will consist of: 1) a stratigraphic analysis of growth and erosional features; 2) a structural analysis of basin evolution from fault geometries and styles; 3) proposing a tectonostratigraphic evolution from the analyses in this study.

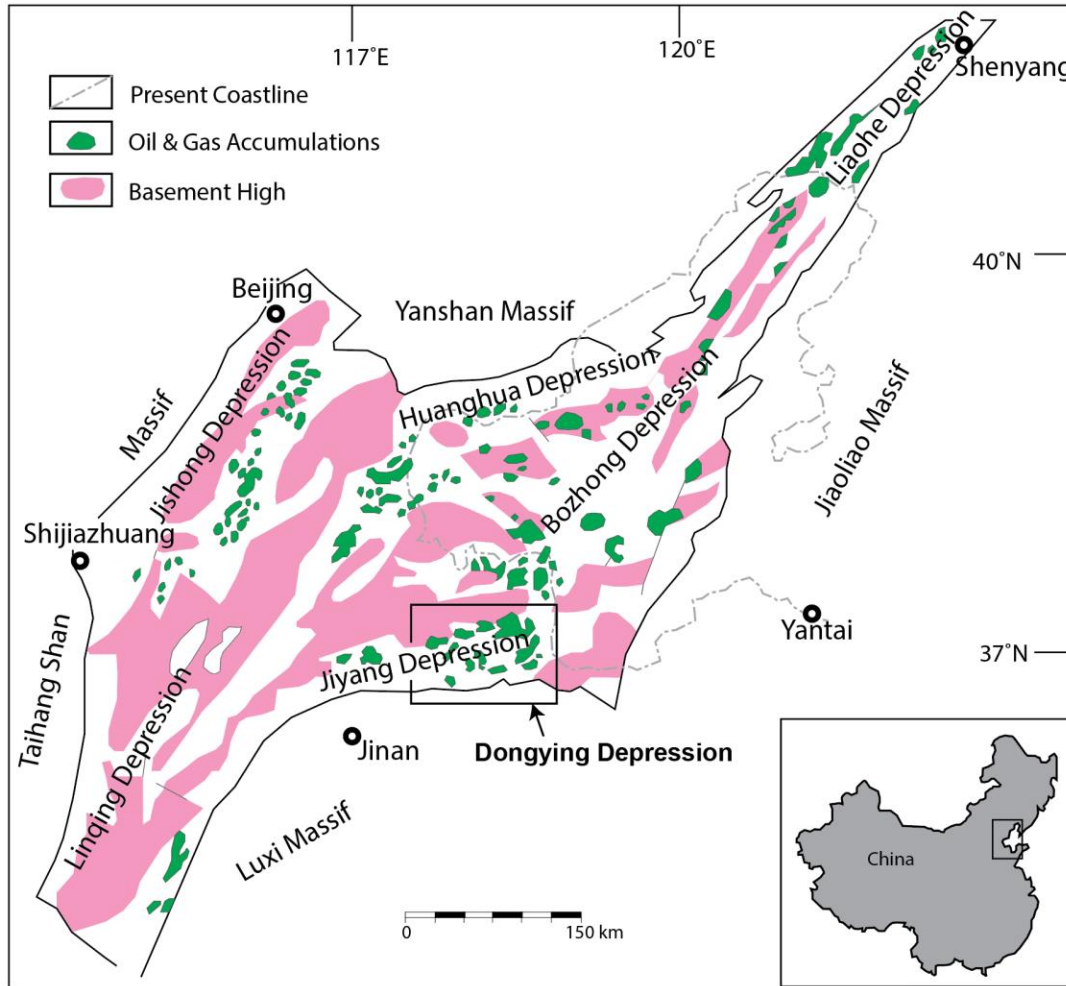


Figure 3.1: Tectonic map of the Bohai Bay basin, eastern China, showing the basin extent, petroleum accumulations and basement uplift locations (redrawn after Lampe et al., 2012.). This study focuses on the Dongying Depression, a petroleum-rich region that is located along the southeastern margin of the Bohai Bay Basin.

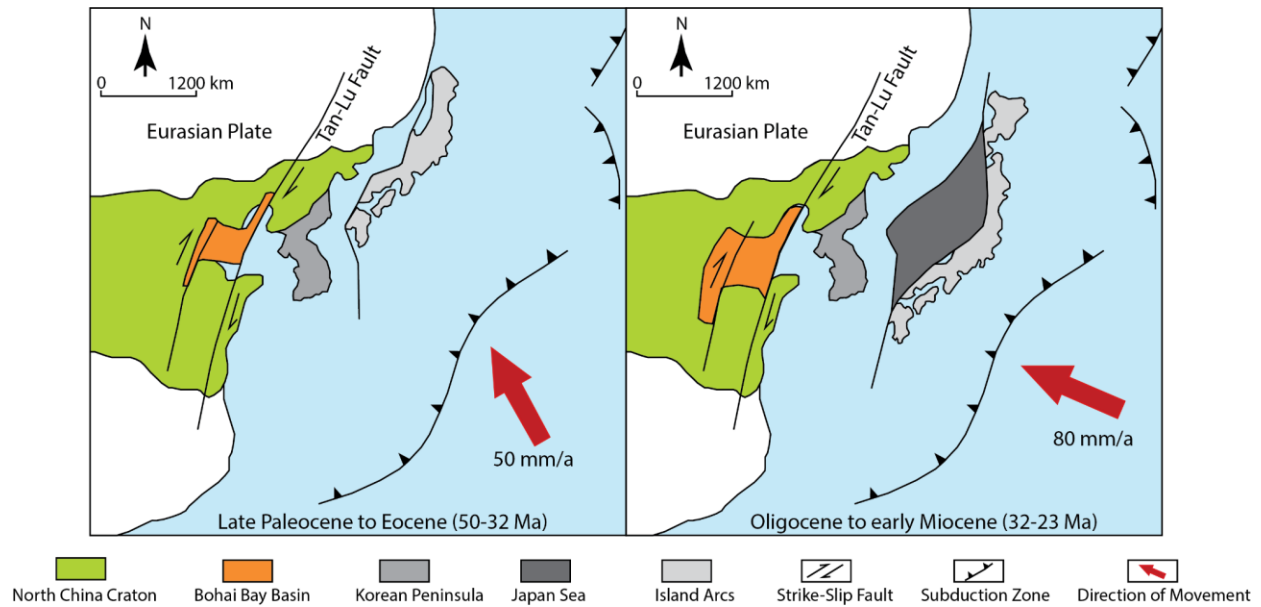


Figure 3.2: Regional plate tectonic history of Bohai Bay Basin, eastern China, showing two distinct phases of Pacific Plate subduction that is attributed to the multistage structural formations of the basin (redrawn after Liang et al. 2016). The shift from an extensional dominated system to a transtensional dominated system ~32 Ma is determined to have been caused by this shift in subduction direction and speed.

3.2 Geologic Setting

3.2.1 Structural Setting

The Dongying Depression is a Paleogene rifting basin that has undergone three tectonic phases since the end of the Cretaceous that include an extensional structural system, a transtensional system, and lastly, thermal subsidence (Chen et al., 2017).

The timeline of basin formation can be divided into three periods: a series of small, isolated basins developed along a major fault during a late Mesozoic to Paleocene rift stage, then from Eocene to the Oligocene, grabens forming synrift, and the last stage is from the Miocene to present day and is considered to be 'post rift' thermal subsidence (Lampe et al., 2012).

There are several faults that occur within the basin that allow for petroleum

migration or that act like seals. Lampe et al. (2012) includes three types of faults for migration in his model: main graben faults, secondary graben faults, and lithology dependent faults. His model also includes four fault scenarios for petroleum distribution: closed faults, open faults, no faults, and assigned faults (Lampe et al., 2012).

Tectonically this area has been tied to the subduction of the Pacific Plate (Fig. 3.2). Some studies suggest the Pacific Plate movement had been consistently moving north-northwest until the Miocene when it changed to a near-westwards motion (Bao et al., 2013). It is speculated that the migration of the Bohai Bay Basin depocenters are controlled by Pacific Plate subduction in terms of both evolution rate and direction. Furthermore, the migration direction of the Bohai Bay Basin depocenters is consistent with the direction of Pacific Plate subduction (Liang et al., 2016). It was concluded that the driving force of the extensional deformation originated from upwelling of the hot mantle due to the subduction of the Pacific Plate (Qi and Yang, 2010

3.2.2 Stratigraphy

The Dongying Depression developed in the early Tertiary and features individual depocenters of lacustrine sedimentation. The Paleogene consists of three formations: the Paleocene Kongdian Formation, the Eocene to Oligocene Shahejie Formation, which includes the main petroleum source rocks in the study area, and the Oligocene Dongying Formation (Fig. 3.4).

The sedimentary cycle with each formation follows this order: alluvial fan deposits, fluvial deposits, coastal lake deposits, shallow to deep lake deposits, ephemeral lake and river deposits, delta-plain deposits, and marsh deposits (Chen et al., 1984). The hydrocarbon accumulations in the depression are sourced from and

mostly accumulated in the Shahejie stratigraphy. The extreme faulting in the region has made understanding migration pathways very difficult. The depression consists of three petroleum systems which contribute to seven reservoir layers (Lampe et al., 2012).

3.3 Methods and Data

3.3.1 Dataset

Data Given

- 2D raster images of 13 N-S lines and 7 E-W lines from 3D seismic data
- Company stratigraphy as a regional framework
 - Seven horizons constrained by wells and biostratigraphy
 - Some misties
- Time depth curve for depth conversion

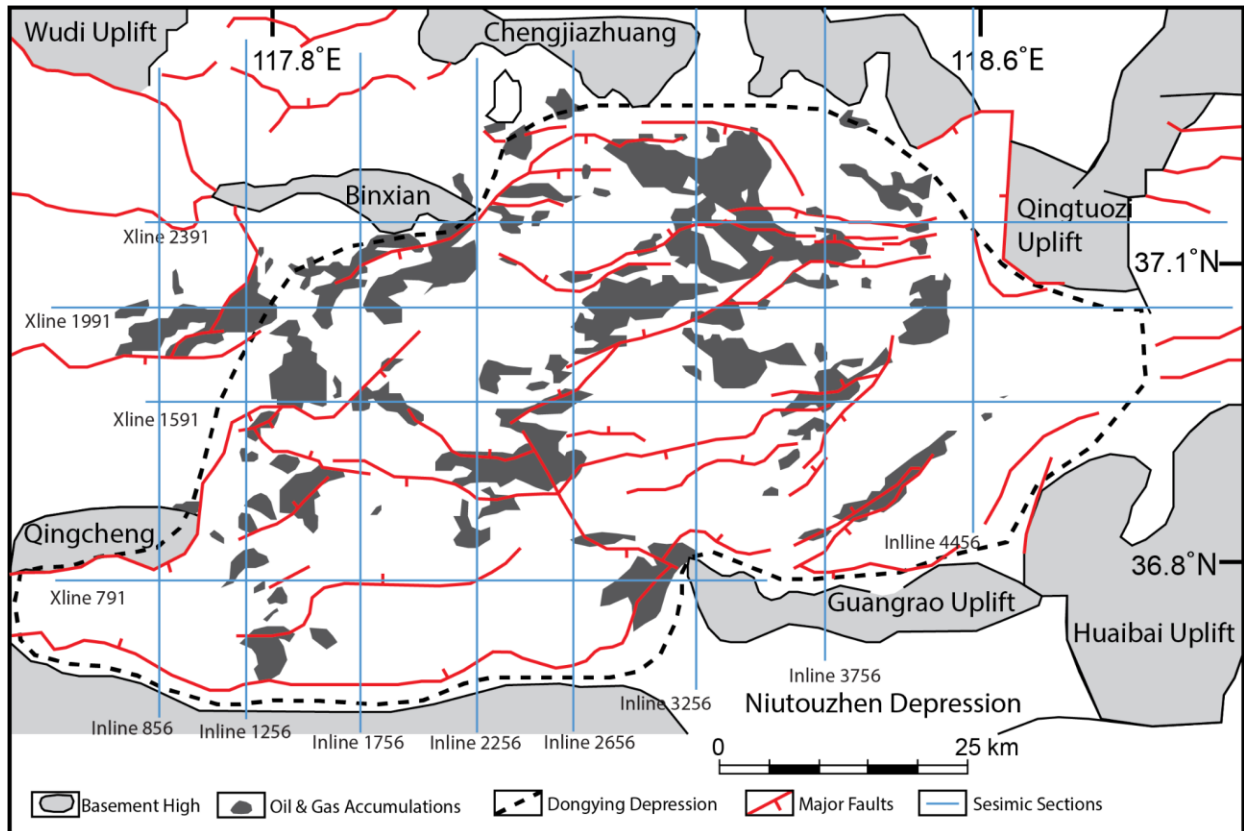


Figure 3.3: Basemap of the Dongying Depression showing the depression extent, petroleum accumulations, basement uplifts, and general locations of the interpreted seismic lines of this study (Basemap modified from Lampe et al. 2012).

The area of the 3D seismic data set covers an area of 1600 km². There has been data collected from 112 wells along with photos of drill cores from 20 different wells. The data includes a proprietary sequence stratigraphic framework developed from petroleum geoscience data which included 7 horizons ranging from the Kongdian - Shahejie contact at 50.4 Ma to the Dongying - Guantao Contact at 24 Ma. No fault interpretation was included in the dataset. The data set consists of 13 inlines spread across the Dongying Depression, 8 of which are shown in Figure 3.4.

The north-south and east-west transects form a grid across the depression with several kilometers between each transect. Because of the large distance between the

transects, correlation of faults and other geologic structures between is overly challenging and thus we rely on maps from previous studies (i.e. fault map in Fig. 3.3) to fill data gaps.

3.4 Results

3.4.1 Seismic stratigraphy

The final three stages of the tectonic evolution of the basin, based on previous studies (Chen et al., 2017), is represented in the company stratigraphy as follows: extensional growth after the Cretaceous to the base of T6, transtensional growth between horizons T6-T1, and thermal subsidence growth above T1 (Fig. 3.4).

From the given data, a seismostratigraphic column was created outwards and revised from the company stratigraphy to visualize the company stratigraphy and additional growth in the region juxtaposed to the changing tectonics (Chen et al., 2017) and local and regional unconformities (from this study) (Fig. 3.4). Additional horizons were added into the interpretation of the seismic to understand growth patterns and to map out other structures (Figure 3.8f and 3.8g). Among the additional horizons interpreted are stratigraphic beds from the Cretaceous, the Kongdian (Tr), and growth strata that does not have a specific age tied to it (Fig. 3.4). The growth strata is represented by a single color but is used to represent growth any time after the Kongdian-Shahejie contact (Figs. 3.8c, 3.8g, 3.8h). Given the scope of this research, the interpreted Cretaceous and Kongdian horizons are meant as a reference point and are not precisely interpreted, but instead represent the general trend of the deep horizons that have distinct features that separate it from the overlying strata (Figure 3.8f). The key indicators of the different aged deep horizons are distinct angular

unconformities that indicate the transition between the different deformation periods (Figure 3.8f).

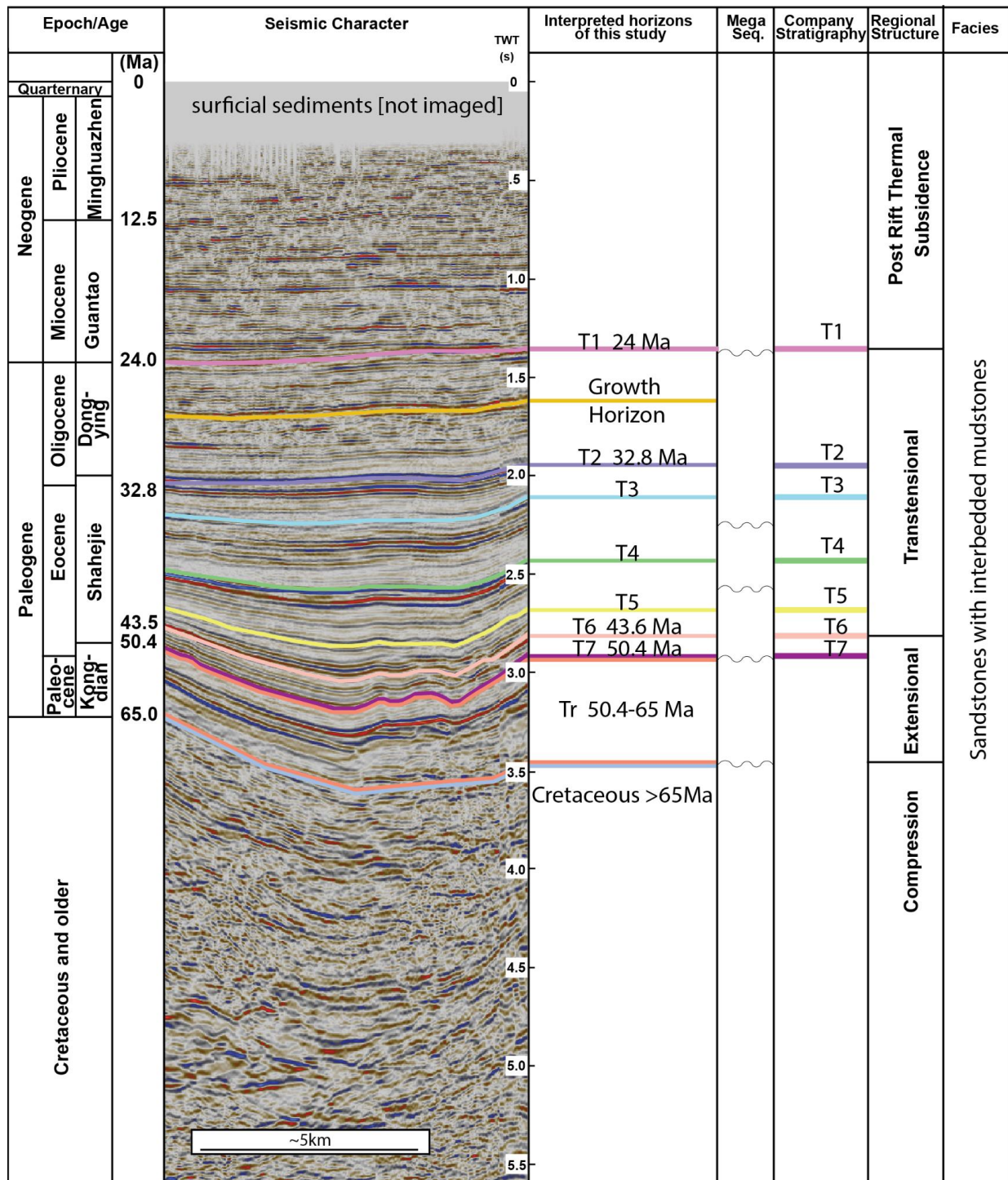
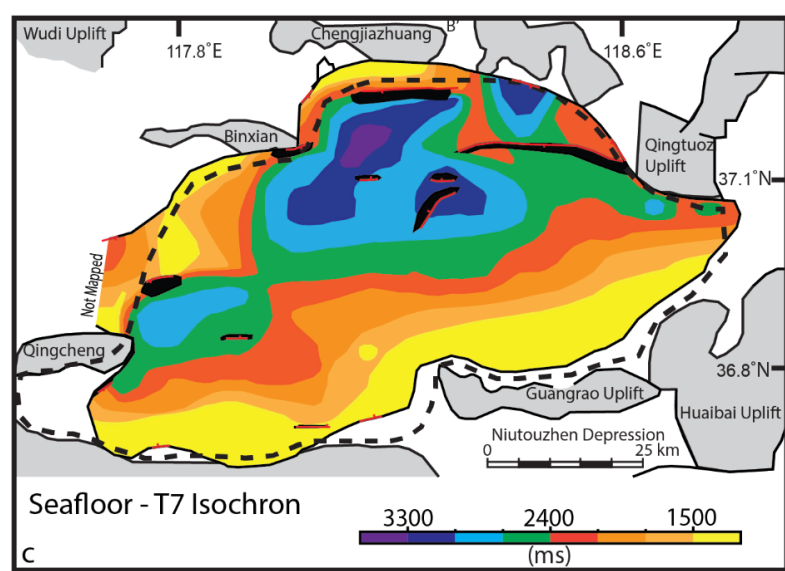
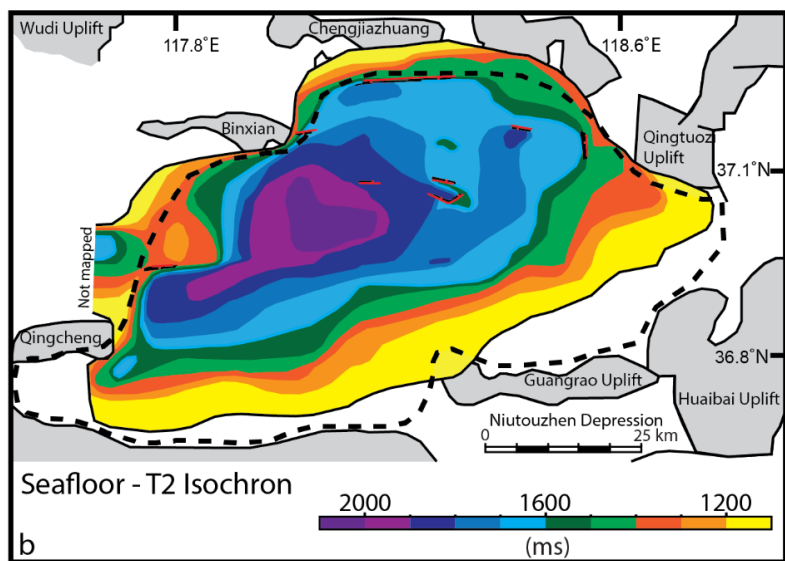
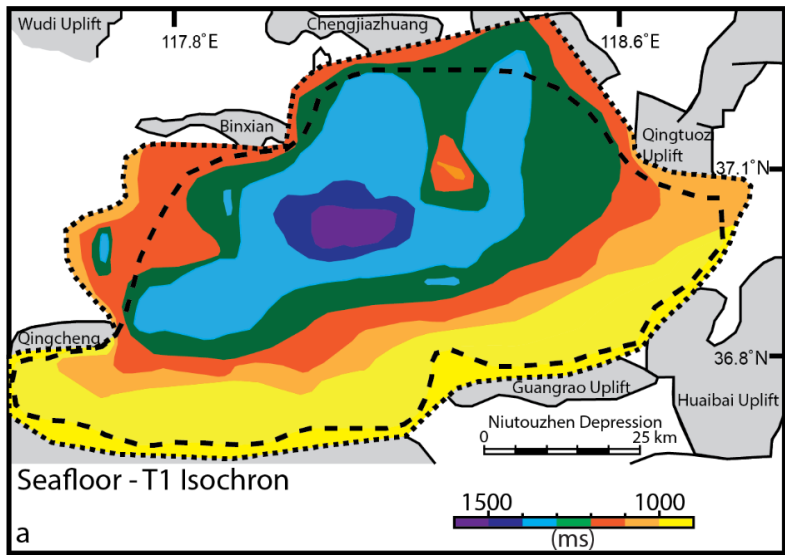


Figure 3.4: Seismostratigraphic column created based on the results from this study showing given company stratigraphy name and age interpreted on a seismic cross section from the given data, the relation of the stratigraphy with regional tectonics, and a simple overview of lithologies. Tr represents all of the deposition during the Kongdian.

Three isochron maps were made to analyze the basin fill patterns in the depression. The depths were determined based on the different tectonic changes that were occurring through time at this location. Looking at the seafloor to T7 isochron (Fig. 3.5a), the deposition is found dominantly in the north-northeastern portion of the basin where the half graben structures were forming. This is also at a depth where faulting has displaced the beds significantly. In the seafloor to T2 isochron (Fig. 3.5b), the depositional center of the depression can be seen to have distinctly migrated southwest to a more west-central location in the basin, which is an indication of a shift in where faults were growing. The depocenter in the seafloor to T1 Isochron (Fig. 3.5a) shifts slightly southeastern to a more centralized location in the depression. The area of deposition is also significantly more spread out than seen in the previous two figures, illustrating a shift to a less localized and more regionalized subsidence. Therefore, in general there is a shift of depocenter from North to south from the Early Cenozoic (~ 50 Ma) to present as well as a spreading out of the depocenter (i.e., more widespread subsidence).

Figure 3.5: Isochron maps showing two-way time thickness of three stratigraphic intervals based on results from this study: a) Surface to T1 (0 to 24 Ma); b) Surface to T2 (0 to ~33 Ma); c) Surface to T7 (0 to ~50 Ma). Basemap modified from Lampe et al. (2012).



3.4.2 Regional Tectonostratigraphy

Eight N-S lines (i.e., inlines) and four E-W lines (i.e., xlines) were interpreted to analyze the structural evolution history of the depression as well as understand erosional and fault patterns and characteristics. Figure 3.6 shows two representative transects that show the typical regional half graben structure, high angle normal faulting, fault termination characteristics, and regional unconformities. A 1:1 scale cross section was made (Fig. 3.6) from the time depth curve given in the original data. Figure 3.7 shows the same regional transects as Figure 3.6 at 1:1 scale that allows a more realistic visualization of the geometry of the high angle (~60°) linear normal faults. A single dominant listric normal fault where the majority of early growth occurred is also very evident (Fig. 3.7).

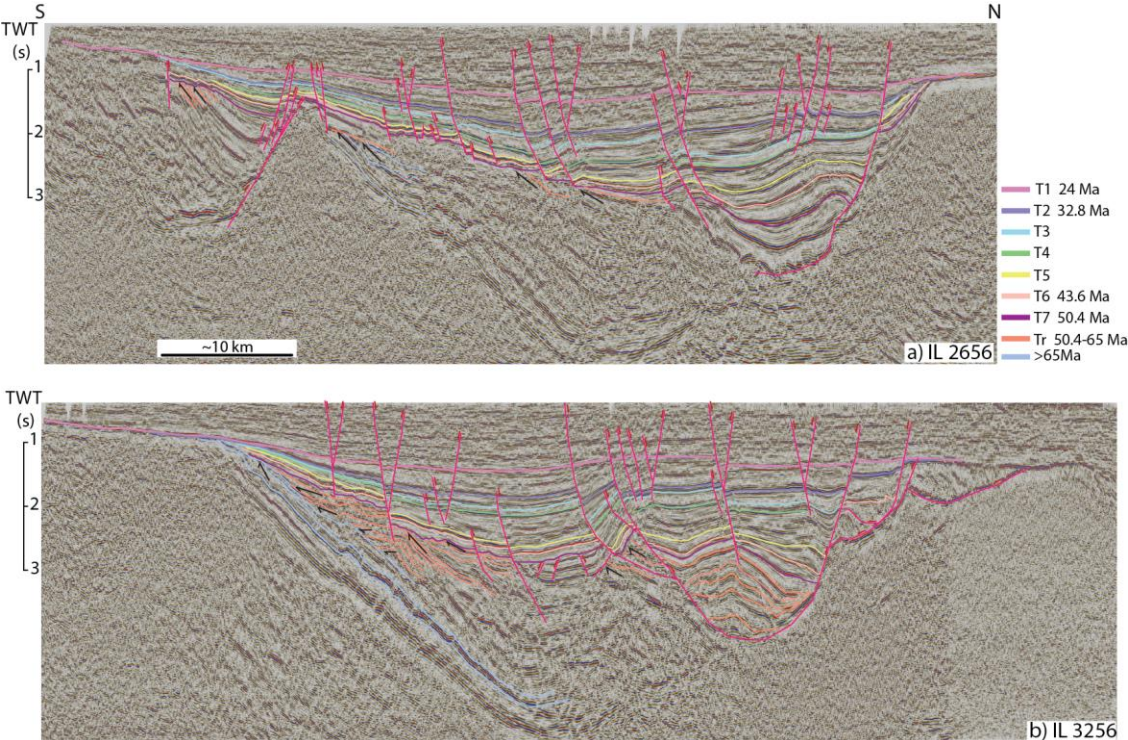


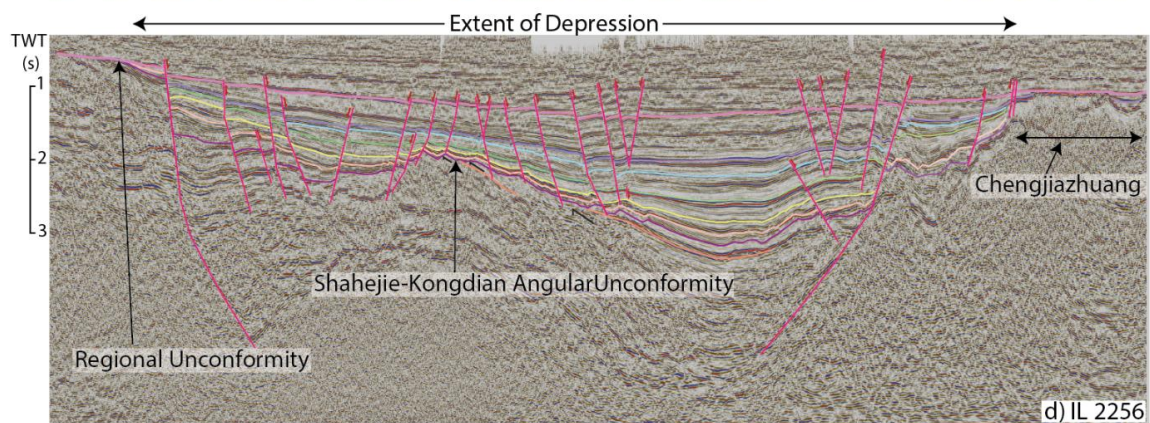
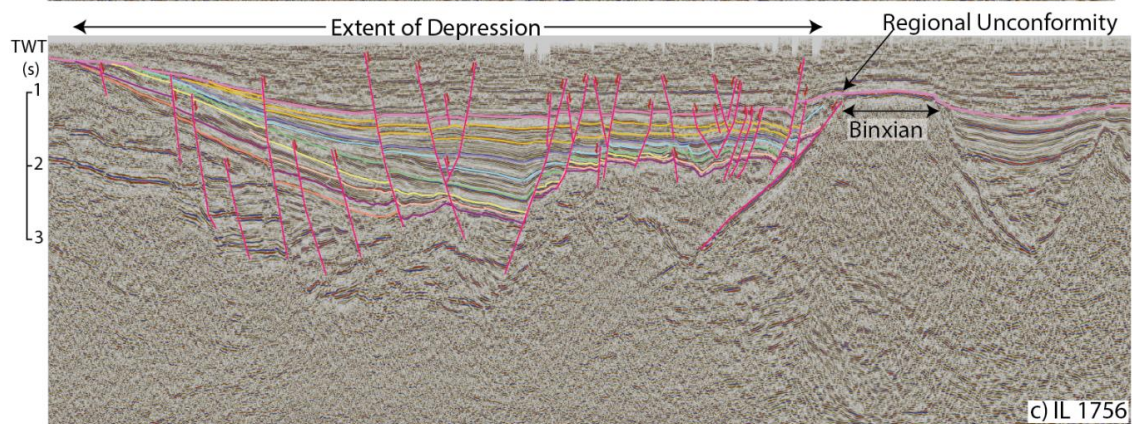
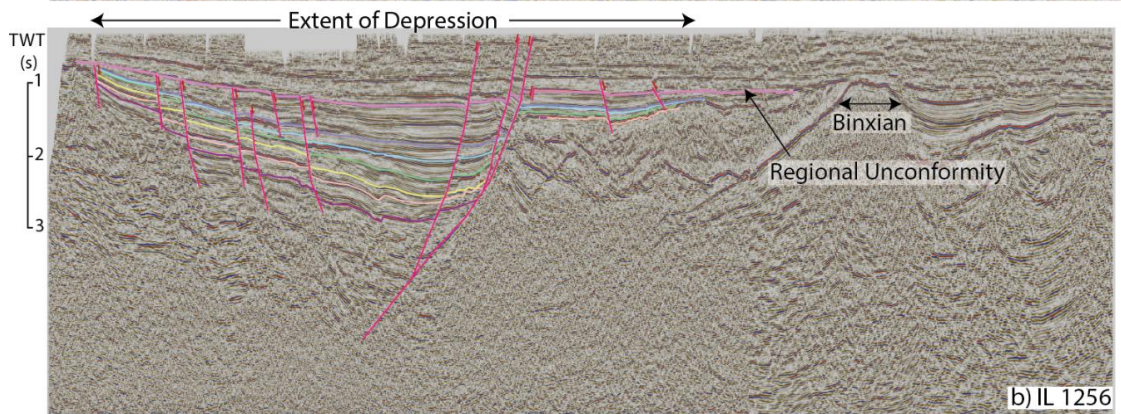
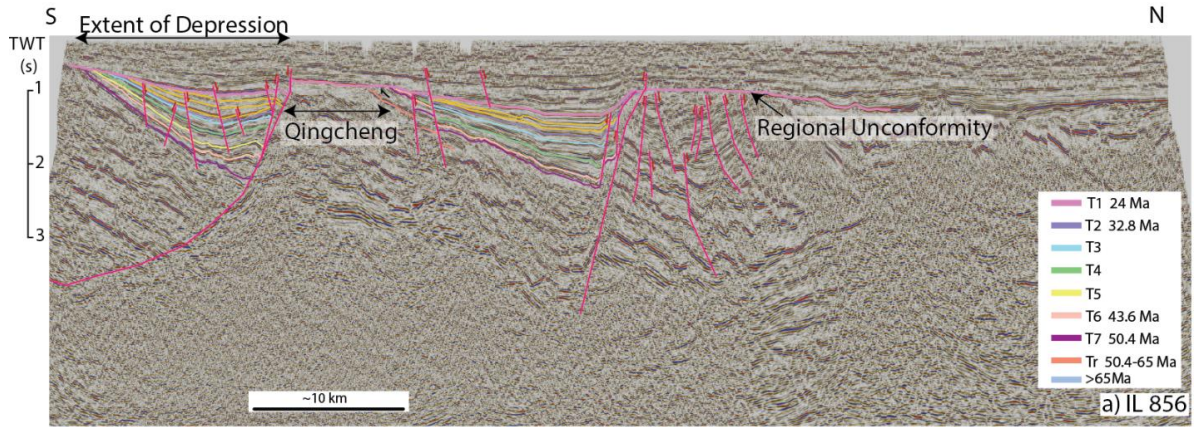
Figure 3.6: Two representative regional seismic transects illustrating the general shape of the depression and the half grabens it is composed of. The transects include interpretations from company stratigraphy (T1-T7) with faults, additional horizons, and stratal terminations added in from this study.

Figure 3.7: Two representative regional seismic transects shown without vertical exaggeration, with an interpreted and uninterpreted version. The transects include interpretations from company stratigraphy (T1-T7) with faults, additional horizons, and stratal terminations added in from this study. Refer to Figure 3.6 for stratigraphy key.



The interpreted N-S lines can be seen in Figure 3.8. Their corresponding uninterpreted version is shown in Figure 3.9. The N-S transects have several characteristic patterns that can be seen throughout the depression. Generally each transect has a dominant south facing listric fault which forms the half graben structure of the depression. Dominantly to the south of three main listric faults is a series of linear synthetic and antithetic growth faults. The north and south borders of the basin are different basement highs which the stratigraphy grows off from the south to the north. A few of the transects have distinctly different features that are not seen everywhere in the depression. Figure 3.8a is the westernmost interpreted transect, where only the southern graben is considered part of the Dongying Depression (Fig. 3.3). The Qingcheng Uplift separates the two half grabens and indicates the end of the depression to the north. Figure 3.8c is the third N-S line from the west and does not have the typical half graben structure. The transect is dominated by synthetic and antithetic faults instead of a single listric fault, causing the depocenter of this transect is shifted south southcentral of the line and migrates north through time. Figures 3.8d and 3.8e are distinct and have two half-grabens in the transect. Each have a larger half graben to the north and a small half graben in the southernmost portion of the depression, but both half grabens do follow the south facing listric fault trend.

Figure 3.8: Interpreted N-S seismic transects at 4x vertical exaggeration showing interpreted seismic horizons with additional older stratigraphy, growth strata, stratal terminations, and faults from this study. All faults interpreted are normal or inverted normal faults. The seismic transects are in order from west to east and consist of areas both inside and outside the Dongying Depression. Location map in Figure 3.3.



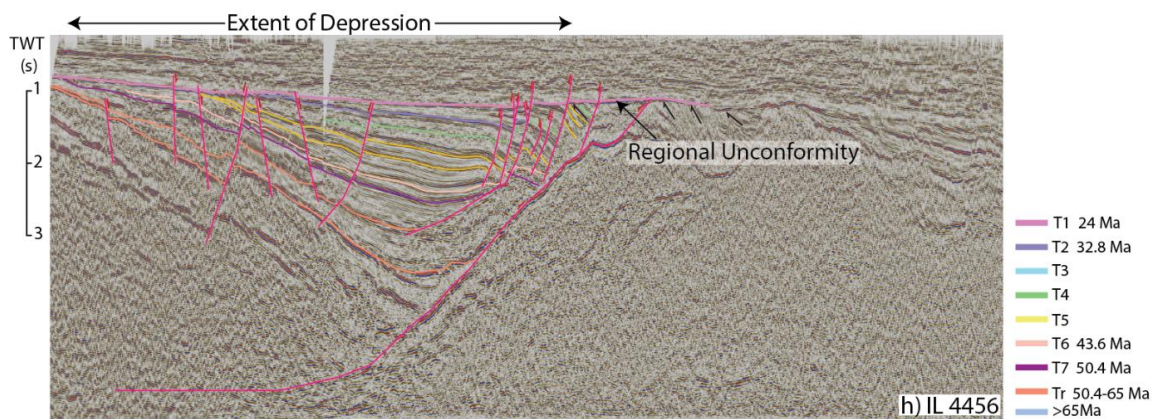
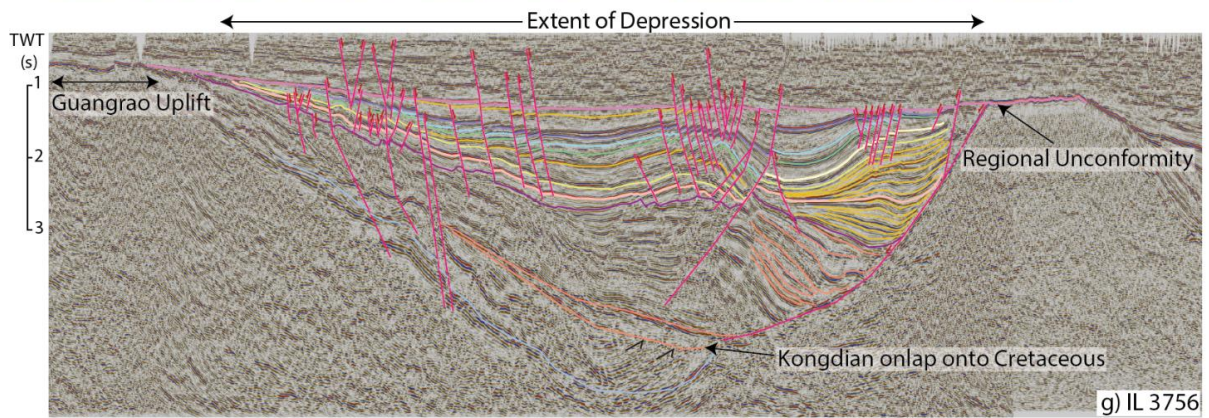
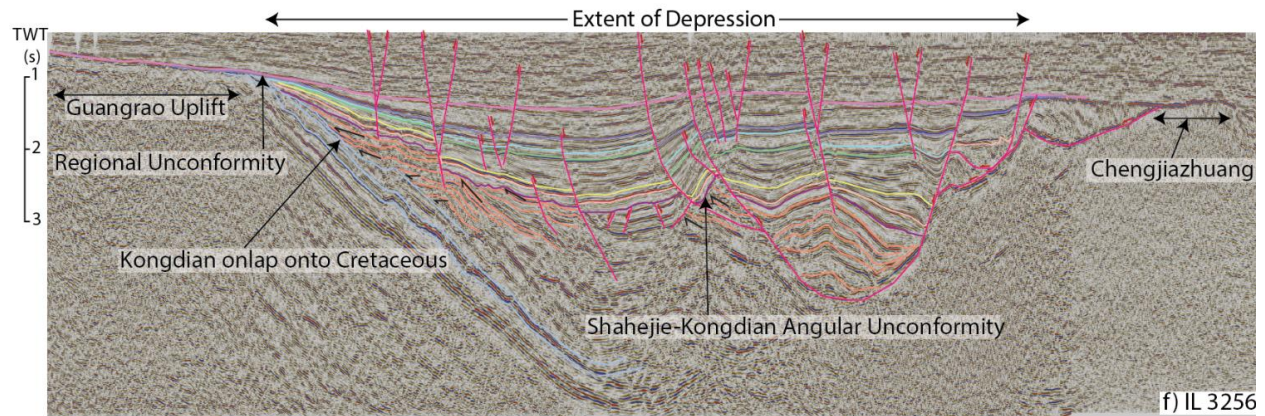
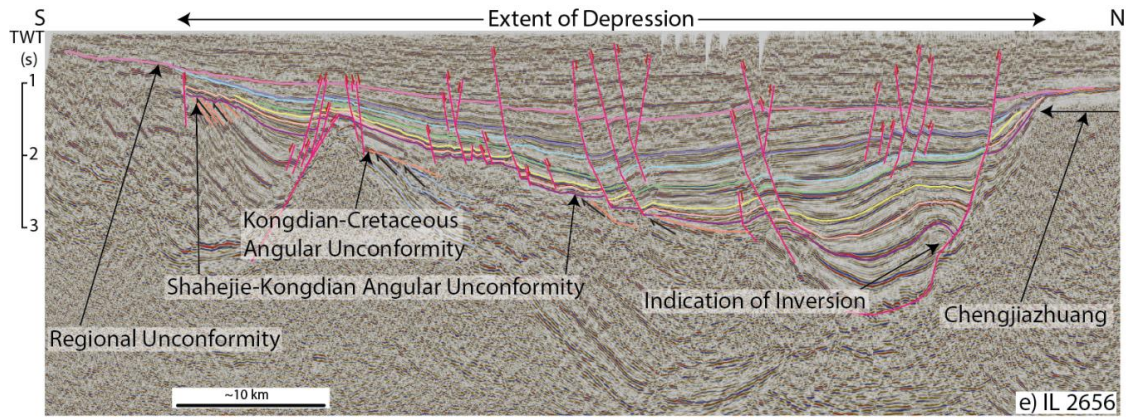
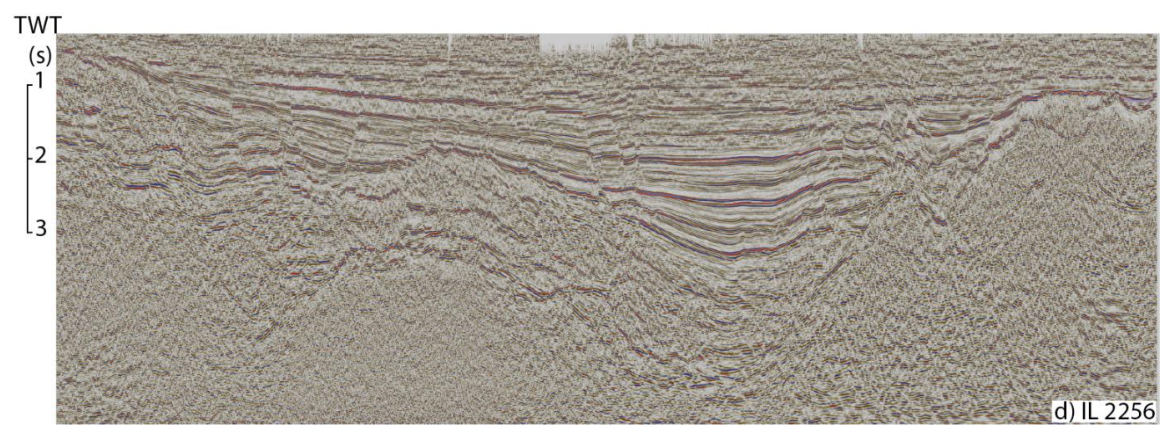
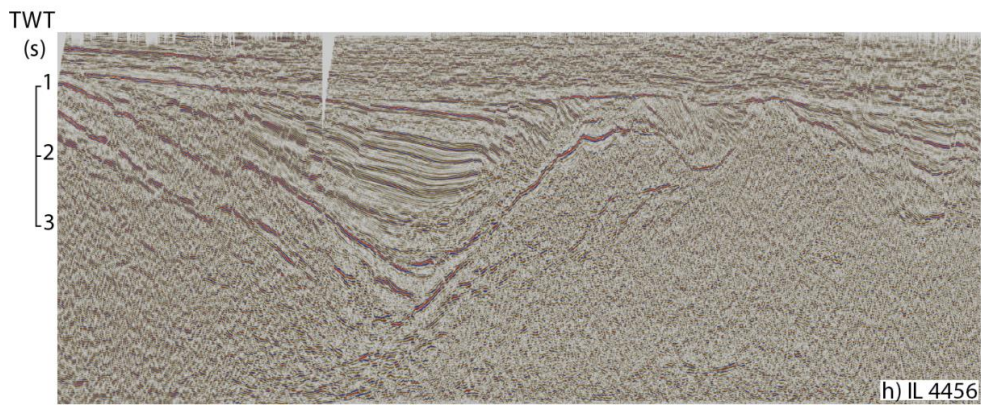
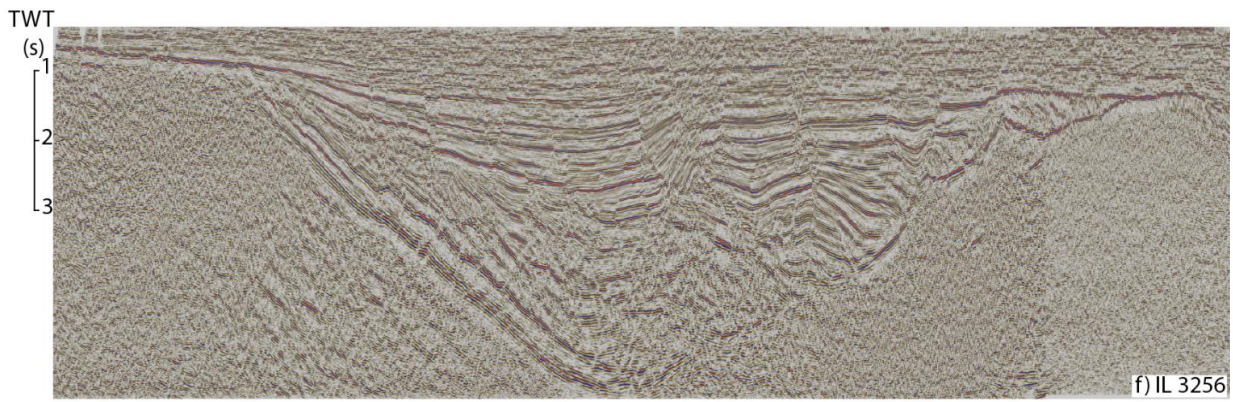


Figure 3.9: Interpreted N-S seismic transects at 4x vertical exaggeration showing the uninterpreted seismic transects. The seismic transects are in order from west to east and can be correlated directly with Figure 3.8 (3.8a is the same seismic transect as 3.9a). Location map in Figure 3.3.





The interpreted E-W lines can be seen in Figure 3.10 and their corresponding uninterpreted version in Figure 3.11. Due to the direction of intersection of the E-W transects, growth will be significantly more evident in the more northern lines than the southern lines. Being that the majority of growth in the basin is due to the formation of half grabens in the north, it makes sense that this is where the growth is more visible. The E-W transactions will be described from north to south. Figure 3.10a is the northernmost E-W transect and shows extreme growth and fault displacement of the stratigraphy from the large listric normal faults trending east to west. The Dongying Depression in the transect is constrained by a basin high on each side of the growth strata which ends abruptly into the basin high. A notable local unconformity is also present and will be talked about later in this paper. Figure 3.10b shows significantly less growth in the stratigraphy but has evidence of important sequence stratigraphy in the form of clinofolds, which proves the depositional environment of the depression. Significant growth can be seen throughout the transect, with extensive deep growth (between T4-T6) on the east side of the depression and shallower growth (above T4) more in the center of the basin. Figure 3.10c shows less growth in the deeper horizons as expected because of its central location in the basin (Fig. 3.3). There is significantly more growth, nearly equivalent to Figures 3.10a and 3.10b, in the younger strata (above T1) which proves the shift of the depocenter southward. Clinofolds are also found in this transect and will be analyzed in detail later in the research. Figure 3.10d is the southernmost interpreted transect and shows the least amount of growth in the deeper stratigraphy except in the far west, which corresponds to the half graben in Figure 3.8a. The shallower stratigraphy, above T1, shows significantly more growth than the deeper

stratigraphy, but not as much as its northern counterparts.

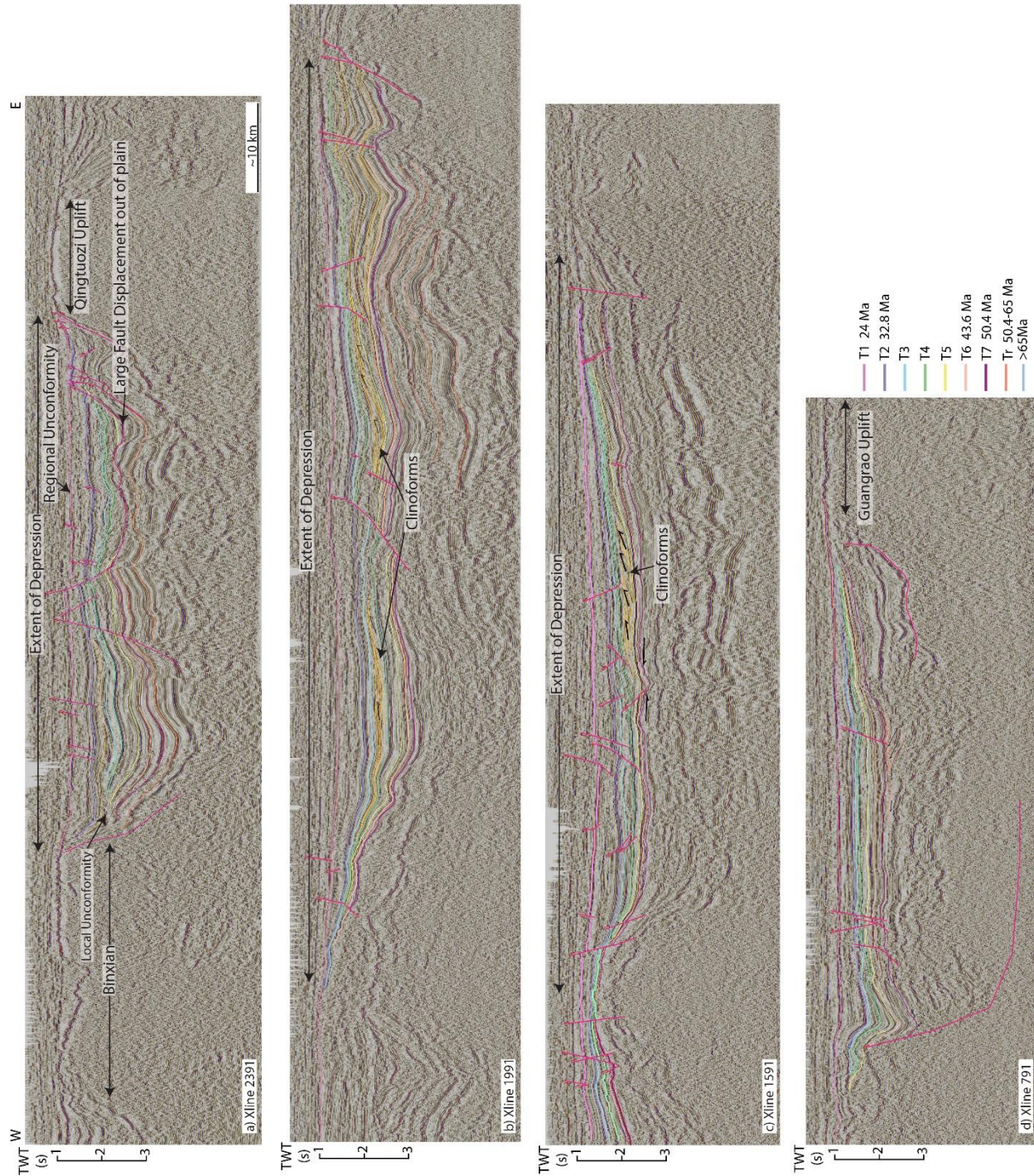


Figure 3.10: Interpreted E-W seismic transects at 4x vertical exaggeration showing interpreted company stratigraphy with additional older stratigraphy, growth strata, stratal terminations, and faults from this study. All faults interpreted are normal faults. The seismic transects are in order from north to south and consist of areas both inside and outside the Dongying Depression. Location map in Figure 3.3.



Figure 3.11: Interpreted E-W seismic transects at 4x vertical exaggeration showing the uninterpreted seismic transects. The seismic transects are in order from north to south and can be correlated directly with Figure 3.10 (Figure 3.10a is the same seismic transect as Figure 3.11a). Location map in Figure 3.3.

3.4.3 Stratigraphic styles

Stratigraphically, the Dongying Depression is dominantly defined by a large regional unconformity at the Dongying-Guantao Contact, represented by T1 (Fig. 3.3). Along the edges of the basin this unconformity is best described as an angular unconformity (Fig. 3.12) but is not as well defined in the central portion of the depression. The regional unconformity is most evident in the eastern side of the depression and likely indicates the direction of erosional events, from east to west (Fig. 3.12). Examples of the regional unconformity can be seen in Figure 3.13. The extent of the unconformity at the edges of the basin as well as the style of sediment deposition around the edges of the depression indicate a constant erosion of the sediment at these locations throughout the Shahejie (Fig. 3.13).

Aside from the distinct regional unconformity, there are several local angular unconformities recognized throughout the interpreted seismic transects which are mapped out together with the regional unconformity in Figure 3.12. Figure 3.12 illustrates the distinct patterns the unconformities have based on the age of the eroded stratigraphy as well as the location of where the unconformity can be seen. Angular unconformities labeled T2-T7 occur locally and are visible only in the northern E-W seismic transects (Fig. 3.12). An example of what this unconformity looks like can be seen in Figure 3.14. Angular unconformities labeled as T7-Tr represent a distinct unconformity that occurs where the upper Kongdian Formation horizons are eroded away and T7 lies on top of these angled beds (Fig. 3.15). This local unconformity lies in the central-north central portion of the depression (Fig. 3.12). Angular unconformities that are Tr and older are the oldest and deepest angular unconformities (Fig. 3.16) and

appear more central-south central in the depression (Fig. 3.12). These unconformities occur where the Tr horizons lie unconformably on top of the underlying Cretaceous beds (Fig. 3.16).

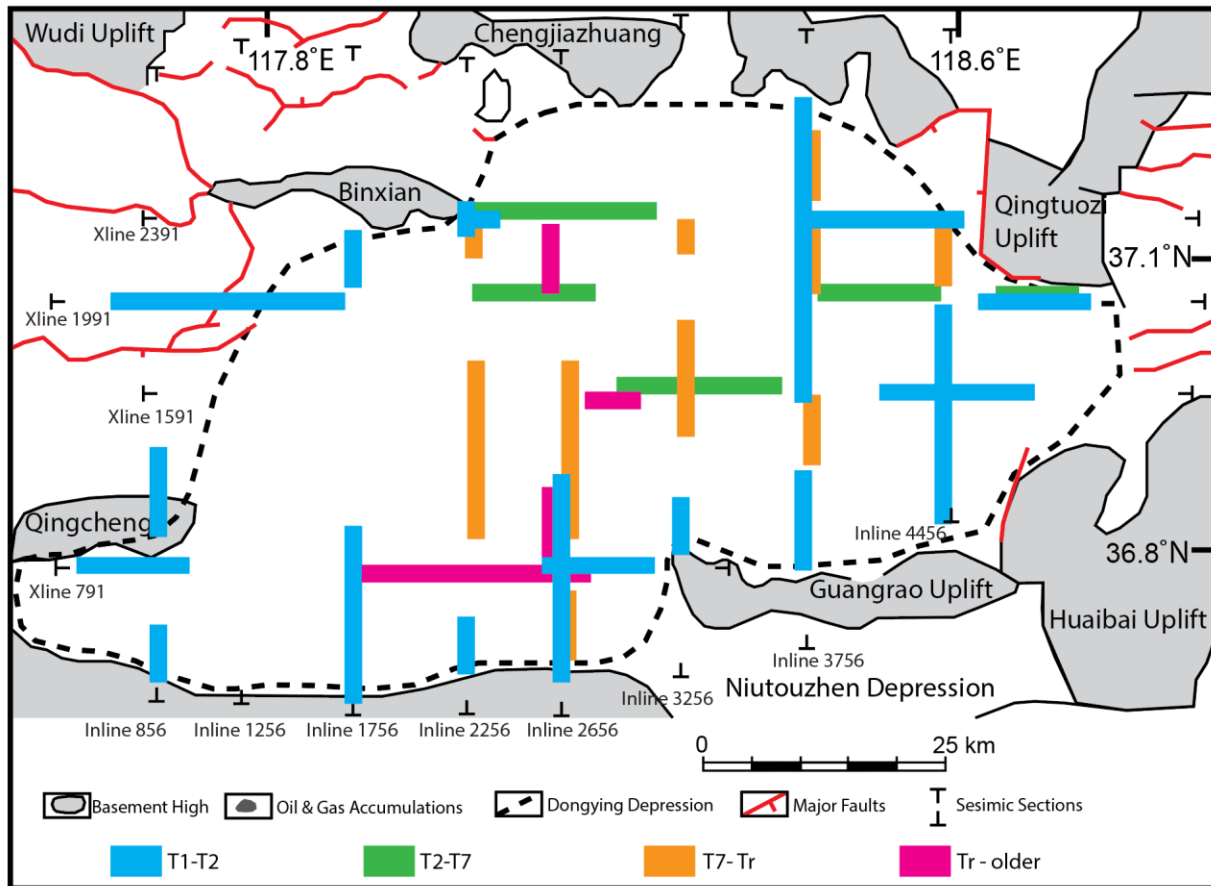


Figure 3.12: Basemap of the Dongying Depression showing the depression extent, petroleum accumulations, basement uplifts, and locations of distinct angular unconformities in seismic transects of this study. Each colored rectangle represents a location on the seismic transect where a distinct angular unconformity can be seen and mapped. The T1-T2 angular unconformity that is represented is the same as the regional Dongying-Guantao Contact unconformity but is only represented where there is a distinct angular unconformity (Basemap modified from Lampe et al. 2012).

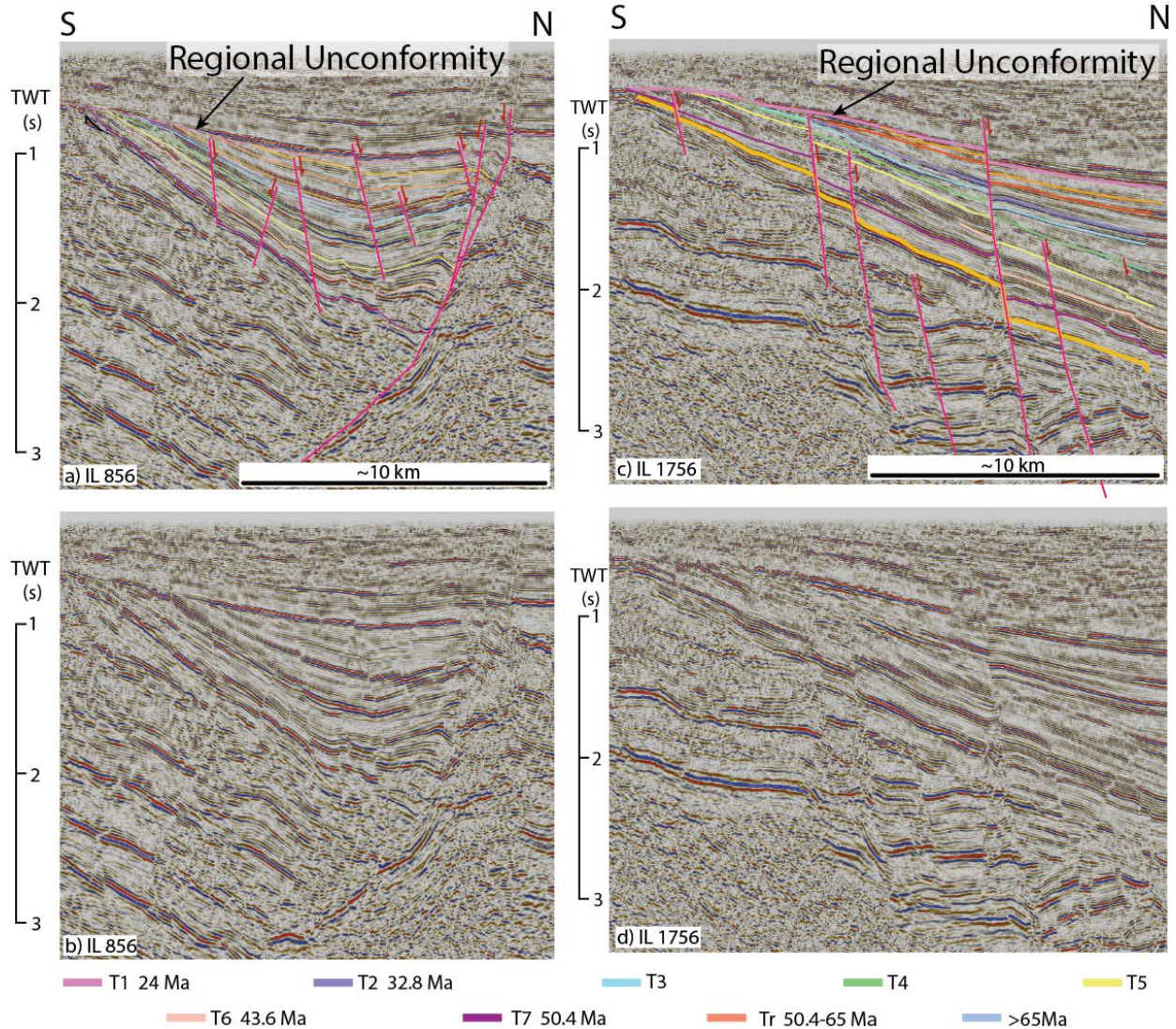


Figure 3.13: Zoomed in images on seismic transects where the Dongying - Guantao contact angular unconformities can be seen. This is represented as T1-T2 in Figure 3.12. Figure 3.13a is from N-S transect IL 856 (Fig. 3.8a) and shows the interpreted stratigraphy along with interpreted faults from this study. Figure 3.13b is the uninterpreted version of Figure 3.13a (see also 3.9a). Figure 3.13c is from N-S transect IL 1756 (Fig. 3.8c) and shows the interpreted stratigraphy along with interpreted faults from this study. Figure 3.13d is the uninterpreted version of Figure 3.13c (see also 3.9c).

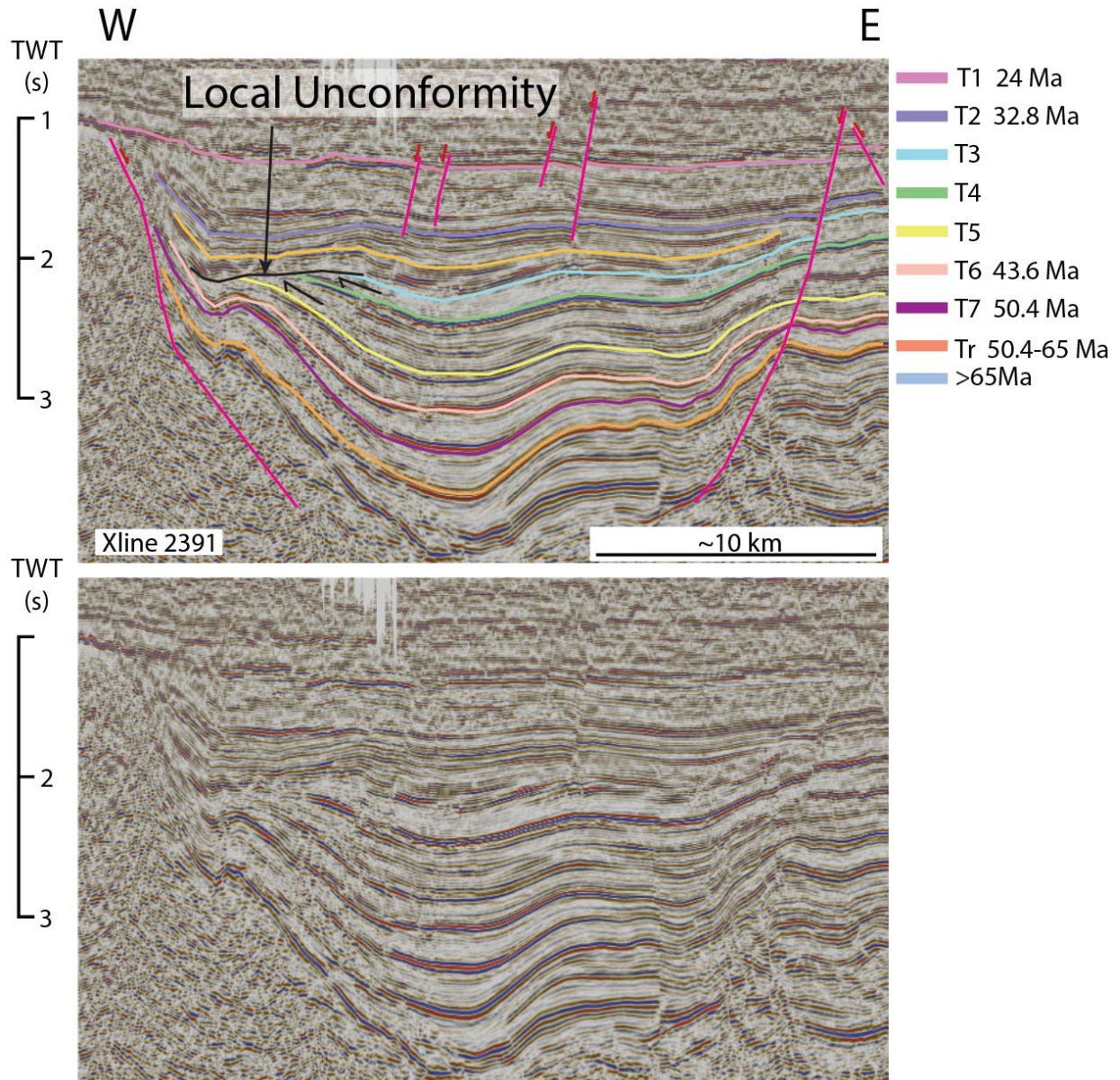


Figure 3.14: Zoomed in example of the Shahejie angular unconformity, represented as T2-T7 in Figure 3.12. Figure 3.14a is zoomed in from the interpreted seismic transect in Figure 3.10a and Figure 3.14b is zoomed in from the uninterpreted seismic transect in Figure 3.11a.

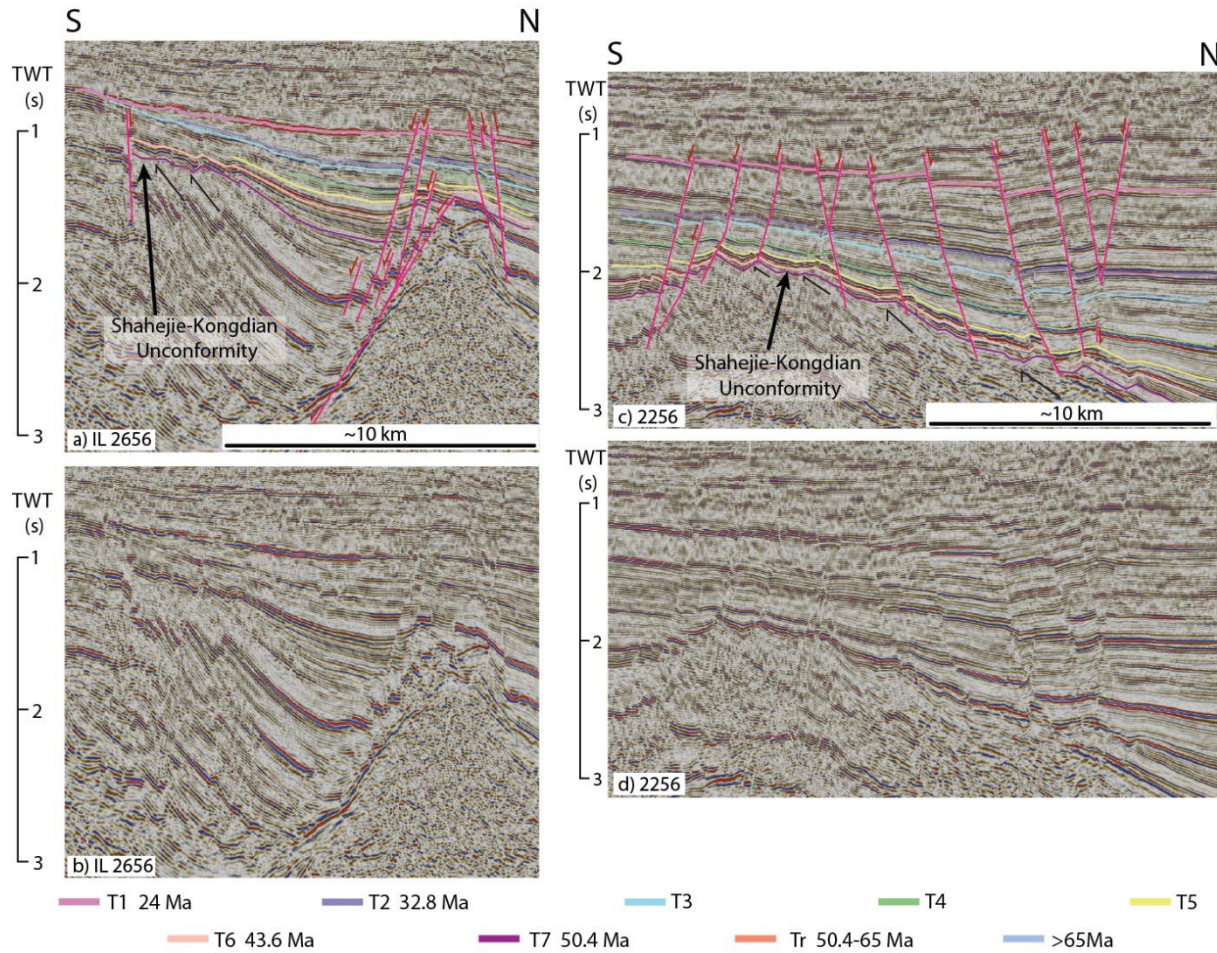


Figure 3.15: Zoomed in example of the Kongdian - Shahejie Contact angular unconformity, seen in Figure 3.12 as T7-Tr. Figure 3.15a is zoomed in from the interpreted seismic transect in Figure 3.9e and Figure 3.15b is zoomed in from the uninterpreted seismic transect in Figure 3.10e. Figure 3.15c is zoomed in from the interpreted seismic transect in Figure 3.9c and Figure 3.15d is zoomed in from the uninterpreted seismic transect in Figure 3.10c.

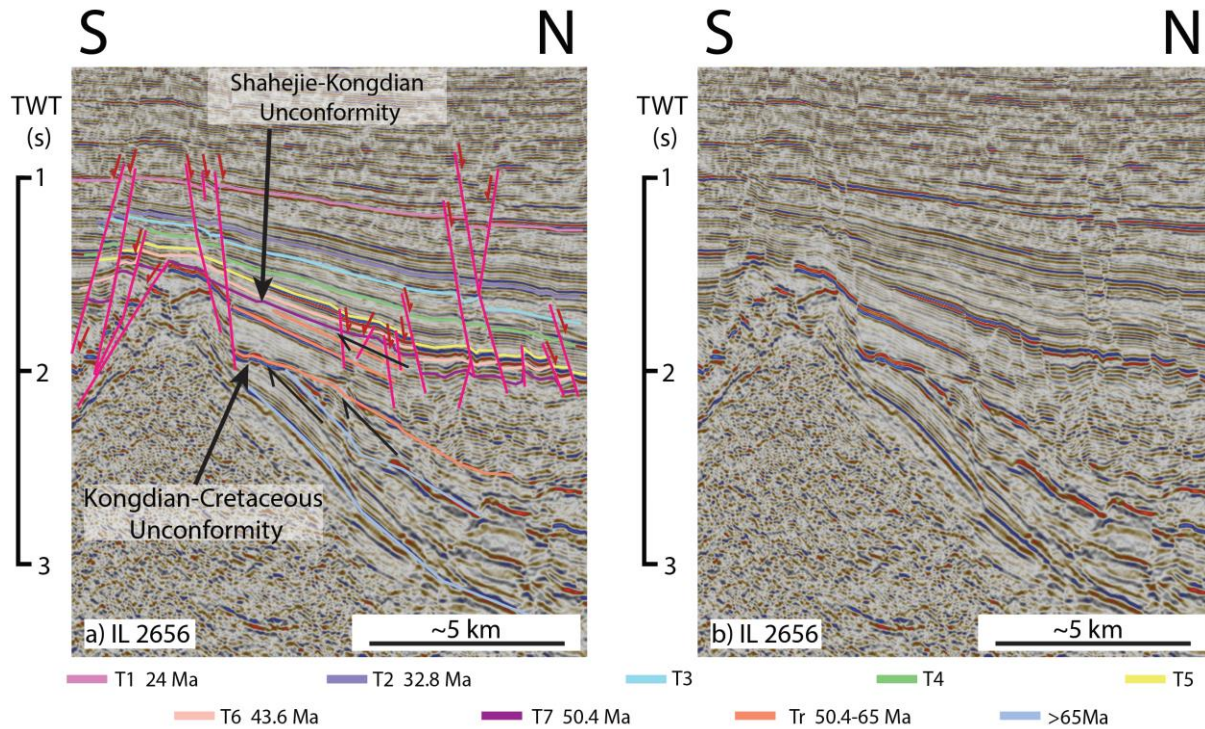


Figure 3.16: Zoomed in example of the Kongdian - Cretaceous angular unconformity, seen in Figure 3.12 as Tr - older. Figure 3.16a is zoomed in from the interpreted seismic transect in Figure 3.9e and Figure 3.16b is zoomed in from the uninterpreted seismic transect in Figure 3.10e.

The interpreted Kongdian horizons are found to be onlapping on to the Cretaceous strata in several locations throughout the model (Fig. 3.17). Often seen at the edges of the basin, this is an indication of sediment deposition and fill due to the beginning and growth of the extensional rifting that followed the Cretaceous compressional phase. The underlying Cretaceous sediment does not appear to have any growth, but the Kongdian sediment can be tracked to have extreme growth to the north of what is imaged in Figure 3.17. In some cases, it is not only the Kongdian sediment that onlaps onto the underlying Cretaceous strata, but also the overlying T6 and T7 horizons (Fig. 3.17a). The onlapping occurs on the south side of the depression because the south side is not as strongly affected by the extensive fault growth to the

north (Fig. 3.20). The extent of the effects of the half graben are indicated by the onlapping as well as give a time narration of when previous studies (Chen et al., 2017) suggest that the extensional system ended (43.6 Ma) and the interpreted transtensional system began (43.6 Ma). This is evidenced by the shift northward of the new sediment package deposition after T6, when the system apparently became transtensional (Chen et al., 2017). This is visible in Figure 3.17a, where the new packages deposited after T6 do not onlap the cretaceous and begin to shift northward. These patterns cannot be seen along all edges of the depression, potentially due to higher rates of erosion or more extensive antithetic or synthetic faulting and growth stratigraphy (Figs. 3.17c and 3.17d).

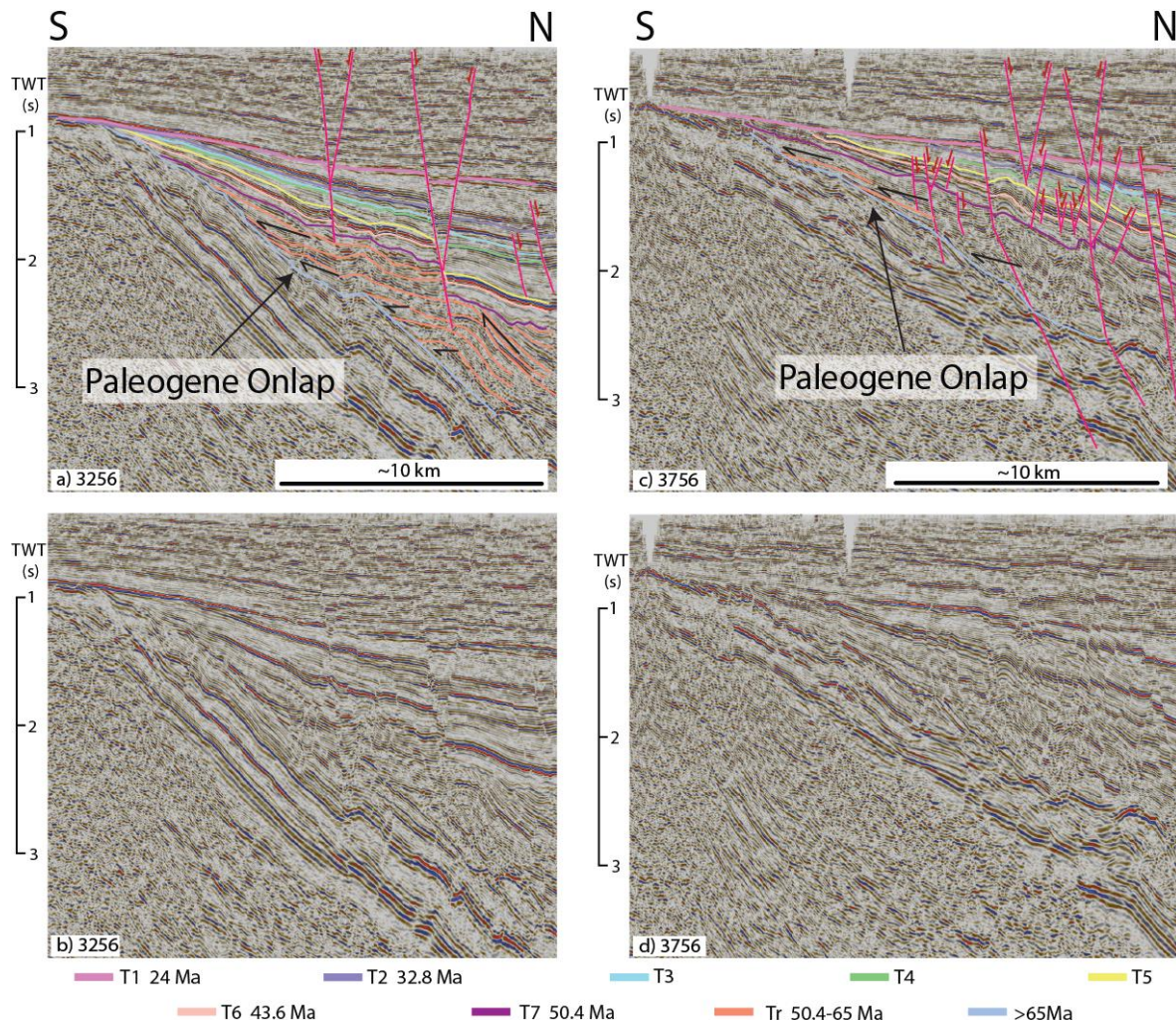


Figure 3.17: Onlap of Kongdian deep horizons onto underlying Cretaceous deposits. Figure 3.17a is zoomed in from the interpreted seismic transect in Figure 3.9f and Figure 3.17b is zoomed in from the uninterpreted seismic transect in Figure 3.10f. Figure 3.17c is zoomed in from the interpreted seismic transect in Figure 3.9g and Figure 3.17d is zoomed in from the uninterpreted seismic transect in Figure 3.10g.

Depositional environments of the area have been discussed at length, describing the deposition of the depression as lacustrine facies, with alluvial fans and deltaic systems (Chen et al., 1984). There is evidence of this in this dataset in the form of clinofolds. Clinofolds can be seen in several E-W transects throughout the depression but are not as easily visible in the N-S transects (Figs. 3.18 and 3.19). These

clinoforms are consistent with the depositional environment being lacustrine and shed light on the direction of deposition of sediment. The clinoform in Figures 3.18a and 3.19a occur between T3 and T4 (~ 35 Ma) and prograde from east to west. The clinoform in Figure 3.18b and 3.19b occurs between T4 and T5 (~ 38 Ma) and prograde from east to west as well. Both clinoforms are visible on the same E-W seismic transect. Figures 3.18c and 3.19c show a clinoform that is around the same age as the clinoform in Figure 3.18b and is located roughly 25 kilometers southwest of the clinoform in figure 3.18b. The deposition amount is significantly less than the more northern clinoforms and therefore affirms the pattern that more deposition occurs in the north than in the south.

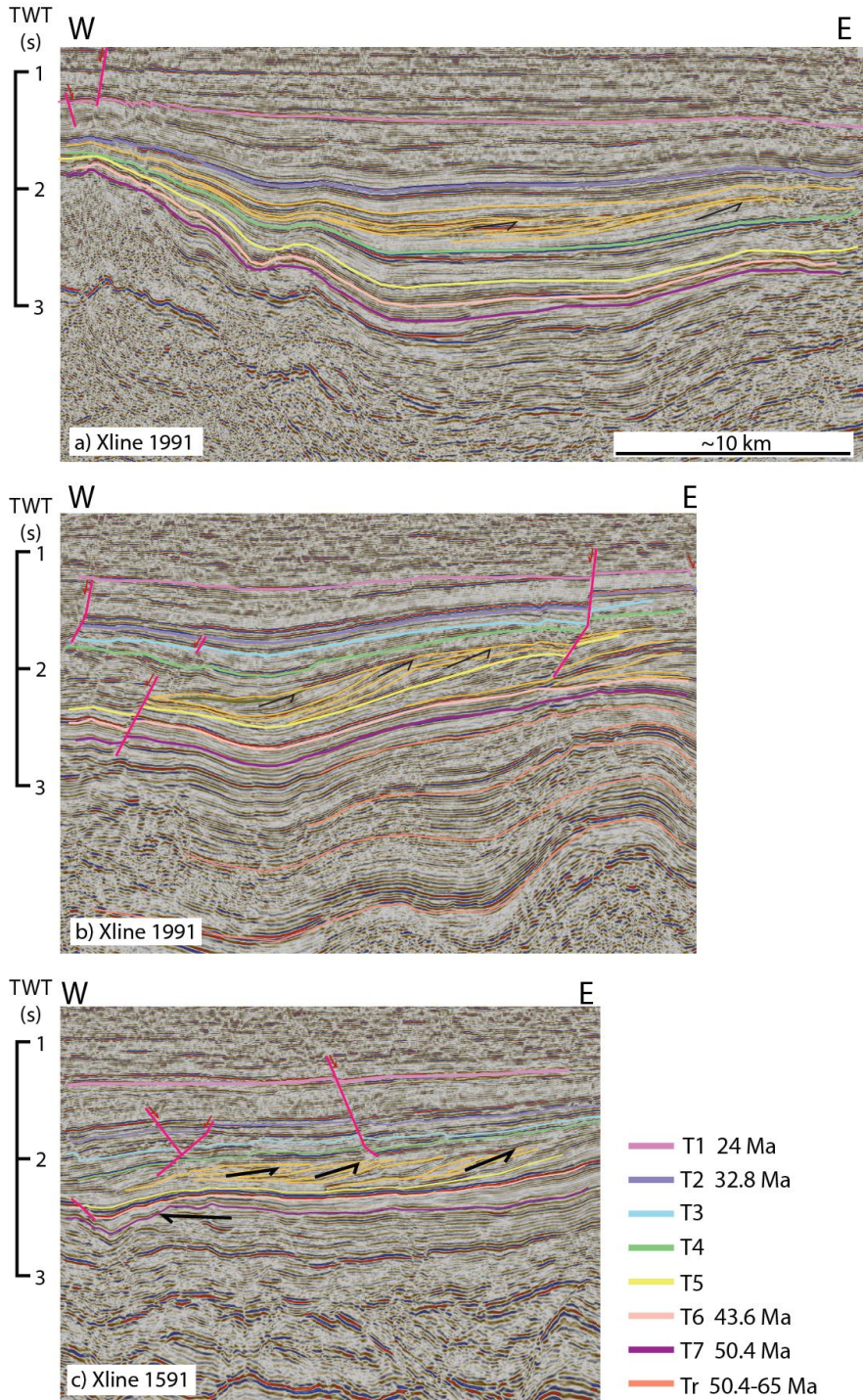


Figure 3.18: Zoomed in images of clinofolds that have been interpreted onto the E-W seismic transects, not a part of company stratigraphy. Figure 3.17a is a zoomed-in interpreted section from the western half of Figure 3.11b. Figure 3.17b is a zoomed-in interpreted section from the eastern half of Figure 3.11b. Figure 3.17c is a zoomed-in interpreted section from Figure 3.11c.

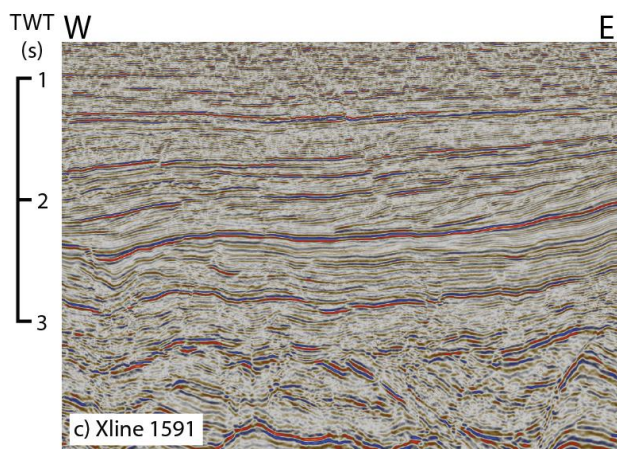
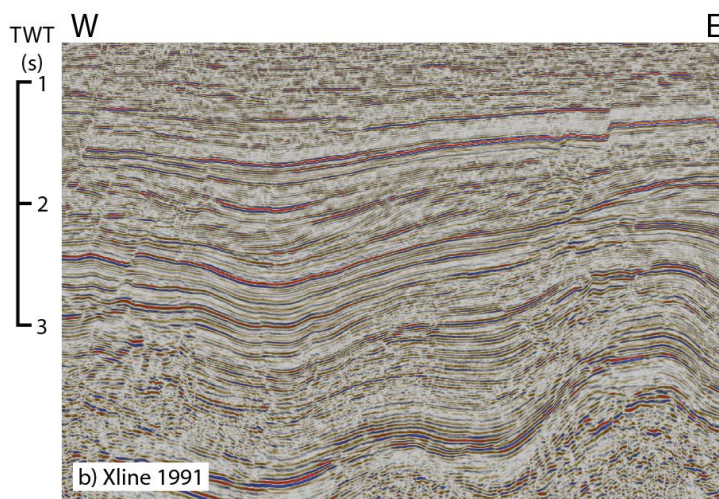
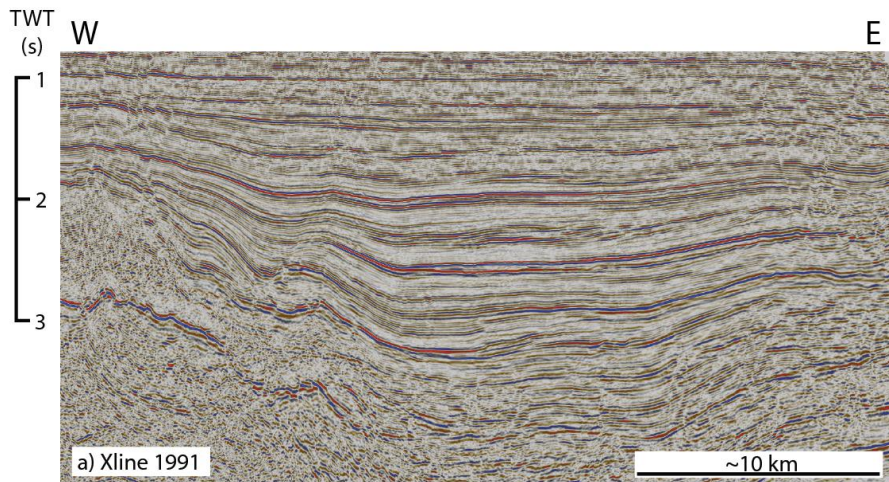


Figure 3.19: Zoomed in images of clinoforms on the uninterpreted E-W seismic transects imaged in Figure 3.17. Figure 3.18a correlates to Figure 3.17a, 3.18b to 3.17b, and 3.18c to 3.17c.

3.4.5 Structural Styles

The structure of the Dongying Depression is a series of south-facing half-grabens (Figure 3.20). The faults can be categorized into groups describing their geometries, fault growth, and upward and downward termination patterns. Resolution of the seismic is a limiting factor in deciding what is the upward termination fault tip. The horizons above T1 (24 Ma) become very discontinuous and difficult to tell if a fault terminates between 0-24 Ma or does not terminate at all, which is why they were grouped together into one category. Upward fault terminations can be categorized into three groups when correlating to tectonic phases in the depression, which are described by previous studies (Chen et al., 2017). Faults that terminate above T1 represent all the faults that continue to grow after transtensional activity ends and thermal subsidence begins to dominate the region. The horizons above T1 become discontinuous (Fig. 3.8c and 3.8e), making it difficult to tell if the faults run to the surface or stop before they reach the surface. The interpreted faults that breach T1 are represented in Figure 3.21. The above T1 fault terminations are very widespread but occur in larger numbers in the northern portion of the depression. Fault terminations between T1 and T6 represent faults that went dormant during or at the end of transtensional activity (Fig. 3.24). These faults are mapped in Figure 3.22 to illustrate the widespread nature of the fault terminations in the depression. Faults that terminate at or below T6 went dormant during the extensional tectonic activity or at the end when the depression became dominantly transtensional faulting (Fig. 3.15a). The deep upward termination faults are mapped in Figure 3.23 and are present in only the southern end of the depression. The extreme lack of T6 and lower terminations indicates that most of the faults remained

active after the system became dominantly transtensional.

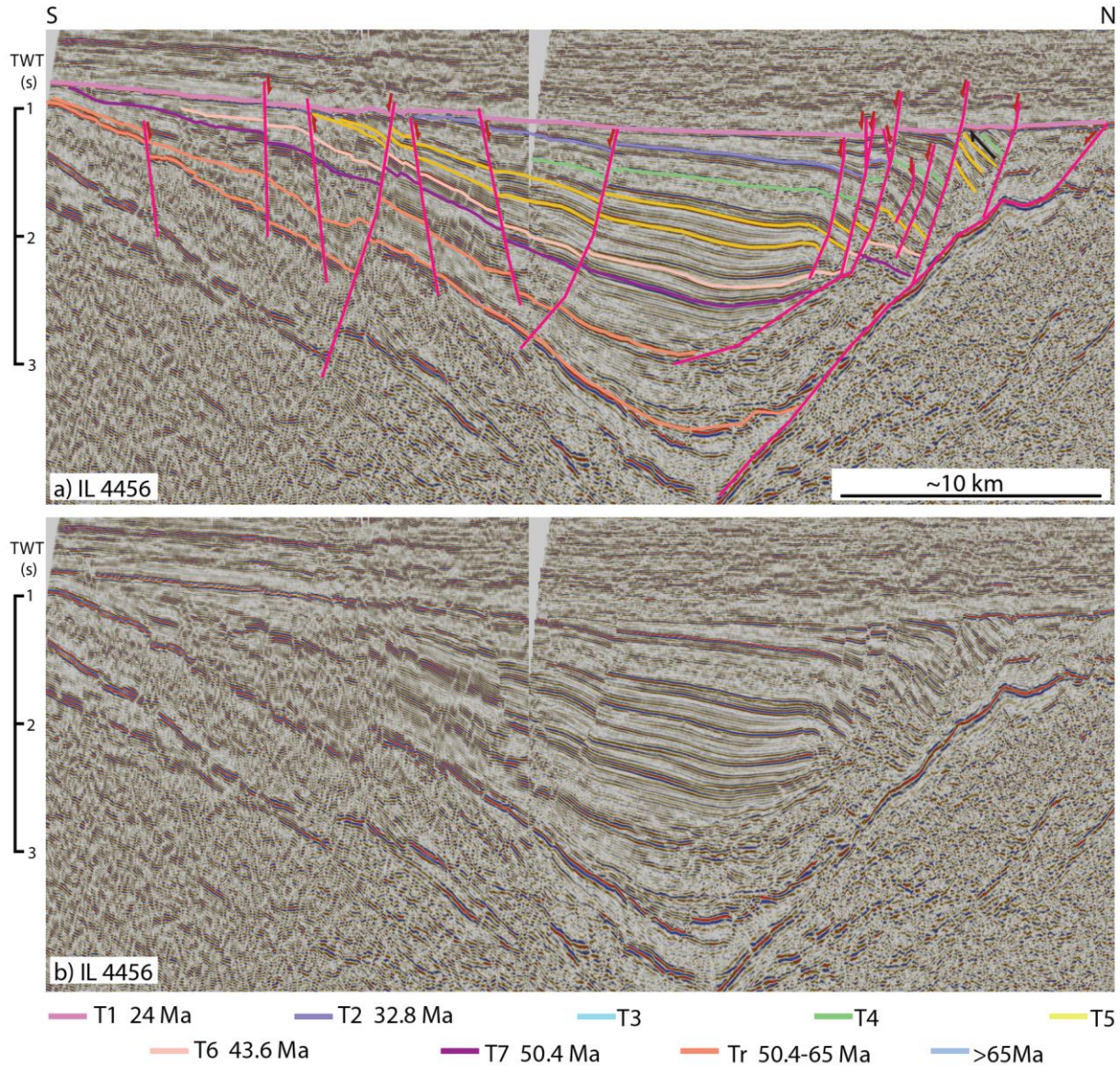


Figure 3.20: Zoomed in image of an example where the half graben geometries of the depression are evident. Figure 3.18a is a part of the interpreted N-S line IL 4456 and is found in zoomed out form in Figure 3.8h. Figure 3.18b is a part of the uninterpreted N-S line IL 4456 found zoomed out in Figure 3.9h.

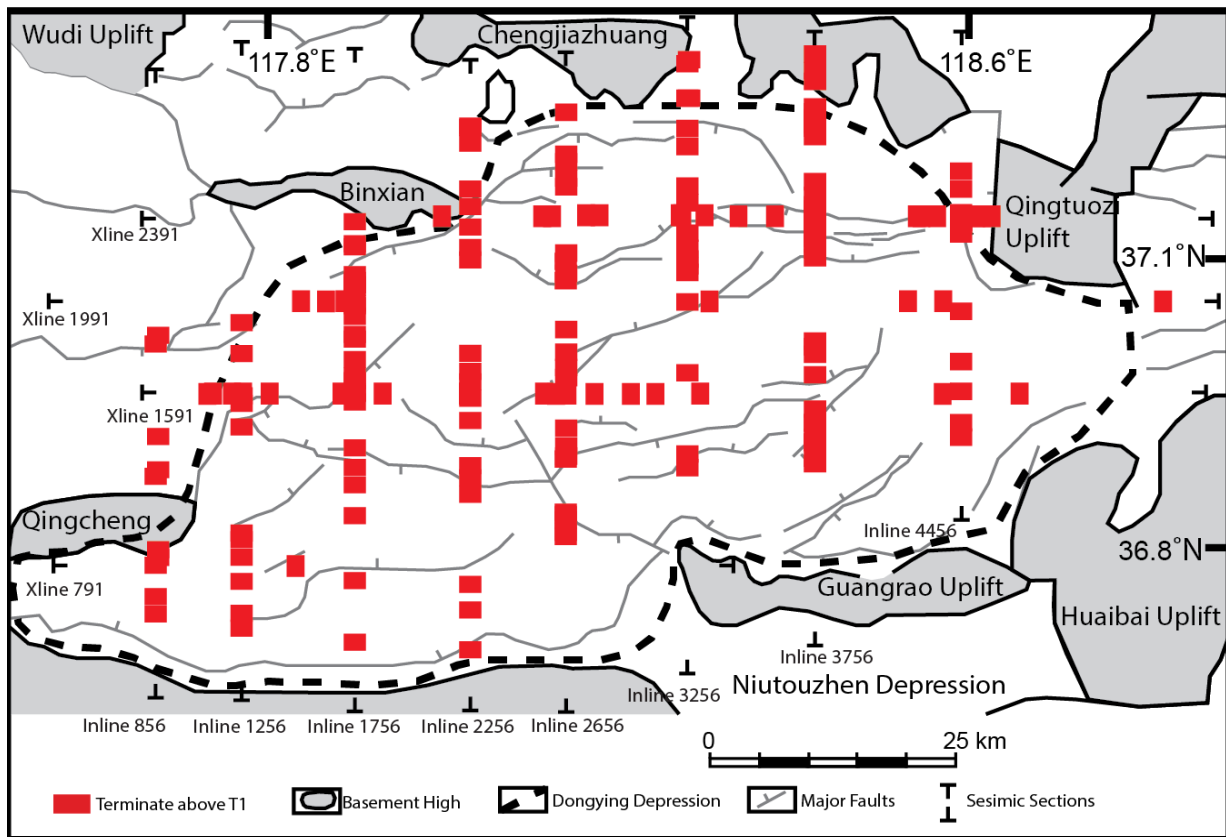


Figure 3.21: Map showing locations of upward fault terminations above the T1 seismic horizon (~ 24 Ma). This represents faults that have been active through thermal subsidence and potentially are active present. (Basemap modified from Lampe et al. 2012)

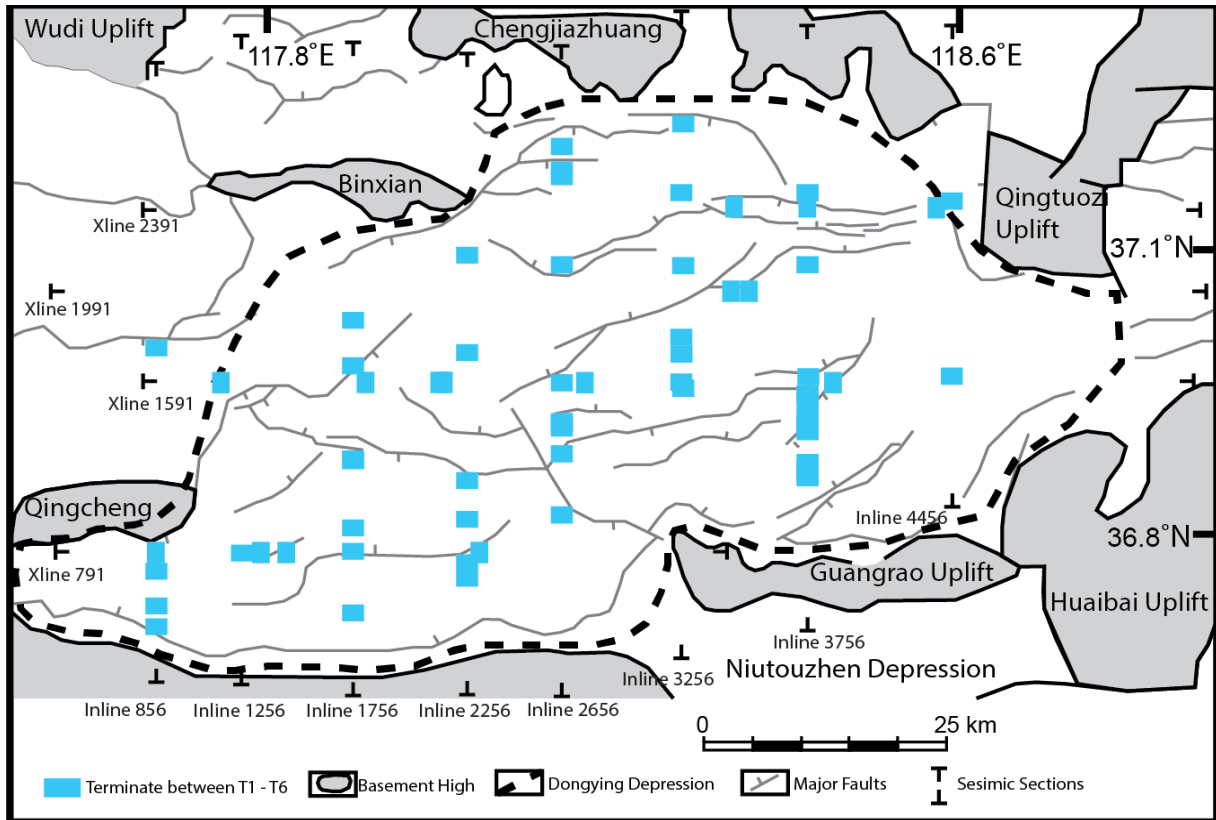


Figure 3.22: Map showing upward fault terminations between the T1 and T6 seismic horizons (~24 to ~43.5Ma). This represents faults that were active during the transtensional phase of the depression but become inactive before the depression becomes dominated by thermal subsidence (Basemap modified from Lampe et al. 2012)

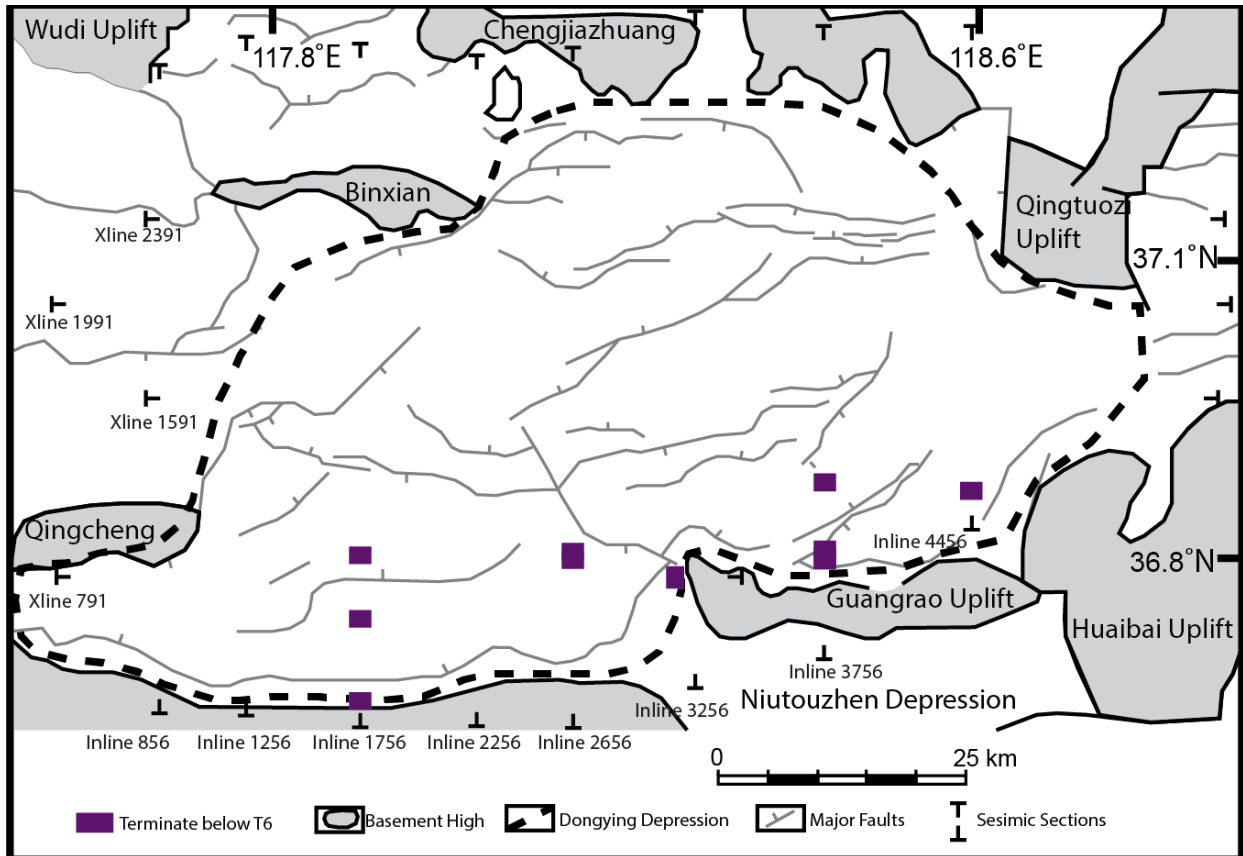


Figure 3.23: Map showing faults that terminate upwards below the T6 seismic horizon (>~43.5 Ma). This represents faults that were active during the extensional phase of the depression but went inactive before the transtensional phase began. (Basemap modified from Lampe et al. 2012)

There are some distinct patterns in the downward fault terminations of the depression. While not all faults in the area follow that specific characteristic, there are a large enough amount of them to note their presence (Fig. 3.24). The downward fault terminations occur at the Kongdian-Shahejie contact (T7), where in some locations there is a distinct angular unconformity (Fig. 3.24). The presence of these fault terminations may indicate a change in mechanical strength between the horizon T7.

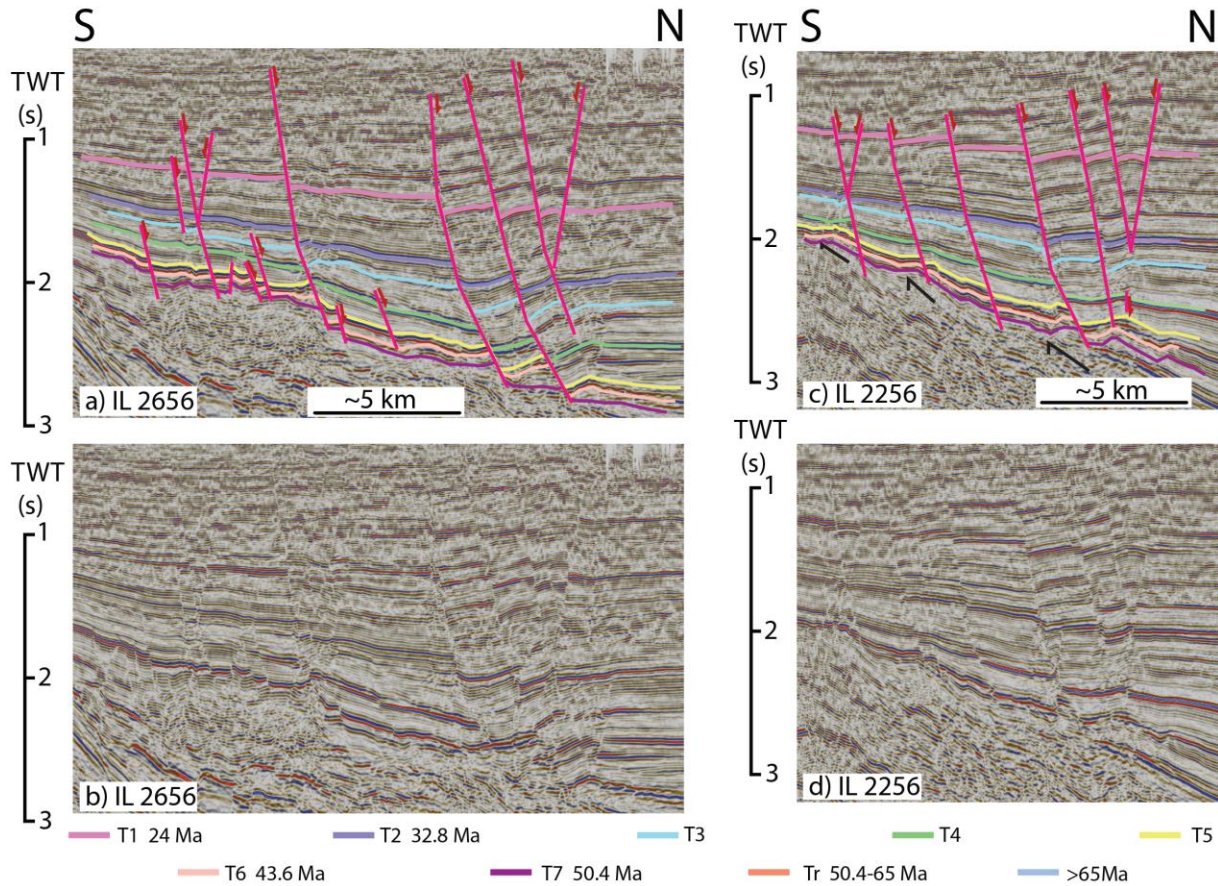


Figure 3.24: Seismic transects that show fault truncation patterns near T7. Figure 3.24a is a zoomed in image from Figure 3.8e and illustrates how many of the faults in this area have a downward termination pattern around T7. Figure 3.24b is a zoomed in image from Figure 3.8d and illustrates a lower termination pattern of faults at T7 as well as the distinct angular unconformity at T7, the Kongdian-Shahejie Contact. This angular unconformity may have a change in rigidity between the two units which causes certain faults to terminate at it. Refer to Figure 3.8 for legend.

3.4.6 Fault Analysis

While the formation of the Dongying Depression has been dominated by large extensional growth, there are two major periods of compression indicated by inversion of the master listric fault and minor antithetic fault in the half graben (Fig. 3.25). The two periods of inversion that stand out are an older occurrence around the time of T6 when a small fold formed in the underlying growth strata, indicated by phase 2 in Figure 3.25a and a large period of inversion that forced the depocenter to shift significantly south as

the underlying growth strata along the master listric fault pushed upward indicated by number four in Figure 3.25a.

Phase 1, indicated by growth strata and arrow 1 (Fig. 3.25a), is deposited due to the master listric fault. This is evidenced by large amounts of growth along the master listric fault that become thinner to the south (Fig. 3.25). Phase 2 (Fig. 3.25a) indicates a period of inversion where the master listric fault becomes a reverse fault. This is evidenced by a small fold that is composed of growth strata (Fig. 3.25). The inversion can be seen in two separate locations of Figure 3.25. One location that the inversion can be seen is in a minor antithetic fault where a significant amount of erosion occurred due to the uplift of the strata, which is then followed by a large amount of growth in the next phase. The other location is where a fold composed of growth strata formed. Two new minor depocenters form on either side of the fold with strata pinching out over the fold. This growth likely occurred with the formation of the fold during the time of compression (Fig. 3.25). Phase 3 is a period that the master listric fault became normal once again. This is indicated by the end of thinning beds on top of the minor fold and shift of new growth stratigraphy being deposited on top of the fold, with the main growth being along the master listric fault (Fig. 3.25a). Phase four indicates a shift back to large reverse faulting where the growth strata along the master listric fault is uplifted significantly. The growth strata in its final stage are at shallower depths than the location where it was deposited (Fig. 3.25). Phase 5 is noted by growth strata at locations far south of where the depocenter once was during extensional growth (Fig. 3.25). This shift was likely because of the uplifting motion to the north.

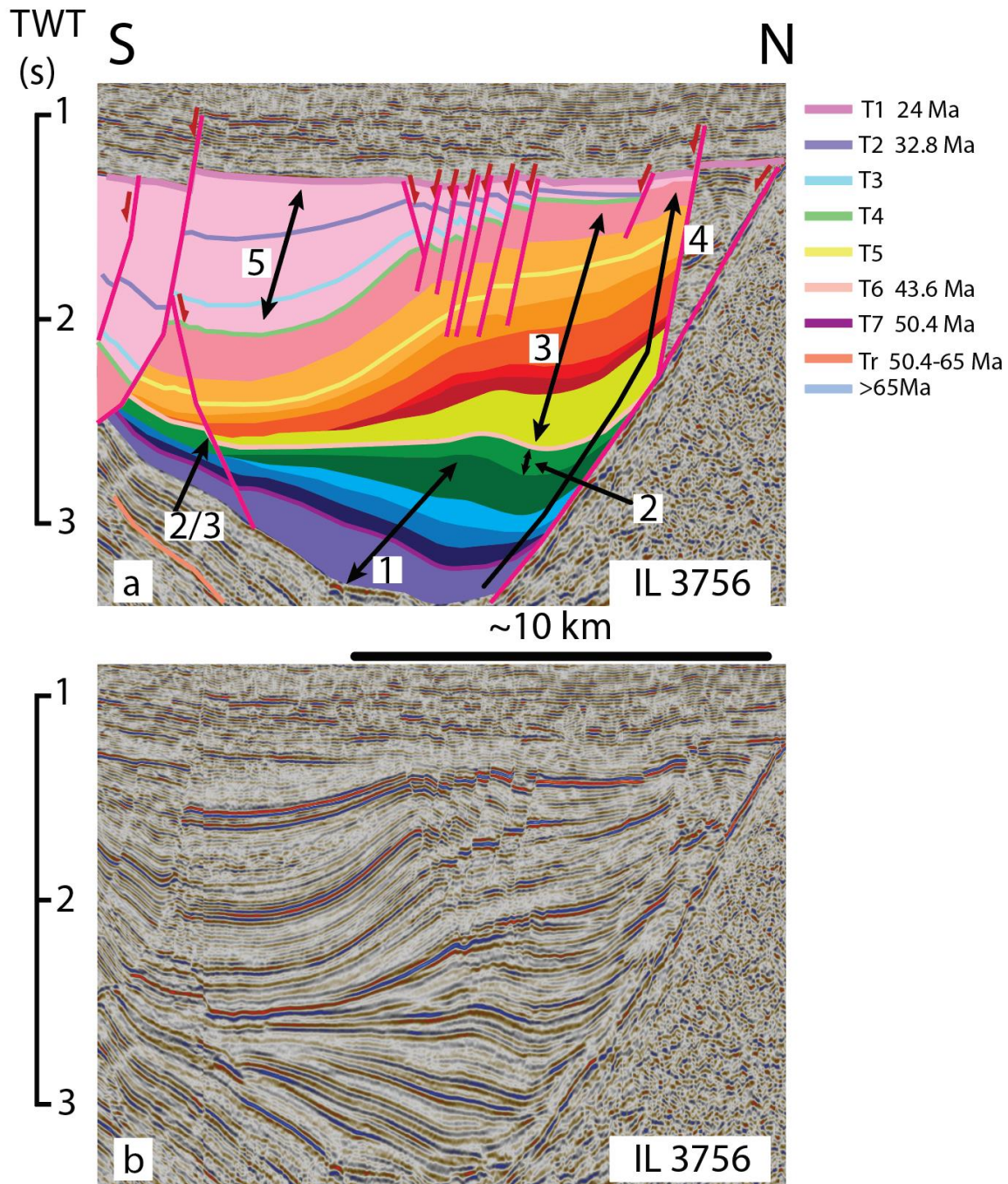


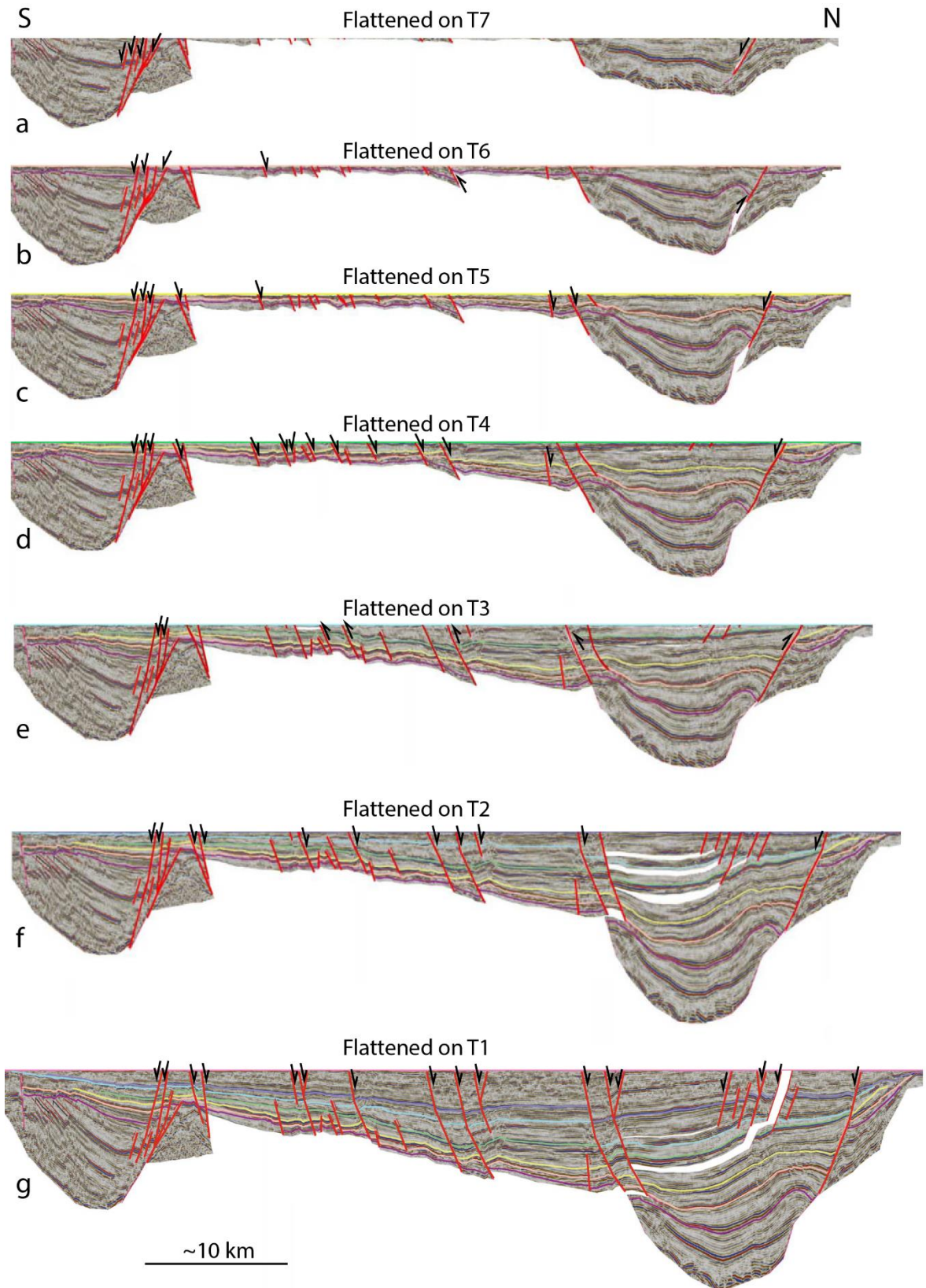
Figure 3.25: Image of Seismic transect 3756 showing evidence of inversion but looking at locations of growth and strata terminations which make up a fold. The different colors in Figure 3.25a are different growth packages, demonstrating minor changes in the growth depocenters of the half graben. The numbered double arrows indicate the periods of growth or inversion in order from first event (1) to most recent event (5). Through this analysis, periods of inversion can be seen where a fold is composed of growth strata. Figure 3.25b is the uninterpreted transect of Figure 3.25a. Phase 1= Extensional Growth; Phase 2 = Inversion; Phase 3 = Extensional/Transtensional Growth; Phase 4 = Inversion; Phase 5 = Transtensional Growth.

3.4.7 Seismic Reconstruction

A seismic reconstruction of N-S transect 2656 shows a backward deformation that implies the timing of possible structural changes such as inversion and strike slip motion (Fig. 3.8e). The reconstruction was created through progressive flattening along the interpreted company stratigraphy using the software Structure Solver (Structure Solver, 2019). Figure 3.26a is the first reconstruction of the depression, where the stratigraphy is flattened along horizon T7. All the prior growth in the image is from the deposition of the Kongdian (Fig. 3.4). Figure 3.26b is flattened along T6 and represents the end of the extensionally dominated growth, as explained by Chen et al. (2017). Laterally there had not been significant growth of the depression, but the growth in stratigraphy was significant in the two depocenters in the north and south ends of the depression. The feature that stands out at this stage is the minor fold of T7 along the main listric fault in the north. Here we note inversion of the main listric fault and one minor antithetic fault south of the half graben. Below T6 the growth strata appears to be filling up the half graben and thinning over the minor fold, indicating that the thrusting event had stopped before the deposition of T6 (Fig. 3.26b). With the deposition of T5 in Figure 3.26c, the main listric fault to the north can be seen with normal fault growth and the stratigraphy has grown to cover the minor fold. After the Deposition of T5 the growth of the half graben shifts southward, seen in Figure 3.26d with large amounts of growth between T4 and T5 south of the main half graben that is more than the growth between T5-T7 at the same location. The growth strata had doubled in some of the central parts of the depression since the deposition of T5 where several new normal faults became active (Fig. 3.26d). Figure 3.26e is flattened along T3 and illustrates the

distinct shift of depocenter to the central part of the depression. This shift in growth can be attributed to the large amount of inversion at the main listric fault and its main antithetic fault in the northern end of the depression. Figure 3.26f shows the transect flattened along T2 and shows that the faults in the depression have become normal faults once again. Along with significant new growth along the dominant listric and antithetic fault, a series of linear faults has displaced the stratigraphy. These faults appear to be strike slip faults, as the seismic strata do not line up well across the faults (Fig. 3.26f). Strike-slip faulting could explain the apparent gaps between the horizons in the reconstruction (Fig. 2.26f) and this provides evidence for transtensional or strike-slip fault motions within the depression. The growth during this period shifts back northward towards the original depocenter of the half graben (Fig. 3.26f). In Figure 3.26g, the growth of the depression shifts back southward where the antithetic faults have significantly more growth than the main listric fault to the north.

Figure 3.26: Image of seismic transect 2656 seen in Figure 3.8e reconstructed from T7 to T1. Figure 3.26a is flattened along the T7 horizon and is the beginning of the reconstruction. Figure 3.8g is flattened along T1 and is the end of the reconstruction. The dashed line in the figure is the extent of growth through this period.



3.5 Discussion

3.5.1 Tectonostratigraphic evolution

The evolution of the Dongying Depression is extremely complex and has several phases of structural deformation, believed to be caused by the evolution of tectonics in the region (Liang et al. 2016). Evidence of the various changes in tectonics can be found in various subtle changes in the structure and stratigraphy of the Dongying Depression.

First events of the formation of the depression lie in the large amount of growth strata which overlies the Cretaceous and has large depocenters in the north of the newly forming master listric fault (Figs. 3.5, 3.17). Without evidence of strike-slip motion, the depression appears to be dominated by extensional faulting with a half graben geometry.

In the southern end of the depression, evidence of local unconformities appearing with the erosion of the Kongdian Formation is overlaid by the newly deposited Shahejie Formation (Fig. 3.15). The Formation is indicated by company stratigraphy T7, deposited around 50.4 Ma (Fig. 3.4). Growth above T7 continues along the master listric fault along with minor synthetic and antithetic linear normal faults (Figs. 3.25 and 3.26).

Around the time of deposition of T6, a shift in tectonics occurs, evidenced by a shift of deposition in the south (Fig. Fig. 3.26) and minor folds developed in the older growth strata to the north (Figs. 3.25 and 3.26). Due to the nature of the reverse faulting, it is difficult to note if the deformation includes strike-slip motion in the depression, compared to other parts of Bohai Bay Basin as noted by (Chen et al.,

2017). This fold could be interpreted as an extensional fold above a fault ramp, as seen in McClay (1989), but we think it is inversion due to the amount of growth strata that composes the fold, as well as its spatial relationship to the main listric fault.

By the deposition of T5, the reverse thrusting had ended, and growth strata shifted back to the northern half graben (Fig. 3.25). A large number of synthetic and antithetic faults form during this extended period of growth in the central portion of the Dongying Depression, this growth begins slowly shifting the depocenter south (Fig. 3.26). The formation of these faults can be extensional or transtensional in nature, the growth is not large enough to be analyzed in a 2d transect.

The Dongying Depression undergoes another shift in structural deformation around the deposition time of company stratigraphy T4 (Fig. 3.25). A major shift to reverse faulting influences a massive shift in deposition location and uplift underlying growth strata along the master listric fault in the north (Fig. 3.25). The inversion not only affects the master listric fault but the minor synthetic and antithetic linear faults which had formed during the previous growth phase in the center of the Dongying Depression (Fig. 3.26).

The next shift in structural deformation is indicated by the formation of linear faults in the main growth package of the half graben (Fig. 3.26). These faults became active around the same time as deposition of company stratigraphy T3. The horizons T1 and T2 were deposited at the same time as these new linear faults were moving. We believe the reconstruction of these horizons proves the potential of strike-slip growth where the underlying stratigraphy did not line up on either side of the fault (Fig. 3.26), although there are many other possibilities such as: a change in shear angle, a horizon

mismapped, or it could be an artifact of flattening algorithm. We can't exclude the cause of the gaps based on the current data set, although the data set is based on a 3D volume that could be analyzed for strike-slip motion.

There is a hiatus of growth in the depression, seen by large angular unconformities along the edges of the depression (Fig. 3.13). These angular unconformities are overlaid by T1, marking the contact between the Dongying and Shahejie Formations. The unconformities are likely caused by a large-scale uplift of the entire depression, with slightly more uplift in the east, as it has endured more erosion than the west (Fig. 3.12).

The final stage of the depression is determined to be thermal subsidence (Chen et al., 2017). This can be seen in the seismic transects with a continued large-scale shift in deposition to the center of the depression, where most of the normal faults remain active and increase in growth compared to previous stages (Fig. 3.5). Overall, the extension that we restored implies a Beta Factor of 1.11, this is a little less than the average Bohai Bay Basin Beta Factor of 1.21, found by Liu et al (2022).

3.5.2 Comparison to Previous Studies

A comparison of the structural deformation of the Dongying Depression can be made with previous studies of the tectonic evolution that affects the overall Bohai Bay Basin area, such the one by Liang et al. (2016). According to Liang et al. (2016), the first phase of tectonic evolution of the Bohai Bay Basin is caused by the Pacific Plate subducting Northwest at a rate of 130 mm/a. This phase lines up well with our interpretation of extensional faulting dominating the Dongying Depression between 64

to 43.6 Ma. A tectonic shift in subduction speed that is noted by an average (Liang et al., 2016), between 50 Ma and 32 Ma. Liang et al. (2016) notes that the rate of subduction reaches an all-time low at 40 Ma, and that this was a peak in subsidence for the Bohai Bay basin, noting an inverse relationship between the two. This study shows the largest growth of stratigraphy in the Dongying Depression to be after the first inversion event after T6, around 40 Ma (Fig. 3.25a). Liang et al. (2016) states that subduction speeds back up and shifts in a westward direction. In the Dongying Depression, several complexes of linear strike-slip faults form after the deposition of T3 and bisect T2 (Fig. 3.26). The deposition of T2 is 32.8 Ma, meaning that this shift in growth of strike-slip faults in the depression occurs during the shift of the Pacific Plate subduction. This shift does not explain the large inversion phase that occurs around the deposition of T4 between 33 - 43 Ma. The final phase according to Liang et al. (2016) is a small change in the strike slip nature of the Japan Sea. This change does not account for the drastic angular unconformities that define the Dongying - Guantao Contact seen in the Dongying Depression (Fig. 3.12).

Compared to another study of the Dongying Depression, Chen et al. (2017) breaks the tectonic evolution of the depression into 5 parts: two rifting phases between 65 - 43.5 Ma, two transtensional rifting phases (43.5 - 24 Ma), and a final thermal subsidence phase (24 Ma- present). These phases line up well with the results from this study, where there are periods of rifting that are broken up by a brief period of compression, but Chen et al. (2017) does not note compression or inversion during their explanation of the phases that compose the Dongying Depression.

3.6 Conclusion

- The Dongying Depression depocenter shifts towards the center of the depression after 43.6 Ma and may reflect the changing regional tectonic setting.
- A stratigraphic analysis of the Dongying Depression reveals several local unconformities throughout the depression that are most strongly developed at 50.4 Ma.
- Most of the faults that activated during the extensional rifting phase (between 65 to 43.6 Ma) remained active through the many changes in tectonics until going dormant during the slow regional growth of the thermal subsidence phase (24Ma - present).
- A large percentage of faults in the region terminate downward around T7 (50.4 Ma), one of the horizons where several local unconformities were found.
- Large amounts of transtensional deformation occur in the depression around 33 Ma.
- The Dongying Depression has three major periods of inversion, one between T7 and T6 (Upper 40 Ma), one around T4 (between 33-44 Ma), and one at T1 (24 Ma).

Chapter 4: Conclusion

Through an extensive approach into designing a workflow to create a virtual field trip for students using 3D digital models of real geologic outcrops from planning surveys to creation of the assignment, the following conclusions were drawn:

- Model selection is critical in finding large well exposed outcrops with

uncomplicated terrain to make survey pre-flight plans. The optimal outcrop has limited vegetation and distinct protruding geologic beds and other geologic features such as dykes, channels, etc. The terrain can be a mixture of dipping and flat terrain, but issues arise if the outcrop has vertical walls and lateral extents as well.

- Survey plans need to be adjusted to the terrain style of each outcrop. This includes carefully selected camera angles, height, size, and shape of survey. Plan the survey during the time of year with the smallest chance of bad weather during flight and cloud coverage and movement is limited to ensure a smooth model without random shadows.
- When exporting a model with the intention of putting it in Unity software, be sure to export it with only one texture for the whole model to limit complications when creating the virtual field trip.
- Create several stops throughout the VFT that walk the student through the process of how to interpret the geology of the area. The order of the stops is not critical, but they need to tie to one another and build the students' knowledge of the area.
- The use of conceptual models to introduce the virtual field trip game functions and specific geologic features to watch for that will help on the real model ensures a smooth transition to the real outcrop model.

Through a structural analysis of the complex geology of the Dongying Depression, the following conclusions were drawn:

- The Dongying Depression depocenter shifts towards the center of the depression with the changing regional tectonics.
- A stratigraphic analysis of the Dongying Depression reveals several local unconformities throughout the depression.
- Most of the faults that activated at the beginning of the extensional rifting phase remained active through the change in tectonics, and either went dormant during the final thermal subsidence phase or are still active.
- A large percentage of faults in the region terminate downward around T7, one of the horizons where several local unconformities were found.
- Large amounts of transtensional deformation occur in the depression around 33 Ma.
- The Dongying Depression has three major periods of inversion, one between T7 and T6 (Upper 40 Ma), one around T4 (between 33-44 Ma), and one at T1 (24 Ma).

Bibliography

AgiSoft PhotoScan Professional (Version 1.7.6) (Software). (2020). Retrieved from <<http://www.agisoft.com/downloads/installer/>> in July, 2021.

Allen, M. B., Macdonald, D. I. M., Xun, Z., Vincent, S. J., & Brouet-Menzies, C. (1997). Early Cenozoic two-phase extension and late Cenozoic thermal subsidence and inversion of the Bohai Basin, northern China. *Marine and Petroleum Geology*, 14(7), 951–972.

Bao, H.Y., Guo, Z.F., Zhang, L.L., Huang, Y., 2013. Tectonic dynamics of eastern China since the formation of the Pacific plate. *Adv. Earth Sci.* 28 (3), 337–346.

Bemis, S. P., Micklethwaite, S., Turner, D., James, M. R., Akciz, S., T. Thiele, S., & Bangash, H.A. (2014). Ground-based and UAV-Based photogrammetry: A multi-scale, high-resolution mapping tool for structural geology and paleoseismology. In *Journal of Structural Geology* (Vol. 69, Issue PA).

Bistacchi, A., Balsamo, F., Storti, F., Mozafari, M., Swennen, R., Solum, J., Tueckmantel, C., & Taberner, C. (2015). Photogrammetric digital outcrop reconstruction, visualization with textured surfaces, and three-dimensional structural analysis and modeling: Innovative methodologies applied to fault-related dolomitization (Vajont Limestone, Southern Alps, Italy). *Geosphere*, 11(6).

Blender (Version 3.1)(Software). (2021) Retrieved from <https://blender.org/download> in July, 2021.

Chen Changming, Huang Jiakuan, Chen Jingshan and Tian Xingyou, 1984. Depositional models of Tertiary rift basins, eastern China, and their application to petroleum prediction. *Basin Analysis: Principles and Applications. Sediment. Geol.*, 40: 73-88.

Chen, S., Liu, X., Cui, Y., Zhao, X., & Zhang, J. (2017). Palaeogene structural evolution of Dongying Depression, Bohai Bay Basin, NE China. *International Geology Review*, 59(3), 259–273.

Chesley, J. T., Leier, A. L., White, S., & Torres, R. (2017). Using unmanned aerial vehicles and structure-from-motion photogrammetry to characterize sedimentary outcrops: An example from the Morrison Formation, Utah, USA. *Sedimentary Geology*, 354.

Eichelberger, N. W., Nunns, A., Perez, N. D., Ball, S., Claroni, D. J., & He, D. (2018). Incorporating simple erosion into structural forward models: The effects of regional erosion on growth strata geometry. *Journal of Structural Geology*, 116, 146–158.

Flacy, M., 2014, Man allegedly shoots down neighbor's drone with shotgun: Digital Trends, 1 Oct. 2014, <http://www.digitaltrends.com/cool-tech/new-jersey-man-allegedly-shoots-neighbors-drone/>.

Github. (2020). *GitHub*. Retrieved from <https://github.com/> in September, 2021.

Guo, X., Liu, K., He, S., Song, G., Wang, Y., Hao, X., & Wang, B. (2012). Petroleum generation and charge history of the northern Dongying Depression, Bohai Bay Basin, China: Insight from integrated fluid inclusion analysis and basin modeling. *Marine and Petroleum Geology*, 32(1), 21–35.

Hird, J. N., Montaghi, A., McDermid, G. J., Kariyeva, J., Moorman, B. J., Nielsen, S. E., & McIntosh, A. C. S. (2017). Use of unmanned aerial vehicles for monitoring recovery of forest vegetation on petroleum well sites. *Remote Sensing*, 9(5).

Hodgetts, D. (2013). Laser scanning and digital outcrop geology in the petroleum industry: A review. In *Marine and Petroleum Geology* (Vol. 46).

Hu, S., O'Sullivan, P. B., Raza, A., & Kohn, B. P. (2001). Thermal history and tectonic subsidence of the Bohai Basin, northern China: a Cenozoic rifted and local pull-apart basin. *Physics of the Earth and Planetary Interiors*, 126(3), 221–235.

James, M. R., Robson, S., d'Oleire-Oltmanns, S., & Niethammer, U. (2017). Optimising UAV topographic surveys processed with structure-from-motion: Ground control quality, quantity and bundle adjustment. *Geomorphology*, 280.

Jordan, B. R. (2015). A bird's-eye view of geology: The use of micro drones/UAVs in geologic fieldwork and education. *GSA Today*.

Jordan, C. J., & Napier, B. (2016). Developing digital fieldwork technologies at the British Geological Survey. In *Geological Society Special Publication* (Vol. 436, Issue 1).

Lampe, C., Song, G., Cong, L., & Mu, X. (2012). Fault control on hydrocarbon migration and accumulation in the Tertiary Dongying depression, Bohai Basin, China. *AAPG Bulletin*, 96(6).

Liang, J., Wang, H., Bai, Y., Ji, X., & Duo, X. (2016). Cenozoic tectonic evolution of the Bohai Bay Basin and its coupling relationship with Pacific Plate Subduction. *Journal of Asian Earth Sciences*, 127.

Liu, Q., He, L., Yi, Z., & Zhang, L. (2022). Anomalous post-rift subsidence in the Bohai Bay Basin, eastern China: Contributions from mantle process and fault activity. *Tectonics*, 41, e2021TC006748.

Madjid, M. Y. A., Vandeginste, V., Hampson, G., Jordan, C. J., & Booth, A. D. (2018). Drones in carbonate geology: Opportunities and challenges, and application in diagenetic dolomite geobody mapping. *Marine and Petroleum Geology*, 91.

Mateos, R. M., Azañón, J. M., Roldán, F. J., Notti, D., Pérez-Peña, V., Galve, J. P., Pérez-García, J. L., Colomo, C. M., Gómez-López, J. M., Montserrat, O., Devantèry, N., Lamas-Fernández, F., & Fernández-Chacón, F. (2017). The combined use of PSInSAR and UAV photogrammetry techniques for the analysis of the kinematics of a coastal landslide affecting an urban area (SE Spain). *Landslides*, 14(2).

McClay, K. R. (1989). Physical models of structural styles during extension. In *Extensional Tectonics and stratigraphy of the North Atlantic Margins*. Memoir 46. Chapter 7: Concepts. Published ID. A156 .

Pix4Dmapper (2017). Pix4D SA. Retrieved from <https://www.pix4d.com> in July, 2021.

Structure Solver (2019). Structure Solver LLC, Verison 4.0.700224317. Retrieved from <<https://structuresolver.com>>

Unity (2019). *Unity - Game Engine*. [online] Available at: <<https://unity3d.com/>>

Uzkeda, H., Poblet, J., Magán, M., Bulnes, M., Martín, S., Fernández-Martínez, D., (2022). Virtual outcrop models: Digital techniques and an inventory of structural models from North-Northwest Iberia (Cantabrian Zone and Asturian Basin), *Journal of Structural Geology*.

Julivert, M., Fontboté, J. M., Ribeiro, A., Conde, L. E., (1972). Mapa Tectónico de la Península Ibérica y Baleares, Escala 1:1.000.000. Instituto Geológico y Minero de España, Madrid.

Mlambo, R., Woodhouse, I. H., Gerard, F., & Anderson, K. (2017). Structure from motion (SfM) photogrammetry with drone data: A low cost method for monitoring greenhouse gas emissions from forests in developing countries. *Forests*, 8(3).

Nesbit, P. R., Durkin, P. R., Hugenholtz, C. H., Hubbard, S. M., & Kucharczyk, M. (2018). 3-D stratigraphic mapping using a digital outcrop model derived from UAV images and structure-from-motion photogrammetry. *Geosphere*, 14(6).

Nesbit, P. R., & Hugenholtz, C. H. (2019). Enhancing UAV-SfM 3D model accuracy in high-relief landscapes by incorporating oblique images. *Remote Sensing*, 11(3).

Nieminski, N. M., & Graham, S. A. (2017). Modeling stratigraphic architecture using small unmanned aerial vehicles and photogrammetry: Examples from the Miocene East Coast Basin, New Zealand. *Journal of Sedimentary Research*, 87(2).

Qi, J., & Yang, Q. (2010). Cenozoic structural deformation and dynamic processes of the Bohai Bay basin province, China. *Marine and Petroleum Geology*, 27(4).

Șerban, G., Rus, I., Vele, D., Brețcan, P., Alexe, M., & Petrea, D. (2016). Flood-prone area delimitation using UAV technology, in the areas hard-to-reach for classic aircrafts: case study in the north-east of Apuseni Mountains, Transylvania. *Natural Hazards*, 82(3).

Tamminga, A. D., Eaton, B. C., & Hugenholtz, C. H. (2015). UAS-based remote sensing of fluvial change following an extreme flood event. *Earth Surface Processes and Landforms*, 40(11).

Tavani, S., Granado, P., Corradetti, A., Girundo, M., Iannace, A., Arbués, P., Muñoz, J. A., & Mazzoli, S. (2014). Building a virtual outcrop, extracting geological information from it, and sharing the results in Google Earth via OpenPlot and Photoscan: An example from the Khaviz Anticline (Iran). *Computers and Geosciences*, 63.

Viana, C. D., Grohmann, C. H., dos Santos Toledo Busarello, M., & Garcia, G. P. B. (2018). Structural analysis of clastic dikes using Structure from Motion - Multi-View Stereo: A case-study in the Paraná Basin, southeastern Brazil. *Brazilian Journal of Geology*, 48(4).

Zahm, C., Lambert, J., & Kerans, C. (2016). Use of Unmanned Aerial Vehicles (UAVs) to Create Digital Outcrop Models; An Example from the Cretaceous Cow Creek Formation, Central Texas. *Gulf Coast Association of Geological Societies*, 5.

Appendix

The TCG Virtual Field Trip Stops

In the Taylor Creek Group Virtual Field Trip, there are 11 stops, labeled sequentially 1 to 11. The stops, although given a numerical order, do not need to be followed sequentially. Each stop has an individual purpose to teach the student something about the outcrop and its geology. Some stops are compared to one another to ensure the student notices changes in the model's structure or stratigraphy. The student will first start in a valley between two small ridges. Much like in real life, visibility is limited and the student must walk to the top of the ridge to see more of the model. In order, each stop is described:

Stop 1: Differential erosion and features seen in the sediment. Dirtbike tracks in the sediment are good for scale as well as indications of human activity that may destroy parts of the outcrop. An image of the location is also included for reference.

Stop 2: Located over the ridge to the east of the spawn point, the hammer is on an eroded slope where one might think to take a strike and dip. The stop is meant to show students that not all surfaces are bedding planes that can have a strike and dip measured on.

Stop 3: Following the distinct ridge forming bed to the North, the hammer is located on a part of the formation that is optimal for both strike and dip. While looking at this stop, the student is asked if this exposed feature is good for measuring a strike and dip. They are also asked which face of the feature is the bedding plane, and how they know this. An image of the rock is included along with a description of the type of rock. The student is asked what depositional environment may have formed a rock like this. This stop is meant to illustrate to the student what a good bedding surface looks like, as well as begin their understanding of the structure of the outcrop as well as its formation history.

Stop 4: Continuing North after Stop 3, Stop 4's hammer is located at the top of a small ridge where the sediment color distinctly changes. Here, the stop is intended to make the student think about the strike of the exposed bedding, and if you can measure the strike of a unit without the dip. This stop will keep the student thinking about the structure of the outcrop, and give them a base to compare to when they walk to the other side of the model.

Stop 5: Stop 5 is visible from Stop 4. It is northwest of Stop four, near the edge of the map. This stop brings the student to another good bedding plane that they can measure the strike and dip of the unit. There is a decrease in the dip angle that the student should notice, but the strike should remain the same. This stop also includes an image of the stop from a distance. The picture of the exposed ridge is taken southwest of where the stop is. What the student learns from this is that looking at geology from afar often is misleading. The beds may look like they are dipping in a completely different direction and it takes getting close to the unit to understand what is really going on.

Stop 6: Directly south of Stop 5 and over 2 ridges is the hammer for Stop 6. It is located on a different colored sediment, much like what was seen at Stop 4. The stop asks the student about this change in color of the sediment and asks if the area is good for strike and dip measurements. This will keep the student thinking about where they can or cannot take these measurements and keep them on the lookout for what might be a good surface.

Stop 7: Located directly west of Stop 6, the hammer for Stop 7 is located on the same bed as Stop 5. This stop asks the student to take a strike and dip measurement and compare it to Stop 5.

Stop 8: Located 3 ridges south of Stop 7, Stop 8 rests on top of a ridge and asks the student to compare the strike of the bed to their measurements at Stop 4. This is intended to point out to the student that the beds no longer strike in the same direction. They can walk the ridge back towards Stop 4 to see the change.

Stop 9: This stop is located several ridges north of Stop 8 and takes you past Stop 7. The hammer is located on top of a small ridge where the sediment color is different from all of the other stops. The stop includes two pictures of the location. Here, the student is asked a question about the depositional environment of the beds at this location. This question is intended to keep the student thinking about the geologic history of the area.

Stop 10: Located between Stop 7 and Stop 9, Stop 10 asks the students to look at the vegetation of the area to see if there are any growth patterns. This will give the student another perspective on other non-geologic features that can indicate underlying geology.

Stop 11: On top of an eroded ridge, east of Stop 10, the student is asked if this location

is good for making a strike and dip measurement. While the rock face looks flat like a bedding plane, it does not fit any of the other locations' strike and dip patterns, which indicates this surface is only an eroded surface and to be disregarded for measurements.

Written Assignment (Blank)

Understanding Field Geology Through Virtual Outcrops

Objective: Learn how to interpret geologic structures by looking at two different virtual outcrops. The first will be an animated and simple outcrop. The second will be a real outcrop where the geologic features are significantly harder to see and find.

Part 1: Methoda Field's Mapping Exercise

Objective of Part 1: Learn basic field techniques to better understand and interpret geologic features in the field with a simple virtual geologic model.

Copy the following link into your internet browser: <https://keatondenzer.itch.io/tcg-part1>

The Password is: TCG

Instructions: Once the game has loaded, click the play button. Explore the small outcrop and do the various questions at each stop (floating rock hammer). There are 7 flags labeled by stop number, but they do not need to be visited sequentially. Utilized the flying feature as much as possible to get both a bird's eye view, and the view from the ground.

After you have explored the model and investigated all the stops, answer the following questions:

Describe the experience of 'walking on the ground' compared to flying over the model.

What challenges does a geologist face when on the ground in the field?

What are some ways to combat these challenges when in the field?

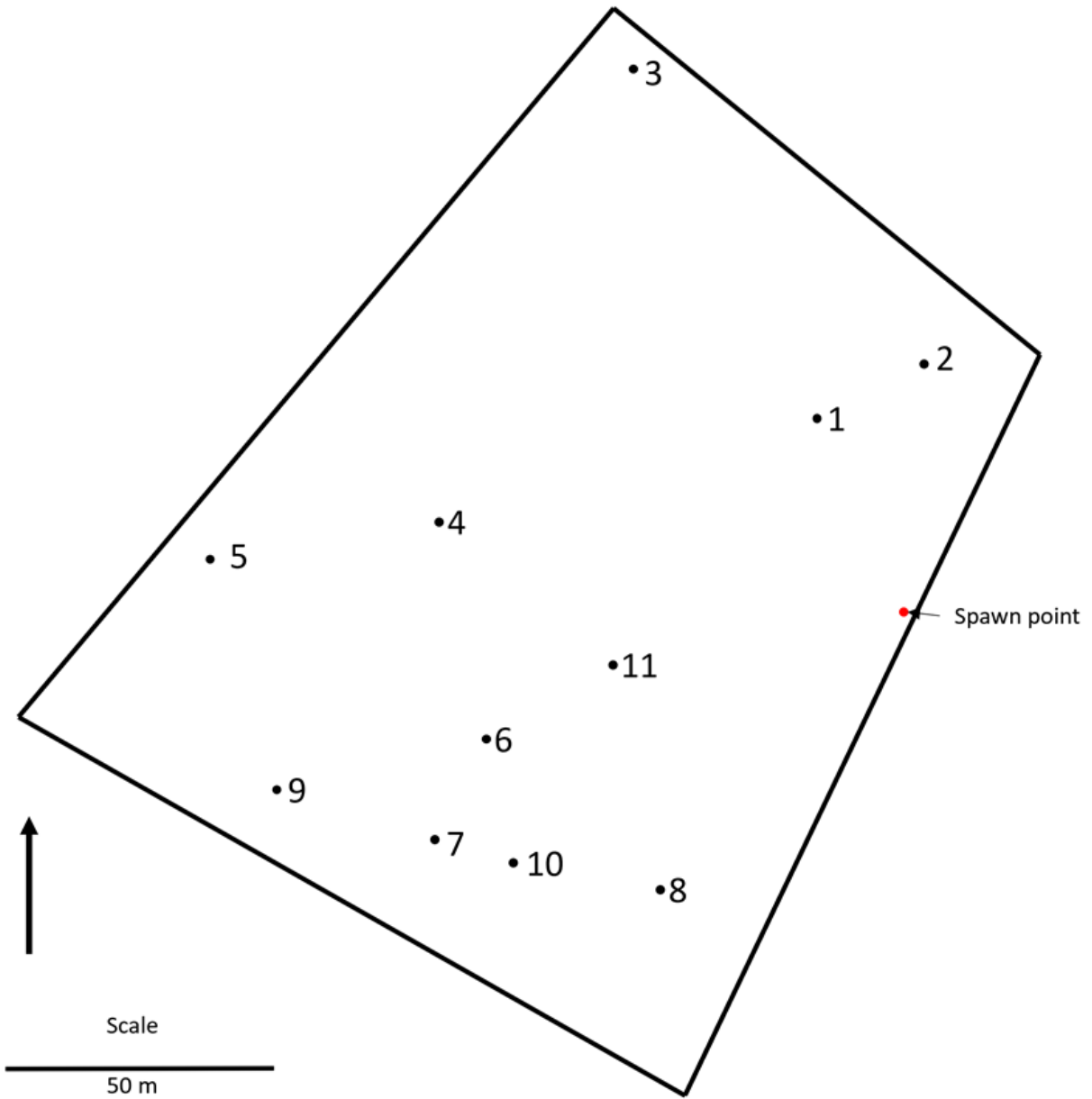
Part 2: Taylor Creek Group Surface Mapping

Objective of Part 2: Use the basic techniques in Part 1 to interpret a real geologic outcrop by walking on the virtual surface of the exposed Taylor Creek Group in British Columbia.

Copy the following link into your browser: <https://keatondenzer.itch.io/tcg-part2>

The Password is: TCG

Instructions: Once the game has loaded, click the play button. You will be dropped onto the model as if you were in the field, this is your spawn point. The jetpack feature will not be accessible for this portion of the lab. Walk around the area and stop at the various locations where there are floating hammers. Answer the questions to the corresponding stop numbers. The stops do not have to be done in order although it is recommended that you save stop 11 to be your last question. Be sure to record the strike and dips in azimuth notation for each question that asks for it.



Stop 1:

Why is the topography so low here? What does this tell you about the potential stratigraphy? What is a good assumption for the lithology under the cover?

Stop 2:

Is this a good location to measure strike and dip? Why or why not?

Stop 3:

Measure and record the strike and dip, then draw it on the blank map.

What makes this location good for taking a strike and dip?

What may have been the depositional environment of a unit such as this one?
(deep marine, shallow marine, deltaic, desert, etc.)

Stop 4:

Measure and record the strike and dip, then draw it on the blank map.

Why can we take a strike measurement here but not a dip measurement?

Stop 5:

Measure and record the strike and dip, then draw it on the blank map.

Compared to stop 3, is the dip at this location more or less? Why might this be?

Stop 6:

How does the color of the sediment here differ from other, more prominent areas? What can this tell you about the stratigraphy?

Is this location good for strike and dip measurements? Why or why not?

Stop 7:

Measure and record the strike and dip, then draw it on the blank map. How do these measurements compare to stop 5?

What does this indicate about the structure of the area?

Stop 8:

Measure and record the strike and dip, then draw it on the blank map.

How does this compare to Stop 4? What does this indicate about the bedding?

Stop 9:

Would this deposition likely be marine or terrigenous in origin?

Stop 10:

Are there any patterns to where the vegetation is growing? How can this be useful in identifying stratigraphy and structures?

Stop 11:

Looking at the surface marked by the red flag, determine if this is a good location to take a strike or dip (Yes or no). If it is, record the strike and dip. If not, explain why.

Measure the thickness of this bed. Is this the true thickness? What else needs to be considered when measuring the thickness of beds?

Draw at least 3 stratigraphic contacts on the blank map that follow the correct strike of the unit. You may want to go record a few more points on your map with the strike of the bedding to help with your accuracy of the bed locations.

Part 3: Taylor Creek Group Aerial Mapping

Objective: Compare ground observations of the Taylor Creek Group Outcrop with what the area looks like aurally.

Copy the following link into your browser: <https://keatondenzer.itch.io/tcg-part3>

The Password is: TCG

Instructions: Click play once the game has loaded. Use the jetpack mode to fly above the model. Look at the outcrop from all directions to better understand what geologic structure(s) are present. Answer the following questions about what you are observing.

Use the Map view to trace out the real bedding contacts. Was your initial interpretation in Part 2 correct? What differences can you see compared to your initial interpretation now that you have an aerial view of the area?

What are the benefits to seeing the structure from ground level?

What are some benefits to seeing the structure from the air?

Draw a rough cross section of what this area might look like between Stop 3 and Stop 5. (Does not have to be to scale)

Try to describe the depositional and structural history of the area. Which structural deformation came first? How many deformations are there?

Key to Assignment

Part 3 varies per student and will not be included

Part 1: Methoda Field's Mapping Exercise

Objective of Part 1: Learn basic field techniques to better understand and interpret geologic features in the field with a simple virtual geologic model.

Copy the following link into your internet browser: <https://keatondenzer.itch.io/tcg-part1>

The Password is: TCG

Instructions: Once the game has loaded, click the play button. Explore the small outcrop and answer the various questions at each stop (floating rock hammer). Be sure to go to the stops in order.

Stop1:

Would this erosional feature be a wind gap or a water gap? Explain your reasoning.

Wind, It was formed by water but the water is now gone

Does the thickness of the unit appear to be thicker or thinner in the river than what the beds true thickness is?

Thicker

Stop 2:

In your own words, what is differential erosion and what can it be used to indicate?

How rocks of different levels of hardness erode over time. Indicates weaker rocks vs harder rocks.

At the location of this stop, are you standing on a cliff forming rock or a slope forming rock?

Slope forming

List Two other examples of lithologies that form cliffs and one other lithology that forms slopes.

Cliff forming: Limestone, Well cemented conglomerates, Basalt, etc.

Slope forming: siltstone, mudstone, etc.

Stop 3:

What is the strike and dip of the blue flag across from Stop 3? Use both Azimuth and Quadrant notation.

Strike 121° Dip 45° SE or S 59° E 45° SE

Mark on the map the strike and dips of all four flags with the correct symbol and include a screenshot of your map view with the correct symbols at the correct locations. Does the strike or dip change in this area?

Answers will vary

Stop 4:

Does this view match what you thought the model would look like in the subsurface? Explain your reasoning.

Answers will vary

Looking at the model from Stop 4, and assuming the structure is not overturned, which unit is the oldest (northernmost unit or southernmost unit) and which is the youngest (northernmost unit or southernmost unit)?

Southernmost is oldest and northern most in youngest

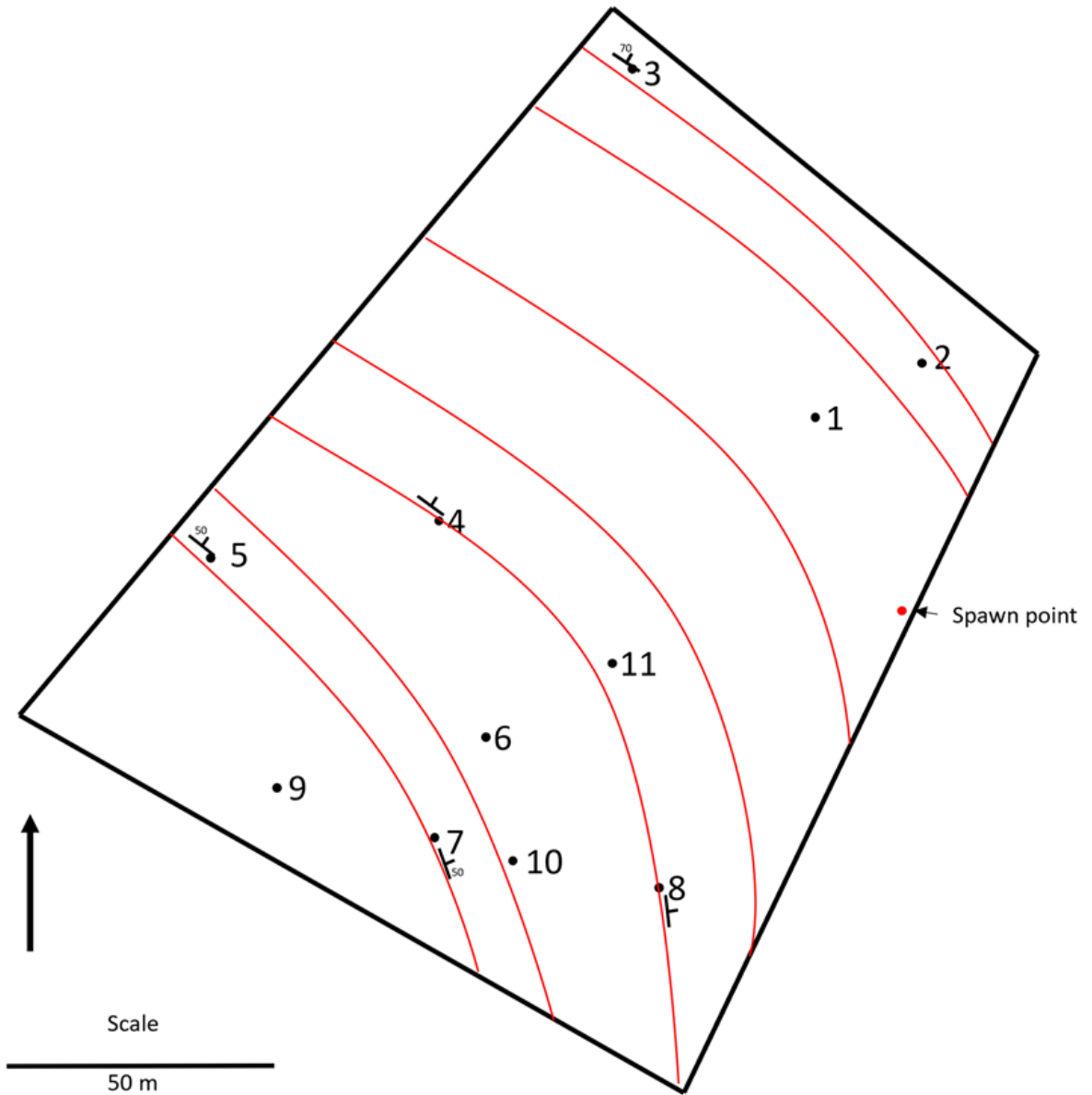
Part 2: Taylor Creek Group Surface Mapping

Objective of Part 2: Use the basic techniques in Part 1 to interpret a real geologic outcrop by walking on the virtual surface of the exposed Taylor Creek Group in British Columbia.

Copy the following link into your browser: <https://keatondenzer.itch.io/tcg-part2>

The Password is: TCG

Instructions: Once the game has loaded, click the play button. You will be dropped onto the model as if you were in the field, this is your spawn point. The jetpack feature will not be accessible for this portion of the lab. Walk around the area and stop at the various locations where there are floating hammers. Answer the questions to the corresponding stop numbers. The stops do not have to be done in order although it is recommended that you save stop 11 to be your last question. Be sure to record the strike and dips in azimuth notation for each question that asks for it.



N

Stop 1:

Why is the topography so low here? What does this tell you about the potential stratigraphy? What is a good assumption for the lithology under the cover?

There was soft rock present that eroded away easier than the ridge material. Likely a shale under the cover.

Stop 2:

Is this a good location to measure strike and dip? Why or why not?

No, there are no good bedding surfaces.

Stop 3:

Measure and record the strike and dip on the blank map.

Strike: 115° Dip: 70°

What makes this location good for taking a strike and dip?

Well exposed surface and can tell which side to measure.

What may have been the depositional environment of a unit such as this one? (deep marine, shallow marine, deltaic, desert, etc.)

Deltaic

Stop 4:

Measure and record the strike and dip, then draw it on the blank map.

-125°

Why can we take a strike measurement here but not a dip measurement?

The color of the bedding allows us to see the strike of the bedding but there is not exposure for us to measure the dip.

Stop 5:

Measure and record the strike and dip, then draw it on the blank map.

Strike: 131° Dip: 50°

Compared to stop 3, is the dip at this location more or less? Why might this be?

Less, answers may vary for why.

Stop 6:

How does the color of the sediment here different from other, more prominent areas? What can this tell you about the stratigraphy?

It is more dark grey. Change in stratigraphy, probably shale or siltstone.

Is this location good for strike and dip measurements? Why or why not?

No, there are no prominent bedding surfaces.

Stop 7:

Measure and record the strike and dip, then draw it on the blank map. How do these measurements compare to stop 5?

Strike: $160-170^{\circ}$ Dip: 50° , The strike has changed significantly but the dip has not changed much

What does this indicate about the structure of the area?

There is a bend in the structure.

Stop 8:

Measure and record the strike and dip, then draw it on the blank map.

Strike: 176°

How does this compare to Stop 4? What does this indicate about the bedding?

It is larger, there is a bend in the bedding

Stop 9:

Would this deposition likely be marine or terrigenous in origin?

Marine

Stop 10:

Are there any patterns to where the vegetation is growing? How can this be useful in identifying stratigraphy and structures?

Yes, the vegetation often grows along the ridge where the shale contacts the conglomerate rock.

Stop 11:

Looking at the surface marked by the red flag, determine if this is a good location to take a strike or dip (Yes or no). If it is, record the strike and dip. If not, explain why.

No, it does not follow the pattern of the rest of the outcrop, it is an eroded surface.

Measure the thickness of this bed. Is this the true thickness? What else needs to be considered when measuring the thickness of beds?

Not the true thickness. Need to take into account the dip of the beds.

Draw at least 3 stratigraphic contacts on the blank map that follow the correct strike of the unit.

Answers will vary